Department of AERONAUTICS and ASTRONAUTICS
STANFORD UNIVERSITY

LECTURE NOTES

ON

PLASMA AND SPACE PHYSICS

prepared by

DR. FREDERICK L. SCARF

for the

ASEE-NASA SUMMER FACULTY INSTITUTE, 1965

Department of Aeronautics and Astronautics
Stanford University
Stanford, California

LECTURE NOTES
ON
PLASMA AND SPACE PHYSICS

prepared by

Dr. Frederick L. Scarf

for the

ASEE-NASA Summer Faculty Institute, 1965

I. INTRODUCTION

In this series of lectures we will discuss some properties of the fully ionized gases which extend over the vast region of space from the base of the solar atmosphere, or corona, to the top of the earth's ionosphere, roughly 300 – 500 kilometers above the surface. In this entire region we have to deal with essentially a single plasma composition, fully ionized hydrogen with a small admixture of helium, but very distinct states of this plasma are encountered because varying densities, temperatures, flow velocities and associated magnetic fields are involved. In order to have a framework in which to begin our detailed discussion, it is convenient at this point to describe roughly some of the main physical features of these regions.

I.1. The Solar Corona

The photosphere or the visible surface of the sun has a radius of 7×10^5 km $(= 1\ R_\odot)$ and a temperature near 6000°K . During total eclipses, information on the much less luminous, rarefied solar atmosphere may be obtained. Between the photosphere and an altitude of $(5 - 15) \times 10^3$km , the density falls and the solar atmosphere remains fairly cool. From this region an emission spectrum with many familiar atomic lines in the visible range is observed, and hence this is called the chromosphere.

Beyond the chromosphere there exists an extremely faint halo which represents primarily photospheric light scattered from the corona. Near the coronal base $(\sim 1.03\ R_\odot)$ the surface brightness is on the order of 10^{-6} that of the disc and at $3\ R_\odot$ the brightness is down by three more orders of magnitude. Since the luminosity is so low, visual observations are useless, and the discovery of the corona is generally assigned to 1851, when the first attempts were made to photograph a solar eclipse. Very limited photographic studies were

carried out in the period 1850 – 1930 (total observing time less than one hour) but after the invention of the coronagraph by Lyot in 1930 it was possible to study the corona out to $(1.7 - 2)R_\odot$ without waiting for eclipses. One of the major advances associated with the coronagraph is the discovery and identification of many extremely weak emission lines in the coronal base region $(r < 1.4\ R_\odot)$. Some of these lines were detected as early as 1898 and attributed to a new element, coronium, but in the period 1939 – 1942 all the coronal lines were definitely identified by Grotrian and Edlén as emissions from very highly ionized states of heavy atoms (Ca 12 – Ca 15 ; Fe 10 – Fe 15 ; etc.) . The ionization potentials for these states are on the order of 200 – 800 ev , and it was realized that the spectrum could be produced by thermal excitation only if T were on the order of 10^6°K .

General confirmation of this surprising temperature estimate was obtained by several independent means in the next decade. The measured total intensities in the solar X-ray spectrum and the radio emission at meter wavelengths yield a coronal electron temperature near 7.5×10^5°K for quiet conditions, and the line widths of emission lines indicate that the temperatures are greater than 10^6°K . During the eclipses of 1952, 1954 and 1955 careful intensity versus radial distance measurements were made at high altitudes, and these were used to calculate electron density profiles, $N_e = N_e(r)$. In the region $R_\odot < r < 3R_\odot$, the results are quite close to those predicted by the equation of hydrostatic equilibrium

$$\frac{d}{dr}(N\kappa T) = -\frac{GM_\odot mN}{r^2} \quad . \tag{I.1}$$

For isothermal conditions Eq. (I.1) yields

$$\begin{aligned} N(r) &= N(r_0)\ \exp\ (GM\ m/\kappa T)(r^{-1} - r_0^{-1}) \\ &\simeq N(r_0)\ \exp\ (-\ GM\ mh/\kappa T R_\odot) \end{aligned} \tag{I.2}$$

and this agrees with the light scattering experiments for $N(r_0) \simeq 2 \times 10^8/cm^3$ at $r_0 \simeq 1.06\ R_\odot$ and $T \simeq (1.1 - 1.6) \times 10^6 °K$. Here G is the gravitational constant (6.67×10^{-8} cgs units), M is the mass of the sun (2×10^{33} gms) and m is the mean mass of a coronal particle (if 90% of the particles are ionized hydrogen and 10% are fully ionized helium, the mean mass is 62% of the proton mass).

I.2. The Interplanetary Medium

For many years it has been accepted that such terrestrial phenomena as the aurora, geomagnetic fluctuations, and geomagnetic storms are associated with the emission of particles from the sun. Long-lived activity centers on the sun (M-regions) apparently cause geomagnetic disturbances at regular intervals of 27 days (the rotation period of the sun as seen from the earth) and individual events such as solar flares may produce identifiable magnetic activity at the earth after a delay of 24 to 70 hours. Since the mean sun-earth distance is 1.5×10^8 km ($= 1$ AU $\simeq 214\ R_\odot$), these delays correspond to average velocities on the order of 600 – 1700 km/sec, assuming radial propagation. The slow speeds clearly refer to moving particles and not to propagation of radiation.

The first suggestion that continuous rather than intermittent solar particle emission might occur is due to Biermann. By analyzing the acceleration and excitation of Type I (fully ionized) comet tails, Biermann concluded that during quiet periods the flow velocities might range from 400 km/sec to 1000 km/sec, and that these particles would form a streaming interplanetary plasma.

Although comet tails cannot be regarded as precision test objects for analysis of the interplanetary medium, in 1958 Parker published an ingenious and bold theory in which he argued that a) the solar corona is not static; b) it continually expands into space reaching supersonic speeds at distances of several solar radii; and c) the expanding solar corona is, in fact, the same as the streaming plasma of

interplanetary space. Parker referred to this as the solar wind.

Parker's analysis led to another conclusion. The postulated solar wind can coexist with an interplanetary magnetic field only if the field lines spiral out from the sun in a rather special pattern, arriving at the earth with a "hose angle" tilted near $45°$ toward the west limb of the sun. Ground based observations of the arrival of energetic ions (in solar cosmic rays with energies on the order of 30 MeV – 1 BeV) emitted during large solar flares strongly supports this prediction, assuming that the high energy particles are guided along the spiral field lines. The study of solar modulation of primary cosmic ray intensities also supports the Parker model.

Although much indirect evidence seemed to favor this theory, Parker's predictions were not generally accepted until 1962. (A 1961 symposium on "The Solar Corona" resulted in a book of more than 300 pages, but the possible existence of continuous coronal streaming is only mentioned in two brief paragraphs.) However, for the first 104 days of 1962, an electrostatic analyzer on the interplanetary probe Mariner 2 directly sampled the solar plasma and found that a finite streaming proton current was always present. The velocity ranged from 250 – 800 km/sec , the mean density appeared to be in the range of $1 - 5$ ions/cm^3 , and the observed spectra were consistent with a mean temperature of 2×10^5°K . Subsequent measurements generally confirm these early observations.

I.3. The Ionosphere and Magnetosphere

Although all information about the corona and much of our knowledge of the interplanetary medium is based on interpretation of ground observations, the study of the plasma surrounding the earth is primarily founded on information collected by instruments on satellites, or rocket probes.

There are some exceptions to this generalization. The propagation of radio waves through the high atmosphere provides a means of studying

the ionosphere or partly ionized gas which exists above $60 - 80$ km altitude. The most common technique utilizes the ionospheric sounder which is essentially a variable frequency radar. When a wave with angular frequency ω and amplitude E_0 encounters a single electron, the electron responds according to

$$m\ddot{x} = - m \omega^2 \Delta x = - eE \qquad (I.3)$$

if collisions and magnetic fields can be neglected. In the entire medium, this generates a net polarization field, $P = - 4\pi Ne \Delta x$, and the displacement is $D = \kappa E_0 \simeq n^2 E_0$, with the index of refraction given by

$$n^2 = 1 - \omega_p^2/\omega^2 \quad , \qquad \omega_p^2 = 4\pi Ne^2/m \qquad (I.4)$$

The quantity ω_p is the electron plasma frequency and the wave is totally reflected for $\omega \leq \omega_p$. By sweeping the frequency and measuring the echo delay time, an electron density versus altitude profile can be obtained. A typical daytime profile is shown in Fig. 1, along with a neutral density curve. Before rockets were available, the latter was calculated from the $N_e(h)$ distribution by assuming hydrostatic equilibrium with slowly varying temperature and a fixed solar radiation flux. The short wavelength solar radiation (UV to X-rays) produces photo-ionization of the neutral atmosphere, and the recombination proceeds slowly enough so that fairly high concentrations of electrons persist throughout the night. The various "layers" are not really very distinct, but the D-region essentially disappears at night, soft solar X-rays are responsible for the permanent E-region, and the He 2 304Å line in the solar spectrum is the main agent for F-region photo-ionization.

Above the F maximum, the almost fully ionized plasma is relatively inaccessible to ground-based observation, although incoherent radar backscatter (i.e., Thompson scattering by electrons) yields $N_e(h)$ for $h \lesssim 4000 - 6000$ km. Another experimental technique is based on the fact that the index of refraction differs drastically from

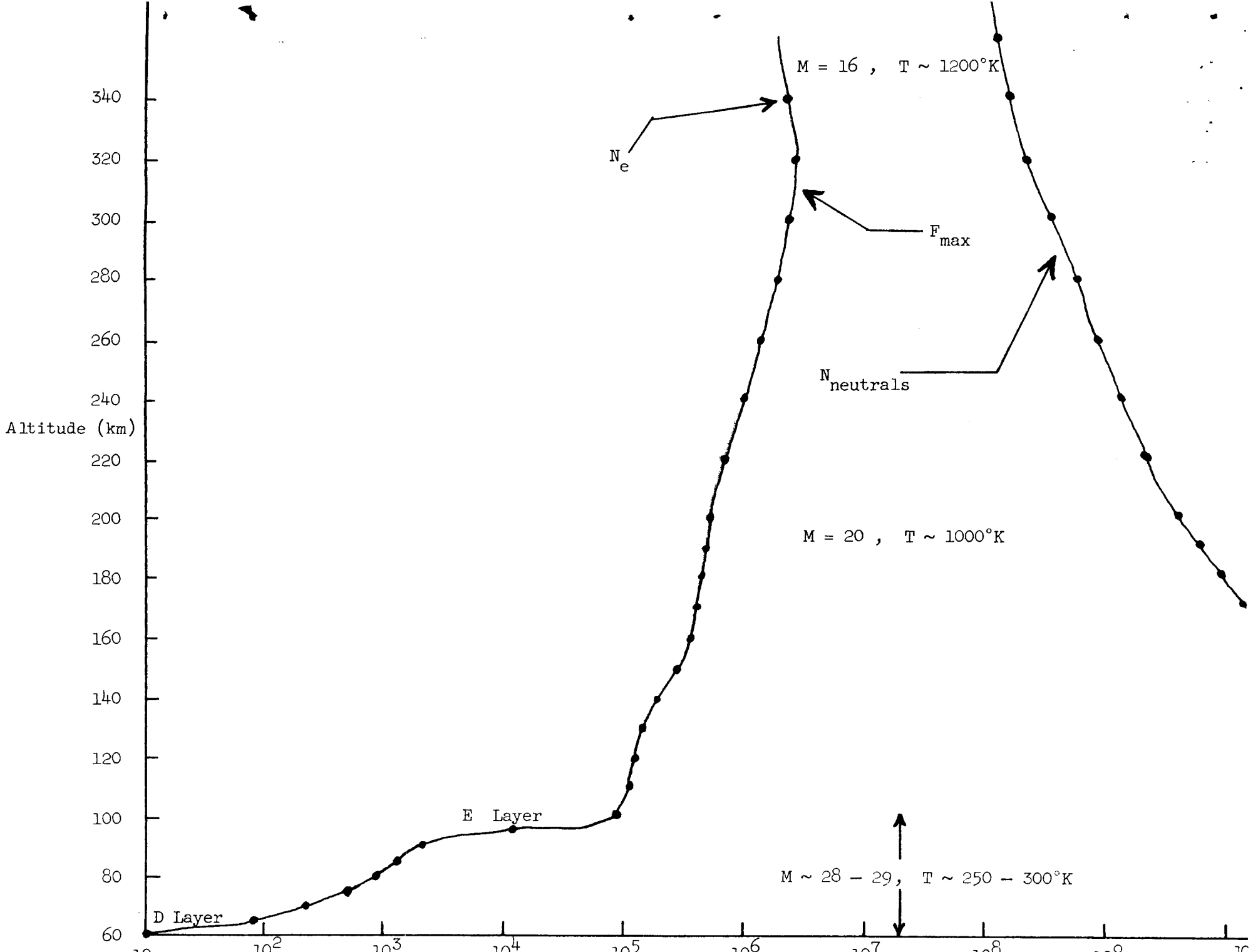
M = 16 , T ~ 1200°K
N_e
F_{max}
$N_{neutrals}$
M = 20 , T ~ 1000°K
E Layer
M ~ 28 – 29, T ~ 250 – 300°K
D Layer
340
320
300
280
260
240
Altitude (km)
220
200
180
160
140
120
100
80
60
10
10^2
10^3
10^4
10^5
10^6
10^7
10^8
10^9
10^{10}
Figure 1

Eq. (I.4) at frequencies below the electron and ion gyrofrequencies. Passbands occur and audiofrequency noise signals (whistlers) and subsonic oscillations (micropulsations) can propagate through the ionosphere. Analysis of these signals leads to a density distribution

$$N_e(r) \simeq 10^4 (R_e/r)^3 \text{ cm}^{-3} \qquad \text{(I.5)}$$

for $2R_e \lesssim r \lesssim 5R_e$ ($1\ R_e = 6371$ km), and it also is known that at altitudes above about 1000 km the gas is essentially a proton-electron plasma; the barometric equation then indicates that in the upper ionosphere ($h \sim 1000$ km) the temperature is on the order of $2000 \pm 1000°K$.

Satellite measurements have yielded relatively little additional information about the low energy or thermal plasma component above the ionosphere. Some experiments indicate that the equivalent electron temperature rises slowly with altitude reaching perhaps 50,000°K to 100,000°K at a geocentric distance of $(8 - 10)R_e$. However, it appears definite that a large non-Maxwellian tail of electrons with $E \sim 100$ev - 2kev is also present, and no good measurements of the proton temperature are available to date.

Perhaps the most spectacular developments since the launching of Sputnik I and Explorer I in 1957-58 are related to the discoveries that the geomagnetic field is permanently distorted and terminated by the solar wind, and that large fluxes of high energy (superthermal) electrons and protons are trapped in the distorted, but ordered, geomagnetic cavity. The region in which trapping by the earth's magnetic field can occur is called the magnetosphere, and a rough sketch of the cavity is shown in Fig. 2; inside the magnetosphere Van Allen "radiation" is found in a trapped or quasi-trapped state, and presumably no solar plasma is present. Upstream from the magnetosphere boundary or magnetopause, a broad complex region of wind-magnetosphere interaction exists. This is called the transition region and some extremely interesting plasma physics phenomena occur here. Apparently the transition region proton flow velocity is on the order of $60 - 90\%$ of the incident

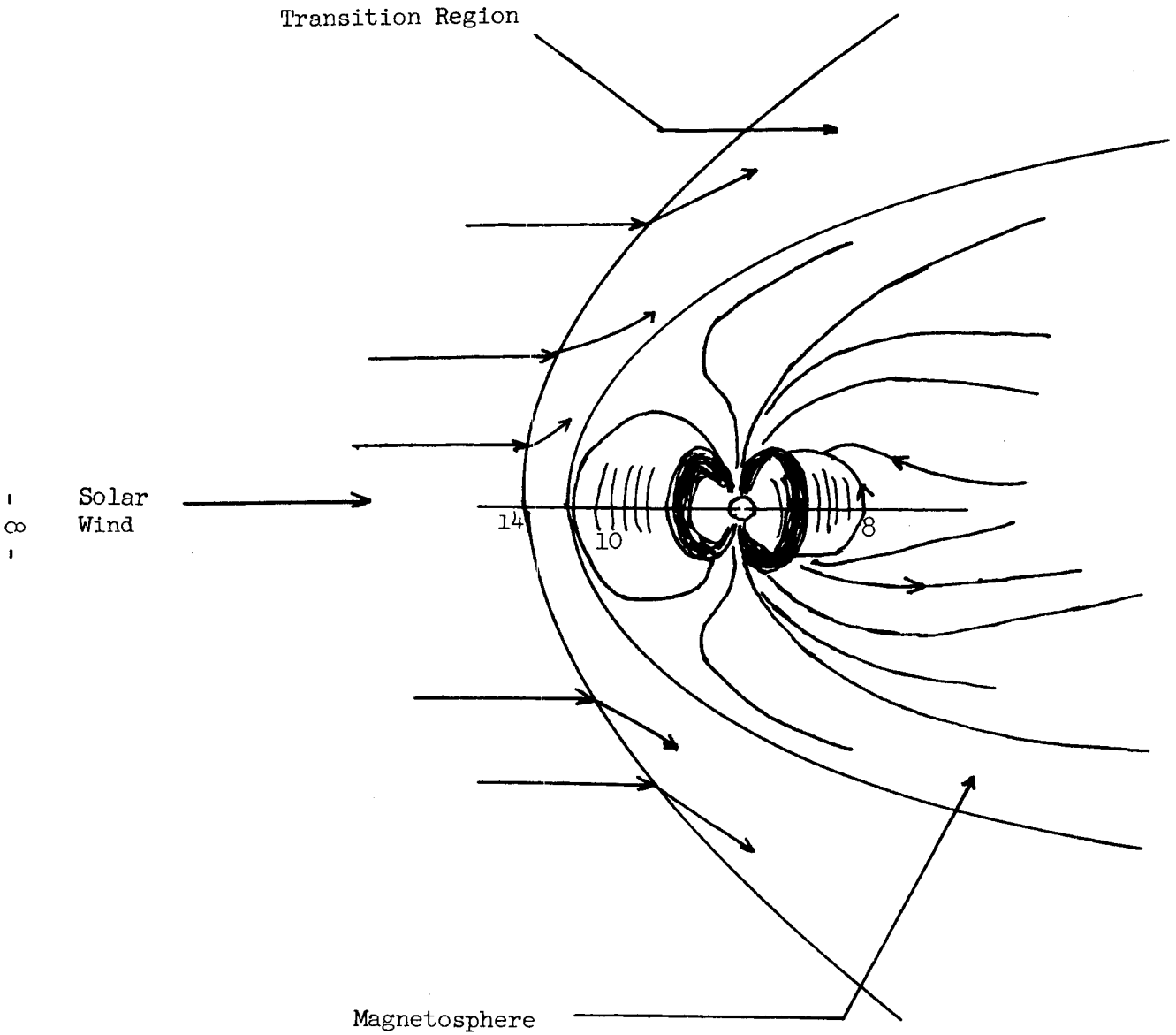

Figure 2

solar wind speed, the proton temperature is on the order of $5 \times 10^5 °K - 10^6 °K$, while the electrons are nearly at rest with temperatures ranging from $10^6 °K$ to $3 \times 10^8 °K$. The outer boundary of the transition region is generally called the "shock boundary," but as we shall see, all of these regions, boundaries, etc., have quite variable locations and characteristics, and they are frequently indistinct.

I.4. Collisions and Plasma Equilibrium

The general properties of the various plasma states were discussed first in order to fix the terminology and offer some familiarity and perspective. However, a much more practical reason for this organization is related to the fact that many different mathematical tools are needed to analyze plasmas with such a wide range of densities, temperatures, etc. Perhaps the most basic classification involves the extent to which the dynamical description of the plasma is governed by inter-particle collisions or correlations. In order to assess the importance of collisions, we must compute the mean free path in the plasma and compare it with some significant scale length for the system.

The mean free path for two-particle encounters is defined by $\ell \sigma N = 1$, where σ is the total scattering cross-section. In a fully ionized hydrogen gas, long range coulomb forces operate and the process is quite similar to ordinary Rutherford scattering. As a first approximation, one can define the distance of closest approach between particles of mass m_1 , m_2 ,

$$\frac{mv^2}{2} = \frac{e^2}{r_{min}} \quad , \qquad \frac{1}{m} = \frac{1}{m_1} + \frac{1}{m_2} \tag{I.6}$$

and the differential scattering cross-section is

$$\sigma(\theta) = \left(\frac{r_{min}}{4}\right)^2 \csc^4 \theta/2 \quad . \tag{I.7}$$

However, Eq. (I.7) demonstrates the familiar fact that the total cross-section for Rutherford scattering diverges, so that no finite

mean free path can be defined for a gas of charged particles with strict inverse square forces between arbitrary pairs.

Fortunately, this is not the case for a true plasma, since a test charge in a fully ionized gas does not actually produce a coulomb field. In fact, if a positive charge is inserted in an electron-proton gas, the mobile electrons form a non-uniform cloud which tends to shield out the field at long range. The electron density distribution around the test charge is obtained by equating the pressure gradient and the force density; as in the deduction of Eq. (I.2) for an isothermal gas, hydrostatic equilibrium implies

$$N_e(r) = N_e(\infty)\, e^{(e\phi(r)/\kappa T)} \simeq N_e(\infty) + eN_e(\infty)\phi(r)/\kappa T + \ldots \tag{I.8}$$

and the potential is given by Poisson's equation

$$\nabla^2\phi = -4\pi(N_p - N_e) \tag{I.9}$$

If the proton distribution is uniform, this yields a shielded coulomb potential

$$\phi(r) = \frac{q}{r}\, e^{-k_D r} \tag{I.10}$$

$$k_D^2 = \ell_D^{-2} = (4\pi N_e e^2/\kappa T) \tag{I.11}$$

The shielding length ℓ_D is called the Debye length and k_D is the Debye wave number. Since the true potential rapidly decreases for $r > \ell_D$, the total cross-section is finite and a mean free path for two-body collisions in a plasma can be defined. The actual evaluation for the shielded potential is rather complex but the final result is clearly related to the original Rutherford scattering expression; the effective total cross-section computed by Spitzer is

$$\sigma_{eff} \simeq 22.8\pi \left(\frac{r_{min}}{4}\right)^2 \ell n\, \Lambda \qquad \text{(I.12)}$$

$$\Lambda = (2\ell_D / r_{min})$$

For electron-proton scattering of thermal particles $(1/2\ m_e v^2 \simeq (3/2)\kappa T_e/\Delta)$, the mean free path is thus

$$\ell = 1.8 \times 10^5 T^2 / N\, \ell n\, \Lambda \quad \text{(cm)} \qquad \text{(I.13)}$$

$$\Lambda = 1.25 \times 10^4 T^{3/2} / N^{1/2}$$

where T is expressed in degrees Kelvin and N in particles per cubic centimeter. The expression for ℓ is essentially independent of particle mass, and the quantity $\ell n\, \Lambda$ varies little for the temperature and density range of interest; we find $15 < \ell n\, \Lambda < 35$ in these regions but it is sufficiently accurate to treat $\ell n\, \Lambda$ as a constant, say $\ell n\, \Lambda = 25$.

Effects of two-particle collisions will govern the plasma behavior if ℓ is small compared to some scale length (L) for the system (in the language of aerodynamics, the Knudson number $K = \ell/L$ is small). In the regions where the barometric relation holds (the ionosphere, the corona) a reasonable definition of the scale length involves the rate of change of density with altitude. The scale height, H, is defined by

$$H(r) = |N/(dN/dr)| \simeq \frac{\kappa T(r)}{M(r) g(r)} \qquad \text{(I.14)}$$

where g is the local acceleration due to gravity (terrestrial or solar) and M is the local mean mass. In the magnetosphere the scale height defined by the density variation is on the order of an earth radius, and in the solar wind, a similar definition gives $H \sim 1$ AU (assuming constant speed so that $N(r) \sim r^{-2}$). The concept of scale height for the transition region is rather obscure, but the scale length, L, is on the order of $4R_e$, the thickness of the transition region.

In Table I.1, we have collected rough estimates of N, T, L for all the regions discussed thus far, and evaluated ℓ in each case. It can be seen immediately that two-body coulomb collisions can be neglected in the outer magnetosphere, transition region and solar wind. In the inner magnetosphere and upper ionosphere, close collisions may have some significance in determining the distribution of low energy particles $(mu^2 \leq 3\kappa T)$, but it should be noted that the mean free path for superthermal particles is considerably larger than the value tabulated. The deduction of $\ell(T,N)$ shows that a particle with speed v will have a mean free path given by

$$\ell(v) \simeq \left(\frac{v}{a}\right)^4 \ell(a) \qquad (I.15)$$

where a is the mean thermal speed, $ma^2 = 3\kappa T$. Thus, the upper ionosphere and magnetosphere should be regarded as essentially collisionless for particles with energies greater than, for example, a few hundred electron volts.

The characteristics of the solar corona are clearly governed by two-body collisions and in this case we may be confident that the plasma is near equilibrium. That is, we anticipate that in some frame of reference the particles can generally be described by an isotropic velocity distribution which is nearly Maxwellian, that a temperature can be defined, and that all species have approximately the same temperature. It appears likely from Table I.1 that the upper ionosphere plasma is in near equilibrium, as defined in this manner. [Note that we do not preclude the transient occurrence of localized non-equilibrium phenomena such as solar flares, aurora, etc.] However, the plasma in the magnetosphere, transition region and solar wind cannot be regarded as being in equilibrium in the same sense. Although individual particles are scattered, accelerated, etc. in these regions, the interaction mechanism is much more complex. Instead of particle-particle scattering, we must investigate here how an individual particle can

TABLE I.1

Region	Density (cm^{-3})	Temperature (°K)	ℓ (cm)	L (cm)
Upper Ionosphere ($h \gtrsim 1000$ km)	5×10^3	2×10^3	6×10^6	$\sim 6 \times 10^7$
Inner Magnetosphere ($r \sim 3R_e$)	500	8×10^3	9×10^8	$\sim 6.4 \times 10^8$
Outer Magnetosphere ($r \sim 8R_e$)	30	5×10^4 (?)	6×10^{11}	$\sim 6.4 \times 10^8$
Transition Region (subsolar)	10 (?)	$5 \times 10^5 - 10^6$ (protons) $10^6 - 3 \times 10^8$ (electrons)	1.8×10^{14} (minimum value)	$\sim 2.5 \times 10^9$
Solar Wind at 1 AU	2	2×10^5	1.4×10^{14}	$\sim 1.5 \times 10^{13}$
Coronal Base	2×10^8	1.5×10^6	8.2×10^7	$\sim 1.5 \times 10^{10}$

interact with an organized group of particles, or a wave.

I.5. General Remarks

Before proceeding with the detailed discussion of the properties of the corona, solar wind, magnetosphere and transition region, it seems advisable to introduce a few cautionary remarks. Space physics, and especially spacecraft physics, is a very young science, and our experimental capabilities in this field are still quite limited. A spacecraft travels on an isolated trajectory in space-time and limited telemetry is available to send back data. Related measurements are generally not made at the same time, on-board correlation techniques are rarely used, and various aliasing difficulties are frequently encountered. Unknown or uncontrollable biases may be present, and sources of contamination involving spacecraft magnetic fields, the plasma sheath surrounding the spacecraft, external noise interference, photoelectron currents, etc., have degraded many experimental programs. Furthermore it is not generally possible to achieve comparable sensitivities for related measurements, such as electron and photon fluxes at the same energy, electric and magnetic intensities at the same frequency. Finally, it must be remembered that any single instrument has a given range and sensitivity — many discoveries of sharp "boundaries" probably represent threshold response for that instrument, and one may anticipate that other detectors will find completely different boundaries.

These problems are serious and it is a mistake to think of space physics as a field in which much certain knowledge has been collected so that we are completely ready for straightforward theoretical analysis. Instead, we should regard these lectures as a series of talks in which tentative theories and explanations are assessed on the basis of incomplete or preliminary measurements.

Chapter I. GENERAL REFERENCES

Space Physics, A. Rosen and D. P. Le Galley, eds., J. Wiley, New York, 1964.

C. de Jager, Structure and Dynamics of the Solar Atmosphere, Handbuch der Physik, Vol. LII, Springer, Berlin, 1959.

E. N. Parker, Interplanetary Dynamical Processes, Interscience, New York, 1963.

Physics of the Upper Atmosphere, J. A. Radcliffe, ed., Academic Press, New York, 1960.

J. W. Chamberlain, Physics of the Aurora and Airglow, Academic Press, New York, 1961.

L. Spitzer, Physics of Fully Ionized Gases, 2nd ed., Interscience, New York, 1962.

II. CONTINUUM PLASMA DYNAMICS

In a region where the Knudsen number is small, the state of the plasma is governed by the effects of collisions, and a statistical description of the ionized gas is appropriate. The basic simplifying assumptions are that all particles of a given type (electrons, for example) are identical and that cooperative effects (many particle correlations) are unimportant with the exception of short-range two-particle collisions. In this case it is possible to describe all particles of one type by a single particle distribution function, $f(\vec{r},\vec{v},t)$, where $f(\vec{r},\vec{v},t)d^3rd^3v$ is defined as the number of particles in d^3r , centered at $\vec{r}$, with velocities within the interval d^3v , centered at $\vec{v}$. The distribution function obeys a differential equation, the Boltzmann equation, and all information about the gas is contained in f .

II.1. Kinetic Theory of a Neutral Gas

For simplicity, let us begin this study of the distribution function by considering a neutral gas of identical particles. The necessary manipulations can be performed more easily for this case, and the appropriate modifications for a gas of electrons and protons will be discussed in the next section.

The classical treatise on continuum dynamics is The Mathematical Theory of Non-Uniform Gases by Chapman and Cowling, and all of the extremely complex mathematical development is carefully discussed there. We shall be content with a more modest mathematical program, supplemented by physical reasoning.

First, consider the dynamical equation for the distribution function. If there were no collisions, each particle would move freely along its trajectory under the influence of an external force, $\vec{F}$; the total rate of change of the distribution function would vanish (Liouville's theorem) and the system would obey

$$\frac{Df}{Dt} = \frac{\partial f}{\partial t} + \vec{v} \cdot \nabla f + \frac{\vec{F}}{m} \cdot \vec{\nabla}_v f = 0 \qquad \text{(II.1)}$$

where the second term expresses the influence of diffusion and the third accounts for the actions of the applied forces. The Boltzmann equation states that when the mean free path is small but finite, Df/Dt is entirely the result of encounters among the particles, and (II.1) becomes

$$\frac{\partial f}{\partial t} + \vec{v} \cdot \vec{\nabla} f + \frac{\vec{F}}{m} \cdot \vec{\nabla}_v f = \left(\frac{\partial f}{\partial t}\right)_{coll} . \qquad \text{(II.2)}$$

Although we shall not evaluate the collision term in any detail, it is useful to write down the general expression. For binary or two-body collisions, four states are involved; if f , f_1 represent the fraction of particles having velocities $\vec{v}$, $\vec{v}_1$ before a collision, and f' , f_1' are the analogous distributions after the collision, then the standard form for $(\partial f/\partial t)_{coll}$ is

$$\left(\frac{\partial f}{\partial t}\right)_{coll} = \int d^3 v_1 \int P(|\vec{v} - \vec{v}_1|, \theta) d\Omega [f' f_1' - f f_1] \qquad \text{(II.3)}$$

where P is the probability that a pair with relative speed $|\vec{v} - \vec{v}_1|$ will be scattered into $d\Omega$ at an angle θ . There are several points of interest to be noted here. First, since the scattering probability is proportional to the differential cross-section, $(\partial f/\partial t)_{coll}$ is essentially proportional to the total cross-section or inversely proportional to the mean free path.

A second aspect of Eq. (II.3) has to do with its relation to the equilibrium distribution for a homogeneous, force-free gas in the steady state. Here $(\partial f/\partial t)_{coll}$ must obviously vanish, yet for ordinary conservative collisions, energy relations such as

$$\frac{mv^2}{2} + \frac{mv_1^2}{2} = \frac{mv'^2}{2} + \frac{mv_1'^2}{2} \qquad \text{(II.4)}$$

have to be satisfied. It can be seen that energy and momentum will be conserved if the equilibrium distribution function is of the Maxwell form,

$$f_0(\vec{v}) = a \exp\left[- b(\vec{v} - \vec{u})^2\right] \qquad \text{(II.5)}$$

where a , b are constants and $\vec{u}$ is a constant vector. We define temperature by $b = (m/2\kappa T)$, (κ is Boltzmann's constant, 1.38×10^{-16} ergs/°K) and f_0 must be normalized so that

$$n = \int d^3v \, f_0(v) \qquad \text{(II.6)}$$

is the density. This requires $a = n(m/2\pi\kappa T)^{3/2}$ and it may be verified that $\vec{u}$ is the average velocity, defined by

$$n\vec{u} = \int d^3v \, \vec{v} \, f_0(\vec{v}) \qquad \text{(II.7)}$$

For the more general case in which f is a function of $\vec{r}$, $\vec{v}$ and t , similar moments of the distribution function can be defined, and the Boltzmann equation leads to a set of moment equations. Let

$$n < A > = \int d^3v \, A(\vec{v}) f(\vec{r},\vec{v},t) \quad . \qquad \text{(II.8)}$$

Since $A = A(\vec{v})$, it is clear that

$$\frac{\partial}{\partial t} (n < A >) = \int d^3v \, A(\vec{v}) \frac{\partial f}{\partial t} \qquad \text{(II.9)}$$

$$\frac{\partial}{\partial x_i} (n < v_i A >) = \int d^3v \, A(\vec{v}) \, (\vec{v} \cdot \vec{\nabla}) \, f \qquad \text{(II.10)}$$

(the summation convention is used for repeated indices), and if $\vec{\nabla}_v \cdot \vec{F} = 0$, a partial integration leads to

$$- n < \vec{\nabla}_v \cdot (\vec{F}A) > = \int d^3v \, A(\vec{v}) \, \vec{F} \cdot \vec{\nabla}_v f \qquad \text{(II.11)}$$

[The condition $\vec{\nabla}_v \cdot \vec{F} = 0$ is not satisfied for arbitrary velocity dependent forces, but $\vec{\nabla}_v \cdot \vec{F}$ does vanish if the velocity dependent term is of the form $(\vec{v} \times \vec{B})$.]

Now let us multiply the Boltzmann equation by $A(\vec{v})$, integrate over d^3v , and examine the result,

$$\frac{\partial}{\partial t} n < A > + \vec{\nabla}\cdot(n < \vec{v}A >) - \frac{n}{m} < \vec{\nabla}_v \cdot (\vec{F}A) > = \int d^3v \; A(\vec{v}) \left(\frac{\partial f}{\partial t}\right)_{coll} \quad . \tag{II.12}$$

Consider $A = 1$ in Eq. (II.12) . Since collisions do not change the number of particles, the right hand side vanishes and we obtain the equation of continuity

$$\frac{\partial n}{\partial t} + \vec{\nabla}\cdot(n\vec{u}) = 0 \quad , \tag{II.13}$$

with

$$< \vec{v} > = \vec{u}(\vec{r},t) \quad .$$

For $A = m\vec{v}$ in Eq. (II.12) (more precisely, A is in turn each one of the components mv_i) , the collision term again has no effect because momentum is conserved upon collision and we have

$$\frac{\partial}{\partial t} (nm\vec{u})_i + m\nabla \cdot n < \vec{v}v_i > - n(\vec{F})_i = 0 \tag{II.14}$$

This can be put into another form if $\vec{v}$, the velocity of a particle, is decomposed into $(\vec{u} + \vec{c})$, where $\vec{u}$ is the mean velocity of flow and $\vec{c}$ is the random or thermal velocity in the rest frame. Then

$$\frac{\partial}{\partial t} (nmu_i) + m\vec{\nabla}\cdot(n\vec{u}u_i) + \frac{\partial P_{ij}}{\partial x^j} - nF_i = 0 \tag{II.15}$$

with

$$P_{ij} = m \int c_i c_j f d^3v \tag{II.16}$$

Since the pressure, $n\kappa T$, is given by $(1/3)(P_{xx} + P_{yy} + P_{zz})$, a separate tensor, the stress tensor, is frequently defined by $p_{ij} = p\delta_{ij} - P_{ij}$, with $\delta_{ij} = 1 \quad (i=j) \quad \text{or} \quad 0 \quad (i \neq j)$.

The final moment equation is obtained when A is set equal to $mv^2/2$; again, since collisions conserve energy, the effect of this term does not appear explicitly, and we find

$$\frac{3}{2}\frac{\partial p}{\partial t} + \frac{3}{2}\frac{\partial (p u_i)}{\partial x_i} + \frac{\partial q_i}{\partial x_i} + P_{ij}\frac{\partial u_i}{\partial x_j} = 0 \qquad \text{(II.17)}$$

with

$$\vec{q} - \frac{m}{2}\int d^3v\, \vec{c}\, c^2 f \qquad \text{(II.18)}$$

[The algebraic manipulations which lead to the energy equation are straightforward but lengthy and we omit the detailed derivation here.]

The system of equations (II.13, 15, 17) describes the state of the gas under the action of the applied force, $\vec{F}$, but it should be clear that the system is not complete. We have five equations and 13 unknowns (n, u_1, q_1, $P_{ij} = P_{ji}$, $i,j = 1-3$; P is contained in P_{ij} and $\kappa T = p/n$). In order to complete this set, it is necessary to go back to the full Boltzmann equation so that collisions can be accounted for in an explicit manner.

We first observe that if the distribution function is given by a modified form of Eq. (II.5),

$$f_0(\vec{r},\vec{v},t) = n(\vec{r},t)(m/2\pi\kappa T(\vec{r},t))^{3/2} \exp\left[-m(\vec{v}-\vec{u}(\vec{r},t))^2/2\kappa T(r,t)\right] \qquad \text{(II.19)}$$

then $\vec{q}$ is zero and P_{ij} is simply $p\delta_{ij}$. This occurs because f_0 is an even function of c_x, c_y, or c_z, while $\vec{q}$ and p_{xy}, etc., are odd so that the integrals over d^3v or d^3c vanish. The resulting Euler equations are closed because only five variables (n, p, $\vec{u}$) appear; however $f_0(\vec{r},\vec{v},t)$ does not satisfy the full Boltzmann equation with collisions. Clearly, $\vec{q}$ and p_{ij} involve energy and momentum transfer by collisions.

Various techniques have been devised to evaluate $\vec{q}$ and p_{ij}, and these generally involve the substitution of some perturbed equilibrium distribution

$$f(\vec{r},\vec{v},t) = f_0(\vec{r},\vec{v},t)[1 + \phi(\vec{r},\vec{v},t)]$$

into the Boltzmann equation. Specific complex forms for ϕ lead to

lengthy nonlinear relations between the unknown moments, derivatives of the simpler ones and integrals involving collision cross-sections. However, if all scale lengths in the gas are sufficiently large, a much simpler technique, roughly equivalent to expanding f in a power series in ℓ/L, is applicable. This Chapman-Enskog method yields

$$\vec{q} = - k(T) \vec{\nabla} T \tag{II.20}$$

and $k(T)$ is identified as the coefficient of thermal conductivity. To see this, we note that $q_i = (1/2)Nm < c^2 c_i >$ and hence q is proportional to $N\kappa T(\kappa T/m)^{1/2}$, but q should also be proportional to the Knudsen number ℓ/L. Since $T \sim L|\vec{\nabla} T|$, a possible (and fairly accurate) expression for k is thus

$$k \sim N\left(\frac{\kappa T}{m}\right)^{1/2} \kappa \ell \tag{II.21}$$

$$\sim \frac{\kappa}{\sigma}\left(\frac{\kappa T}{m}\right)^{1/2}$$

The total cross-section, σ, depends only on temperature, and therefore k has the same dependence.

A similar development leads to the identification of p_{ij} with the viscous stress tensor. The strain is defined by

$$\tau_{ij} = \frac{\partial u_i}{\partial x_j} + \frac{\partial u_j}{\partial x_i} - \frac{2}{3}\delta_{ij}(\vec{\nabla}\cdot\vec{u}) \tag{II.22}$$

and the coefficient of viscosity, μ, relates stress and strain by

$$p_{ij} = \mu \tau_{ij} \tag{II.23}$$

The two transport coefficients are not independent and the ratio $\kappa\mu/mk$ is generally a constant (called the Prandtl number). The closed set of equations (II.13, 15, 17, 19, 23) are known as the Navier-Stokes equations.

II.2. The Equations of Magnetohydrodynamics

When the gas is composed of fully ionized hydrogen, a development similar to that of Section II.1 yields the equations of motion. However, several complications can be anticipated because the two species have different electric charges and different masses. Just as in the neutral case, momentum and energy are conserved when electrons collide with electrons, or protons collide with protons, but electron-proton collisions can transfer energy from one gas to another. Furthermore, electrons and protons respond in different ways to electric and magnetic fields so that charge and current densities will enter the equations of motion. These quantities must, of course, be related to the ambient electric and magnetic fields by Maxwell's equations.

We assume that a separate distribution function can be defined for each species and consider the moments of the two Boltzmann equations. It is clear that the continuity equations are unchanged, so that

$$\frac{\partial n_e}{\partial t} + \vec{\nabla}\cdot(n_e\vec{u}_e) = 0$$

$$\frac{\partial n_i}{\partial t} + \vec{\nabla}\cdot(n_i\vec{u}_i) = 0 \qquad \text{(II.24)}$$

These can be rewritten in terms of the mass density $\rho = n_e m_e + n_i m_i = (n_e + n_i)m$, the charge density $\rho_e = n_e q_e + n_i q_i$, the mean velocity vector $\rho\vec{u} = n_e m_e \vec{u}_e + n_i m_i \vec{u}_i$ and the current density $\vec{j} = n_e q_e \vec{u}_e + n_i q_i \vec{u}_i$, and (II.24) becomes

$$\frac{\partial \rho}{\partial t} + \vec{\nabla}\cdot(\rho\vec{u}) = 0$$

$$\frac{\partial \rho_e}{\partial t} + \vec{\nabla}\cdot\vec{j} = 0 \qquad \text{(II.25)}$$

The two equations for conservation of momentum can now be written

$$n_e m_e\left(\frac{\partial}{\partial t} + \vec{u}_e\cdot\vec{\nabla}\right)\vec{u}_e = n_e q_e\left(\vec{E} + \frac{\vec{u}_e \times \vec{B}}{c}\right) - n\, m\, \nabla\phi - \vec{\nabla}\cdot\vec{\vec{P}}_e + \vec{C}_{ei} \qquad \text{(II.26)}$$

$$n_i m_i\left(\frac{\partial}{\partial t} + \vec{u}_i\cdot\vec{\nabla}\right)\vec{u}_i = n_i q_i\left(\vec{E} + \frac{\vec{u}_i \times \vec{B}}{c}\right) - n_i m_i \nabla\phi - \vec{\nabla}\cdot\vec{\mathbf{P}}_i + \vec{C}_{ie} \tag{II.26}$$

Here it has been assumed that the external force may be decomposed into a Lorentz force and a force derived from a potential, $(\vec{\nabla}\cdot\vec{\mathbf{P}})_i$ is $\partial P_{ij}/\partial x_j$, $\vec{C}_{ei}$ represents the momentum per unit volume transferred to the electrons by the ions, etc. If the system is isolated, the overall momentum must be conserved, and therefore $\vec{C}_{ei} = -\vec{C}_{ie}$.

The momentum conservation equations analagous to (II.25) are obtained by adding (II.26), multiplied by unity or $q_{e,i}$. However, the nonlinear $nm(\vec{u}\cdot\vec{\nabla})\vec{u}$ terms preclude an exact reduction to a simple system involving the new variables ρ, $\vec{u}$, ρ_e, $\vec{j}$. Instead, it is customary to use the fact that $m_e/m_i \ll 1$ to obtain an approximate reduction. If the space charge and current densities are sufficiently small [$|n_e - n_i| \ll n_i$, $|\vec{u}_e - \vec{u}_i| \ll |\vec{u}_i|$], then

$$n_e m_e \vec{u}_e\cdot\vec{\nabla}\vec{u}_e + n_e m_i \vec{u}_i\cdot\vec{\nabla}\vec{u}_i \simeq \rho(\vec{u}\cdot\vec{\nabla})\vec{u}_i \quad , \tag{II.27}$$

$$\simeq \rho(\vec{u}\cdot\vec{\nabla})\vec{u} \quad ,$$

and (II.26) yields

$$\rho\frac{\partial\vec{u}}{\partial t} + \rho(\vec{u}\cdot\vec{\nabla})\vec{u} = \rho_e\vec{E} + \frac{\vec{j}\times\vec{B}}{c} - \rho\vec{\nabla}\phi - \vec{\nabla}\cdot\vec{\mathbf{P}} \tag{II.28}$$

with $\vec{\mathbf{P}} = (\vec{\mathbf{P}}_e + \vec{\mathbf{P}}_i)$. The corresponding equation for $\partial\vec{j}/\partial t$ is even more complex. If terms of order m_e/m_i, $|\vec{u}_e - \vec{u}_i|/|\vec{u}_i|$ and $|n_e - n_i|/n_e$ are neglected, Eq. (II.26) leads to

$$\frac{m_e}{n_e q_e^2}\frac{\partial\vec{j}}{\partial t} = \vec{E} + \frac{\vec{u}\times\vec{B}}{c} + \frac{\vec{j}\times\vec{B}}{n_e q_e c} - \frac{1}{n_e q_e}\vec{\nabla}\cdot\vec{\mathbf{P}} + \frac{\vec{C}_{ei}}{n_e q_e} \tag{II.29}$$

The physical significance of (II.29) can be seen by considering the stationary response of a plasma to an electric field only. If there are no stresses, (II.29) yields $\vec{E} = -\vec{C}_{ei}/n_e q_e = \vec{C}_{ei}/n_e e$, but the collision-dominated plasma should obey Ohm's law. We therefore set

$\vec{C}_{ei} = \overleftrightarrow{\eta}\, n_e e\vec{j}$, where $\overleftrightarrow{\eta}$ is the resistivity, which is generally a tensor. With this replacement, Eq. (II.29) may be regarded as a form of Ohm's law for a magnetized, non-stationary plasma with finite stresses. This definition of resistivity merely assumes that the momentum exchanged between electrons and ions is proportional to their relative velocity, or current. A rough estimate of η can be obtained from the force equation

$$\left\langle \frac{\partial j}{\partial t} \right\rangle \sim \frac{j}{t_{coll}} \sim \frac{ne^2 E}{m}$$

and since $\ell \simeq (\kappa T/m)^{1/2} t_{coll}$ for thermal particles,

$$\eta \simeq m(\kappa T/m)^{1/2}/Ne^2\ell \qquad \text{(II.30)}$$

$$\simeq m\sigma \left(\frac{\kappa T}{m}\right)^{1/2}$$

The energy equation is not seriously modified by the fact that two species of charged particles are present. If the total heat flux vector is defined as $\vec{q} = \vec{q}_e + \vec{q}_i$, the generalization of (II.17) is simply

$$\frac{3}{2}\frac{\partial p}{\partial t} + \frac{3}{2}\frac{\partial (pu_i)}{\partial x_i} + \frac{\partial q_i}{\partial x_i} + P_{ij}\frac{\partial u_i}{\partial x_j} - j_i E_i = 0 \qquad \text{(II.31)}$$

Aside from numerical factors, the rough expressions for η , k and μ are fairly accurate. The resistivity varies as $\ell n\, \Lambda/T^{3/2}$, k and η both vary as $T^{5/2}\, \ell n\, \Lambda$, as indicated by Eqs. (II.21), (II.30) and the expression for ℓ discussed in the first chapter. For hydrogen, the precise expressions taken from Physics of Fully Ionized Gases, by Spitzer, are

$$k = 1.9\left(\frac{2}{\pi}\right)^{3/2} \frac{(\kappa T)^{5/2}\kappa}{e^4 m_e^{1/2} \ell n\, \Lambda} \qquad \text{(II.32)}$$

$$\simeq 7.2 \times 10^{-7} T^{5/2} \quad \text{ergs/cm sec °K}$$

$$\mu = \frac{0.406\, m_i^{1/2} (\kappa T)^{5/2}}{e^4 \ell n\, \Lambda} \qquad \text{(II.33)}$$

$$\simeq 0.9 \times 10^{-16} T^{5/2} \quad \text{gm/cm sec}$$

$$\eta = \frac{\pi^{3/2} m_e^{1/2} e^4 \ell n \Lambda}{1.16(2\kappa T)^{3/2}} \qquad \text{(II.34)}$$

$$\simeq 1.6 \times 10^5 \, T^{-3/2} \quad \text{ohm cm}$$

[All numerical values are computed for $\ell n \Lambda = 25$; because some ambiguity exists in treating the shielded coulomb potential, other treatments lead to values for η , μ , k which may differ by as much as $25 - 30\%$ from these.] It should be noted that electrical and thermal conduction is associated with the electron gas, while viscous dissipation primarily involves the ions. In very strong magnetic fields ($eBt_{coll} \geq m_i c$) all of these transport coefficients become tensors. The values for $\eta_{\parallel}$, $k_{\parallel}$, $\mu_{\parallel}$ (parallel to B) are unchanged, but $k_{\perp}$, $\mu_{\perp}$ are drastically reduced while $\eta_{\perp}$ is increased.

To complete our statement of the kinetic equations for the plasma, the Maxwell equations must be specified. In our system of units these are

$$\vec{\nabla}\cdot\vec{E} = 4\pi\rho_e \quad , \qquad \vec{\nabla}\cdot\vec{B} = 0$$

$$\vec{\nabla}\times\vec{E} = -\frac{1}{c}\frac{\partial\vec{B}}{\partial t} \quad , \quad \vec{\nabla}\times\vec{B} = \frac{4\pi\vec{j}}{c} + \frac{1}{c}\frac{\partial\vec{E}}{\partial t} \qquad \text{(II.35)}$$

Generally, no distinction is made in plasma physics between $\vec{H}$ and $\vec{B}$, etc. Instead, all currents and charge densities are explicitly included in $\vec{j}$ and ρ_e .

II.3. General Properties of MHD Equations

The complete set of equations developed to describe the dynamics of a conducting fluid is obviously extremely complex, and it is unlikely that all consequences of these equations are completely understood at present. However, certain approximations were made in deriving (II.28), and we must discuss the self-consistency of the assumptions that the plasma locally remains almost neutral and that the currents are not large.

The validity of the assumption of quasi-neutrality can best be assessed by examining the response of the electrons only to an initial density perturbation. If the effect of collisions can be neglected and if $\vec{B}$, $\vec{\nabla}\phi$, and $\vec{\nabla}\cdot\vec{\vec{P}}$ vanish, then Eq. (II.26) gives

$$n_e m_e \frac{\partial u_e}{\partial t} + n_e m_e (\vec{u}_e \cdot \vec{\nabla})\vec{u}_e = - n_e e \vec{E} \qquad \text{(II.36)}$$

and we must also have

$$\frac{\partial n_e}{\partial t} + \vec{\nabla}\cdot(n_e \vec{u}_e) = 0$$

$$\vec{\nabla}\cdot\vec{E} = 4\pi e(n_i - n_e) \qquad \text{(II.37)}$$

For $n(\vec{r},t) = N_e + n'(\vec{r},t) + \ldots$, these yield

$$\frac{\partial n'}{\partial t} + N_e \nabla\cdot u_e = 0$$

$$\vec{\nabla}\cdot\vec{E} = - 4\pi e n' \qquad \text{(II.38)}$$

$$\frac{\partial u_e}{\partial t} = - \frac{eE}{m_e} + \ldots$$

where terms with u_e^2 have been discarded since the perturbations are assumed to be small. Thus

$$\frac{\partial^2 n'}{\partial t^2} = - N_e \frac{\vec{\nabla}\cdot\partial\vec{u}_e}{\partial t}$$

$$= \frac{N_e e}{m_e} \vec{\nabla}\cdot\vec{E} \qquad (II.39)$$

$$= \frac{- 4\pi N_e e^2}{m_e} n'$$

and the electrons oscillate with $n' = n'_0 \sin \omega_p t$, so that the time average density perturbation vanishes. The plasma frequency, $f_p = \omega_p/2\pi \simeq 9 \times 10^3 N_e^{1/2}$, is generally very high and therefore these electron plasma oscillations are important even in the presence of collisions, for $f_p t_{coll} \gg 1$. Thus, a microscopic property of the plasma, the occurence of high frequency electrostatic waves with little damping, can be used to justify the assumption that $\rho_e \ll e\rho$.

Perhaps the most general basic statement about the restriction to moderate currents has to do with the fact that quasi-neutrality (i.e., $n_e \simeq n_i$) requires $\vec{u}_e$ and $\vec{u}_i$ to obey exactly the same continuity equation, so that large deviations which violate the restriction

$$\vec{\nabla}\cdot[n(\vec{u}_e - \vec{u}_i)] \simeq 0 \qquad (II.40)$$

are excluded. This restriction, however, is an extremely weak one. In practice, the arguments concerning the treatment of Ohm's law are based on the numerical size of the resistivity, η .

Consider the simple $(\vec{B} = 0)$ form of Ohm's law, $\eta\vec{j} \simeq \vec{E}$. Since

$$\frac{\partial \rho_e}{\partial t} = - \vec{\nabla}\cdot\vec{j} \simeq - \frac{1}{\eta} \vec{\nabla}\cdot\vec{E} \simeq - \frac{4\pi}{\eta} \rho_e \quad , \qquad (II.41)$$

space charge and electric fields will decay as $\exp(-4\pi t/\eta)$. For typical temperatures the resistivity is small ($T = 10^6$°K gives $\eta = 1.6 \times 10^{-4}$ ohm cm versus $\eta \simeq 2 \times 10^{-6}$ for a good conductor such as copper) and E vanishes rapidly. The decay rate for a magnetic field is quite different. If the displacement current is neglected, Ampere's law leads to

$$\vec{\nabla} \times (\vec{\nabla} \times \vec{B}) = - \nabla^2 \vec{B} = \frac{4\pi}{\eta c} \vec{\nabla} \times \vec{E}$$

$$= - \frac{4\pi}{\eta c^2} \frac{\partial B}{\partial t} \qquad \text{(II.42)}$$

This is a diffusion equation and B goes as $\exp(- \eta c^2 t/4\pi L^2)$ where L is the scale length for the system $(L^2 \nabla^2 B \simeq B)$. The slow decay or diffusion of the magnetic field illustrates the basic principle of the conventional mhd approximation; the plasma is assumed to be perfectly conducting, permanent electric fields are neglected, and magnetic decay is not treated.

More explicitly, the customary mhd idealization $\eta \to 0$, j finite, requires $\vec{E} + \vec{u} \times \vec{B}/c = 0$, and if displacement current can be neglected, Ampere's law, $\vec{\nabla} \times \vec{B} = 4\pi \vec{j}/c$, allows one to eliminate $\vec{j}$ from the momentum equation. This proceeds as follows

$$\frac{\vec{j} \times \vec{B}}{c} = \frac{(\vec{\nabla} \times \vec{B}) \times \vec{B}}{4\pi} = \frac{(\vec{B} \cdot \vec{\nabla})\vec{B}}{4\pi} - \frac{\vec{\nabla} B^2}{8\pi} \qquad \text{(II.43)}$$

so that E and j no longer appear in the equations of mhd.

$$\frac{\partial \rho}{\partial t} + \nabla \cdot (\rho \vec{u}) = 0$$

$$\frac{\rho \partial \vec{u}}{\partial t} + \rho(\vec{u} \cdot \vec{\nabla})u + \vec{\nabla} p + \rho \vec{\nabla} \phi - \vec{\nabla} \cdot (\mu \vec{\tau}) = \frac{- \vec{\nabla} B^2}{8\pi} + \frac{(\vec{B} \cdot \vec{\nabla})\vec{B}}{4\pi}$$

$$\frac{3}{2} \frac{\partial p}{\partial t} + \frac{3}{2} \frac{\partial p u_i}{\partial x_i} - \frac{\partial}{\partial x_i} k \frac{\partial T}{\partial x_i} + p \frac{\partial u_i}{\partial x_i} - \mu \tau_{ij} \frac{\partial u_i}{\partial x_j} = 0 \qquad \text{(II.44)}$$

$$\vec{\nabla} \times (\vec{u} \times \vec{B}) = \frac{\partial \vec{B}}{\partial t} \quad , \qquad \nabla \cdot B = 0$$

The last of these is Faraday's law with $\vec{E} = - \vec{u} \times \vec{B}/c$, and η has been set equal to zero in the energy equation. These equations have some interesting consequences. Faraday's law now resembles a type of continuity equation, and its significance can be understood only by examining the rate at which magnetic flux, Φ , changes with time. Since the surface of interest will move with the fluid, we have

$$\begin{aligned}\frac{d\Phi}{dt} &= \frac{d}{dt}\int \vec{B}\cdot d\vec{s} \\ &= \int \frac{\partial \vec{B}}{\partial t}\cdot d\vec{s} + \oint \vec{B}\cdot\vec{u}\times d\vec{\ell} \\ &= \int \frac{\partial \vec{B}}{\partial t}\cdot d\vec{s} - \oint (\vec{u}\times\vec{B})\cdot d\vec{\ell} \\ &= \int \left[\frac{\partial \vec{B}}{\partial t} - \vec{\nabla}\times(\vec{u}\times\vec{B})\right]\cdot d\vec{s} = 0\end{aligned} \tag{II.45}$$

and the total flux through any surface is constant. As in superconductivity analysis, this is interpreted as "frozen-in" flux which is carried by the moving medium.

Another relation of interest may be obtained from the momentum equation. Consider $u = \phi = 0$, with $\vec{B}$ of the form $\vec{B} = B(x)\vec{i}_z$, for instance. Then the last term vanishes, and the equation can be integrated to yield

$$p + \frac{B^2}{8\pi} = \text{constant} \tag{II.46}$$

This useful conservation equation illustrates the general diamagnetic behavior of a perfectly conducting fluid. If non-magnetic plasma exists in a region of space bounded by a plasma-free magnetic field, the plasma is, in principle, confined by the fields with p (region I) $= B^2/8\pi$ (region II). Also, if a magnetic field is embedded in a plasma, any attempt to increase the field will lead to a decrease in pressure, and hence in density.

The customary mhd idealization, $\eta \to 0$, clearly leads to a simpler set of equations from which convenient generalities (frozen-in flux, diagmagnetic properties, $\vec{E} = -\vec{u}\times\vec{B}/c$, etc.) can be extracted. It is dangerous, however, to go too far in interpreting these phenomena. For instance, it is convenient to eliminate any permanent long-range electric field using $\vec{E} + \vec{u}\times\vec{B}/c = 0$, but it is frequently much more instructive to retain $\vec{E}$. As an example, let us demonstrate the existence in the plasma of a new mode of wave propagation, the Alfvén mode. This is a transverse wave which can only

appear in a magnetized plasma (transverse waves cannot propagate in ordinary fluids). Consider a static magnetic field $\vec{B} = B\vec{i}_x$. To a first approximation (u^2 negligible, $\nabla p = \nabla \phi = \mu = 0$) , the momentum equation yields

$$\rho \frac{\partial u_y}{\partial t} = \frac{j_z B}{c} \tag{II.47}$$

and $E_z(r,t) = u_y(r,t)B/c$. Maxwell's equations also give

$$\begin{aligned} \nabla \times (\nabla \times E) &= 4\pi \nabla \rho_e - \nabla^2 E \\ &= -\frac{1}{c} \nabla \times \frac{\partial B}{\partial t} \\ &= -\frac{4\pi}{c^2} \frac{\partial \vec{j}}{\partial t} - \frac{1}{c^2} \frac{\partial^2 E}{\partial t^2} \end{aligned} \tag{II.48}$$

But $\partial j/\partial t = c(\rho/B)(\partial^2 u/\partial t^2) = (c^2\rho/B^2)(\partial^2 E/\partial t^2)$, and we finally obtain

$$\begin{aligned} \nabla^2 \vec{E} &= -4\pi \vec{\nabla} \rho_e + \left(\frac{1}{c^2} + \frac{4\pi\rho}{B^2}\right) \frac{\partial^2 \vec{E}}{\partial t^2} \\ &\simeq \frac{4\pi\rho}{B^2} \frac{\partial^2 \vec{E}}{\partial t^2} \quad , \qquad n_e \simeq n_i \end{aligned} \tag{II.49}$$

This describes propagation with the Alfvén phase velocity

$$\frac{\omega}{k} = V_A = \frac{B}{(4\pi\rho)^{1/2}} \tag{II.50}$$

and although the same result can be derived using (II.44), it seems more complete to include the actual finite electric field. An Alfvén wave involves a velocity disturbance with a related electric field vector, and they oscillate in phase with $\vec{E} = -(\vec{u} \times \vec{B})/c$, where B is static.

There are other reasons for believing that the mhd equations frequently suppress too many physical quantities. First, consider the plasma oscillations discussed at the beginning of this section. These waves are purely "electrostatic" in the general sense that

$$\vec{E} = -\vec{\nabla}\phi \quad , \qquad \phi = \phi_0 \sin(\vec{k} \cdot \vec{r} - \omega t) \tag{II.51}$$

and there is no associated magnetic wave vector. Furthermore, our initial generalization of Ohm's law was based on the assumption that an electric field exists but that it is sufficiently small that the potential energy gained across one mean free path is negligible compared to κT . If this assumption is not satisfied, the acceleration term, $\partial\vec{j}/\partial t$, dominates, and the electrons gain energy indefinitely. However, the mean free path varies as $(u/a)^4$, so that for sufficiently large fields or large velocities, this assumption of small currents must always break down and a "runaway" phenomenon will occur. The critical or runaway field is on the order of $E_c \simeq \kappa T/e\ell$, and if $E > E_c$ our restriction to "small" currents is invalid.

Finally, if the electric fields associated with various waves in the plasma are not examined, this means that we will ignore any acceleration processes since it is essentially only the electric field that can change the energy of a particle.

Chapter II. GENERAL REFERENCES

S. Chapman and T. G. Cowling, The Mathematical Theory of Non-Uniform Gases, Cambridge, 1958.

W. B. Thompson, An Introduction to Plasma Physics, Addison-Wesley, New York, 1962.

L. Spitzer, Jr., Physics of Fully Ionized Gases, Interscience, New York, 1962.

III. THE SOLAR CORONA AND SOLAR WIND

All models of the solar atmosphere are based on the continuum equations, and several additional idealizations are usually employed. It is assumed that the atmosphere is in a steady state with complete spherical symmetry, and the effects of viscosity, the solar magnetic field, and solar rotation are not generally explicitly included. If the only force acting on the fluid is the gravitational attraction of the sun, Eq. (II.44) then yields

$$\frac{1}{r^2}\frac{d}{dr}(r^2 nu) = 0$$

$$nmu\frac{\partial u}{\partial r} + \frac{d}{dr}(n\kappa T) + \frac{nGM_\odot m}{r^2} = 0 \qquad \text{(III.1)}$$

$$\frac{3}{2}u\frac{dp}{dr} + \frac{5}{2}\frac{p}{r^2}\frac{d}{dr}(r^2 u) + \frac{1}{r^2}\frac{d}{dr}(r^2 q) = 0$$

with $p = n\kappa T = p_e + p_i$, $q = -k(dT/dr)$. Here $n = n_e + n_i$, and $nm = n_e m_e + m_i n_i$. Thus, for fully ionized hydrogen $n = 2n_e$, $m \simeq (1/2)m_{proton}$. The energy equation in this form is actually an equation of state for the coronal gas. If $\vec{\nabla}\cdot\vec{q} = 0$, the energy and continuity equations yield the familiar adiabatic relation, $pn^{-5/3} = \text{constant}$, showing that the coronal fluid behaves as if it is composed of single particles with mass m , density n , and three degrees of freedom per particle.

III.1. The Static Chapman Model

Chapman (1957) was the first to attempt to construct a quantitative model of the corona. He considered the simplest case, a static atmosphere, and used the conductivity appropriate for ionized hydrogen, $k(T) = k(T_0)(T/T_0)^{5/2}$. In this case (III.1) yields

$$\frac{d}{dr}(n\kappa T) = -\frac{nGM_\odot m}{r^2} \quad , \qquad \text{(III.2)}$$

$$\frac{d}{dr}\left(r^2 T^{5/2}\frac{dT}{dr}\right) = 0 \quad . \tag{III.3}$$

Equation (III.3) has a simple solution, $T(r) = T_0(r_0/r)^{2/7}$, and when this distribution is inserted into Eq. (III.2), the density profile can be obtained. We find

$$\frac{1}{n\kappa T}\frac{d}{dr}(n\kappa T) = -\frac{GM_\odot m}{\kappa T_0 r_0^{2/7}}\left(\frac{1}{r}\right)^{12/7}$$

and hence,

$$\begin{aligned} n\kappa T &= n(r_0)\kappa T(r_0)\ \exp\left[\frac{7}{5}\frac{GM_\odot m}{\kappa T_0 r_0^{2/7}}\left(\frac{1}{r^{5/7}} - \frac{1}{r_0^{5/7}}\right)\right] \\ &= n(r_0)\kappa T(r_0)\ \exp\left[-\frac{7}{5}\frac{GM_\odot m}{\kappa T_0 r_0}\left(1 - \left(\frac{r_0}{r}\right)^{5/7}\right)\right] \end{aligned} \tag{III.4}$$

The coefficient in the exponent is a very large number; for $r_0 = 1.06\ R_\odot$, $T_0 = 10^6 °K$, $(7GM_\odot m/5\kappa T_0 r_0)$ is equal to 12. However, the density at the base is also large $(n(r_0) \simeq 3 \times 10^8/cm^3 = 2n_e(r_0))$ and the $r^{2/7}$, $r^{5/7}$ variations are quite weak. It can be verified that the above parameters and Eq. (III.4) give $n_e = n_i \simeq 300/cm$, $T_e = T_i \simeq 2 \times 10^5 °K$ at $r = 1$ A.U., indicating that the solar corona has an enormous extent.

This surprising prediction of the simple static model sets the stage for the entire study of sun-earth relations. It serves to demonstrate that the solar atmosphere, whatever its state, must reach to the earth and beyond, and that it must contain a considerable amount of kinetic energy near 1 A.U. . Although the actual state of the solar corona differs considerably from the form shown in Eq. (III.4), it is still true that the earth is best regarded as an object embedded in the solar atmosphere.

Before turning to the other models, it is worth examining the static model in more detail. It is clear that Eq. (III.4) predicts a finite pressure at infinity, and using $T \sim r^{-2/7}$, it can be seen that

the predicted density diverges asymptotically with $n(r) \to r^{2/7}$, $r \to \infty$. This behavior is quite peculiar, and we must consider the possibility that this solution represents an unphysical description of an arbitrary stellar atmosphere.

Perhaps the first point to examine involves the assumption that the continuum model and the conductive heating term can be used in the unmodified form out to infinity, since these expressions are valid only if $\ell/L \ll 1$. In fact, the mean free path varies as $T^2/n \sim T^3 \sim r^{-6/7}$ for this model, and thus ℓ actually decreases with increasing distance. Furthermore, Eq. (III.4) shows that the scale height, $H = p/|dp/dr|$, increases as $r^{12/7}$. We therefore conclude that the condition $\ell/L \ll 1$ is not violated by the simple static model at any distance.

However, a significant change does arise when we try to correct for the apparent density divergence in (III.4). When the coronal gas attains a sufficiently large density, its self-attraction becomes important and Eqs. (III.1,2) must be modified. The correct form of the hydrostatic equilibrium equation is then

$$\frac{d}{dr}(n\kappa T) = -\frac{nGM_\odot m}{r^2} - \frac{4\pi mGm^2}{r^2}\int_{r_0}^{r} r'^2 n(r')dr' \qquad \text{(III.5)}$$

and the nonlinear correction term is extremely important in those cases for which $n(r)$ becomes large when the correction is omitted. Thus, if $u = 0$, $T = T_0(r/r_0)^{-2/7}$, as in the Chapman model, $n \to r^{2/7}$ without coronal self-attraction and a divergent contribution has been ignored. The corrected Chapman model obeys (III.5), with the same temperature variation, and it can be verified that the correct asymptotic form is now

$$\left.\begin{aligned} n(r) &\to r^{-16/7} \to 0 \\ p(r) &\to r^{-18/7} \to 0 \end{aligned}\right\} \quad r \to \infty \qquad \text{(III.6)}$$

With these new expressions, it is necessary to re-examine the r -dependence of ℓ/L . The scale height varies as $18r/7$ and $\ell \sim T^2/n \rightarrow r^{12/7}$ so that in this case ℓ/L <u>increases</u> (as $r^{5/7}$) with increasing distance. It is clear that at some finite radius the condition $\ell \approx L$ will be encountered and the continuum model, dominated by collisional heat transfer, will break down.

The problem then resembles the one met in trying to discuss evaporation or the escape of gases from a planetary atmosphere. A critical layer or zone is defined by the shell $\ell \approx H$; beyond this zone we have the "exosphere" in which the particles travel freely on ballistic orbits, modified by collisions which occur whenever they penetrate the inner region. There are complications which arise if the gas is a fully ionized plasma, since the species have different values of q and m . This causes electric fields to develop at the exospheric level (Spitzer, 1951) because of charge separation effects.

The main point of this digression is to note that the static model is a perfectly acceptable description of a possible stellar atmosphere. We reject it, however, not because of any inherent defect in the physics, but because it does not describe the observed properties of the solar corona.

III.2. Parker's Hydrodynamic Coronal Model

With the benefit of hindsight we can state that it is very unlikely that any static model could describe an atmosphere such as the corona. The earth's atmosphere is heated from above by dissipation of radiant flux incident from the sun, and such energy transfer does not generally impart momentum to the gas. Thus, a static terrestrial atmosphere is quite understandable. However, the coronal case is very different, since an enormous energy flux must be supplied from below to raise the temperature three orders of magnitude and maintain this temperature despite the large conductive heat loss. [Chapman's model yields a net energy loss of about $(5 - 10) \times 10^{26}$ ergs/sec by outward conduction; this is considerably larger than the radiative loss in the corona because the corona is fully ionized and such loss must then proceed via an inefficient

bremsstrahlung process (Zirin, 1957). We shall henceforth neglect radiative effects.]

The origin of the high coronal temperature is not completely understood, but it is generally agreed that mechanical motions generated beneath the photosphere are responsible for heating of the solar chromosphere and corona. Various wave modes are capable of propagating upward into the corona and heating mechanisms based on dissipation of hydromagnetic (Alfvén) waves, acoustical shock waves and internal gravity waves (slow, low frequency disturbances roughly analogous to surface waves on water) have been considered as the principal heat source. These mechanisms have one major feature in common; net momentum as well as energy is transferred to the corona and it is therefore logical that the restriction $u = 0$ should be abandoned. In fact, the continuity equation in (III.1) shows that since $nur^2 =$ constant , a finite streaming speed at one radius (say the coronal base) implies $u > 0$ at all finite distances.

Parker's theory was not primarily motivated by consideration of the conditions at the base, but by concepts associated with the expansion of the solar corona into the near vacuum of interstellar space. If we imagine the hot atmosphere to be confined near the sun, and then suddenly released, it seems reasonable to expect the final flow pattern to be the one with the lowest asymptotic pressure. This boundary conditions leads unambiguously to the solar wind solution.

The model considered first by Parker (1958) was based on several simplifying assumptions. The observed scale heights, as determined from $n_e(r)$ measurements, indicated no appreciable decrease in coronal temperature out to $(10 - 20)R_\odot$, although the uncertainties do become significant beyond about $8R_\odot$. Parker idealized these observations as follows: it was assumed that the corona is isothermal with temperature T_0 in a region between the base $(r = a)$ and a radius $r = b$ $(8R_\odot < b < 20R_\odot)$, with an adiabatic temperature distribution $[T(r) = T(b)(n(r)/n(b)^{2/3}]$ beyond $r = b$. Since $T(r)$ is completely specified in terms of the density distribution, it is not necessary to consider the energy equation. For $a < r < b$,

Eq. (III.1) yields $nur^2 = n_0 u_0 a^2$, and therefore

$$nmu \frac{du}{dr} + \frac{GM_\odot mn}{r^2} = - \kappa T_0 \frac{dn}{dr}$$

$$= + \kappa T_0 \frac{n}{u} \frac{du}{dr} + \frac{2n\kappa T_0}{r} \qquad \text{(III.7)}$$

This may be rewritten as

$$\frac{1}{2}\left[1 - \frac{\kappa T_0}{mu^2}\right] \frac{d}{dr}(mu^2) = + \frac{2\kappa T_0}{r} - \frac{GM_\odot m}{r^2} \qquad \text{(III.8)}$$

and the general solution can then readily be obtained,

$$\frac{mu^2(r)}{2} - \frac{mu^2(a)}{2} - GM_\odot m\left[\frac{1}{r} - \frac{1}{a}\right] + \kappa T_0 \ell n \frac{u(a)a^2}{u(r)r^2} = 0 \qquad \text{(III.9)}$$

The initial discussion of the general solution is best carried out by examining the differential equation, (III.8). It is clear that a singular point occurs at the radius $r_c = GM_\odot m/2\kappa T_0$, since both sides of (III.8) must vanish there. If mu^2 and $d(mu^2)/dr$ remain finite, then at $r = r_0$, we must have $mu^2(r_0) = \kappa T_0$ or $d(mu^2)/dr = 0$.

Parker drew attention to the first of these possibilities. Near the coronal base the kinetic energy is small, but if $d(mu^2)/dr$ remains finite in the isothermal region, it can be seen that the flow becomes supersonic near $r = r_c$ (actually, the sound speed is $(\kappa T_0/m)^{1/2}$, if T is constant , and $mu^2(r)$ continues to climb until $r = b$. In order to evaluate $u(b)$, Eq. (III.9) can be rewritten in terms of the values at b and r_c ,

$$\frac{1}{2} mu^2(b) = \frac{1}{2} mu^2(r_c) + \frac{GM_\odot m}{b} - \frac{GM_\odot m}{r_c} + \kappa T_0 \ell n \frac{u(b)b^2}{u(r_c)r_c^2} \ ,$$

$$= \kappa T_0 \ell n \frac{u(b)b^2}{u(r_c)r_c^2} + \frac{GM_\odot m}{b} - \frac{3}{2}\kappa T_0 \ , \qquad \text{(III.10)}$$

and it follows that an approximate solution for large $u(b)$ is

$$\frac{1}{2} mu^2(b) \simeq 2\kappa T_0 \ell n \frac{b}{r_c} + \kappa T_0 \bigcirc \left(\ell n \frac{mu^2}{2} \right) + \ldots \qquad \text{(III.11)}$$

Let us consider some simple numerical examples. If $T_0 = 1.5 \times 10^6 {}^\circ K$, then $r_c = 2.67$ R and $u(r_c) = 155$ km/sec. At $r = b$ the velocity is multiplied by $2(\ell n\, b/r_c)^{1/2}$ and $b = 5r_c = 13.2$ R yields $u(b) = 500$ km/sec. However, $r = a$ may also be chosen as a reference point and assuming $u(a) \ll u(r)$, we find

$$u(a)a^2 \simeq u(r)r^2 \exp\left[-\left(2r_c/a - 3/2\right)\right] \qquad \text{(III.12)}$$

For $a = 1.06\ R_\odot$, the exponent is 3.5 and $u(a) \simeq 30$ km/sec. Thus, in the isothermal region, the coronal fluid is accelerated from a speed of 30 km/sec at the base, through the sonic transition, to a speed of 500 km/sec at $r = b \simeq 13\ R_\odot$.

Before going on to discuss the subsequent flow in the adiabatic region, let us briefly examine the other solutions to (III.9), (III.10). We shall refer to the critical solution just described as the solar wind solution, and a natural question has to do with the behavior of the fluid if $u(a) > u$ (solar wind, a). In this case, it turns out that no physical solution is possible, since $mu^2(r)$ soon turns back toward $r = a$ as $d(mu^2)/dr$ becomes infinite near r_c. This is shown in Fig. 3. All other cases have $u(a) < u$ (solar wind, a) and at $r = r_c$ they have $d(mu^2)/dr = 0$, $mu^2(r_c) < \kappa T_0$. Thus, these are completely subsonic, and as illustrated in Fig. 3, the velocity begins to fall again beyond $r = r_c$.

Since $mu^2(r_c) < \kappa T_0$ for these solutions, the largest possible value for $u(b)$ can be found using (III.10) with $mu^2(r_c) = \kappa T_0$; this gives

$$u(b) < \left(\frac{\kappa T_0}{m}\right)^{1/2} (r_c/b)^2 \exp\left(\frac{3}{2} - \frac{2r_c}{b}\right) \qquad \text{(III.13)}$$

and with the above base parameters $u(b) < 20$ km/sec.

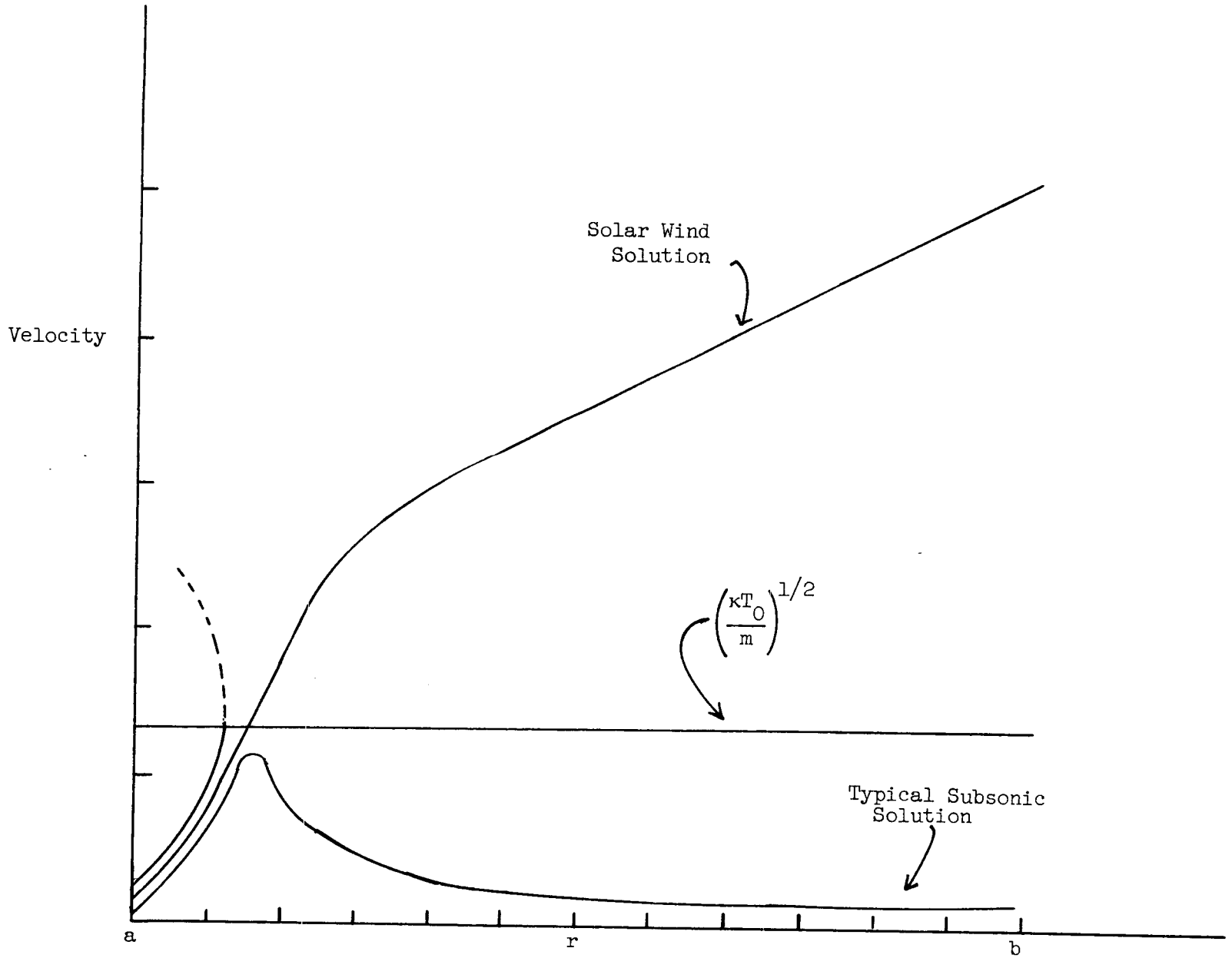
Velocity
Solar Wind
Solution
$\left(\frac{\kappa T_0}{m}\right)^{1/2}$
Typical Subsonic
Solution
a
r
b

Figure 3

In the adiabatic region beyond $r = b$, the continuity equation and the law $p \sim n^{5/3}$ yield

$$u^2(r)\, T^3(r) = u^2(b)\, T_0^3\, (b^4/r^4) \tag{III.14}$$

and the remaining momentum equation can be written in several convenient forms. Since

$$\frac{1}{n}\frac{d}{dr}\, n^{5/3} = \frac{5}{3}\, n^{-1/3}\, \frac{dn}{dr} = \frac{5}{2}\, \frac{d}{dr}\, n^{2/3} \tag{III.15}$$

it is easy to show that the second equation in (III.1) is equivalent to

$$\frac{mu^2}{2} + \frac{5}{2}\, \kappa T - \frac{GM_\odot m}{r} = E \tag{III.16}$$

where E is a constant of motion for adiabatic flow. However (III.14) and (III.15) can also be combined to recast the momentum equation in a form similar to that of Eq. (III.8),

$$\frac{1}{2}\left(1 - \frac{5}{3}\, \frac{\kappa T}{mu^2}\right)\frac{d}{dr}\, (mu^2) = \frac{10}{3}\, \frac{\kappa T}{r} - \frac{GM_\odot m}{r^2} \tag{III.17}$$

The last expression suggests the possibility that a sonic transition might occur even in the adiabatic region. That is, at $r_c' = 0.3\, GM_\odot m/\kappa T$, it appears possible that we might have $mu^2 = 5\, \kappa T/3$ so that u would again increase smoothly past $(\kappa T/m)^{1/2}$ even for the "slow" solutions of (III.13). However, this possibility is not a real one; Eq. (III.16) shows that such a transition requires $E = 0$, and in this singular case mu^2, κT must both vary as r^{-1}, so that one variable cannot decrease faster than the other. We conclude that in the adiabatic region the flow remains subsonic or supersonic, and Eqs. (III.14), (III.15) then yield the appropriate solutions. The constant E is given by $E = (1/2)\, mu^2(b) + (5/2)\, \kappa T_0 - GM_\odot m/b$ and thus as $r \to \infty$, the solar wind streaming energy tends to

$$\frac{1}{2}\, mu^2(r) \to 2\kappa T_0\, \ell n\, \frac{b}{r_c} + \frac{5}{2}\, \kappa T_0 - \frac{GM_\odot m}{b} \tag{III.18}$$

with $T(r) \to r^{-4/3}$, $n(r) \to r^{-2}$. On the other hand, the slow solutions have asymptotic forms with $\kappa T \to 2E/5$, $u(r) \to r^{-2}$, $n(r) \to n_\infty > 0$. Parker observed that only the solar wind solution has an asymptotic pressure which vanishes $(p(r) \to r^{-10/3})$ and he therefore argued that the solar wind is inevitable. Actually, as pointed out by Chamberlain (1960), this statement requires some qualification. When $E = 0$, $u \to r^{-1/2}$, $n \to r^{-3/2}$ and $p \to r^{-5/2}$ as $r \to \infty$. This type of flow also satisfies the "stability condition," $p(\infty) = 0$, and Chamberlain referred to this as a "solar breeze." The predictions of the two models are quite different. At the earth, the solar wind flow speed is on the order of $500 - 600$ km/sec , while the breeze type of solution has $u(1 \text{ A.U.}) \simeq 20$ km/sec . Of course, just as in our treatment of Chapman's model, nonlinear corrections can be inserted to bring $p(\infty)$ to zero for all cases, and as we shall see, when heat conduction terms are inserted, all possible flow patterns can actually be supersonic at $r = \infty$. Thus, in a technical sense, a solar wind is indeed inevitable, if this is taken to refer to the supersonic flow at infinity. However, if we restrict the term "solar wind" to refer only to a solution of the type shown in Fig. 3, with a sonic transition near the coronal base, then Parker's original contention remains valid; at any large but not astronomical distance from the sun, the solar wind flow is the one with the lowest pressure. To the extent that an asymptotic pressure relation governs the flow pattern, a solar wind is therefore inevitable. (This statement should not be taken to imply universal agreement that the pressure distribution at large distances does indeed determine the flow. We shall return to this point later.)

The supersonic and subsonic solutions are quite similar below $r = r_c$, but the velocity distributions beyond r_c are very different, and since $nur^2 =$ constant, the predicted density profiles are also distinct. For instance, if $u(1.06\ R_\odot) \simeq 30$ km/sec , $n(1.06\ R_\odot) = 2n_e \sim 3 \times 10^8$ cm^{-3} , then at 1 A.U. $= 214 R_\odot$, $n_e \simeq 50$ cm^{-3} if $u(1 \text{ A.U.}) \simeq 550$ km/sec , but $n_e \simeq 1500$ cm^{-3} if $u(1 \text{ A.U.}) \simeq 18$ km/sec . The most direct way to verify that the corona is in the solar wind state is to measure $u(1 \text{ A.U.})$, $n_e(1 \text{ A.U.})$, and recent plasma probe measurements do yield densities and velocities which **are**

very much closer to Parker's predictions than to the values associated with any of the subsonic solutions. However, even before such plasma measurements were made, it was possible to rule out the subsonic solutions using observational evidence. Since $u(r)$ increases monotonically for the solar wind, $n_e(r)$ falls smoothly as $(ur^2)^{-1}$, but if u is subsonic, it rapidly decreases beyond r_c, and the resultant density curve develops a "knee," as shown in Fig. 4. Although such comparisons were not made until recently, the observed $n_e(r)$ curve is certainly smooth and in much better agreement with the simple solar wind prediction than with any of the others.

Parker also discussed the physical origin of the solar wind. He noted that the driving mechanism is the pressure gradient in the approximately isothermal base, and he pointed out that the entire process is analogous to the expansion of gas from high pressure through a Laval nozzle into a vacuum. In Parker's words, "the gravitational field plays the role of the throat in the nozzle, making possible the transition from subsonic to supersonic flow."

III.3. Conductive Heating of the Solar Wind

In Parker's solar wind model it is necessary to assume that the temperature remains high in a large base region in order to have pressure gradients strong enough to generate the transition to supersonic flow. The physical origin of the large temperature was indirectly investigated by Parker (1960), who solved the momentum equation for an effective equation of state, $p \approx n^{\alpha}$, with the polytrope index, α, varying between unity (isothermal flow) and $5/3$ (adiabatic flow) to account for different energy sources. However, it was suggested (Chamberlain, 1960) that no reasonable heat source from the solar interior could have the magnitude required and also possess the spatial variation necessary to maintain such a large approximately isothermal region in the presence of fast expansion (see also Noble and Scarf, 1962). Chamberlain therefore emphasized the possibility that the solar breeze solution was the appropriate one.

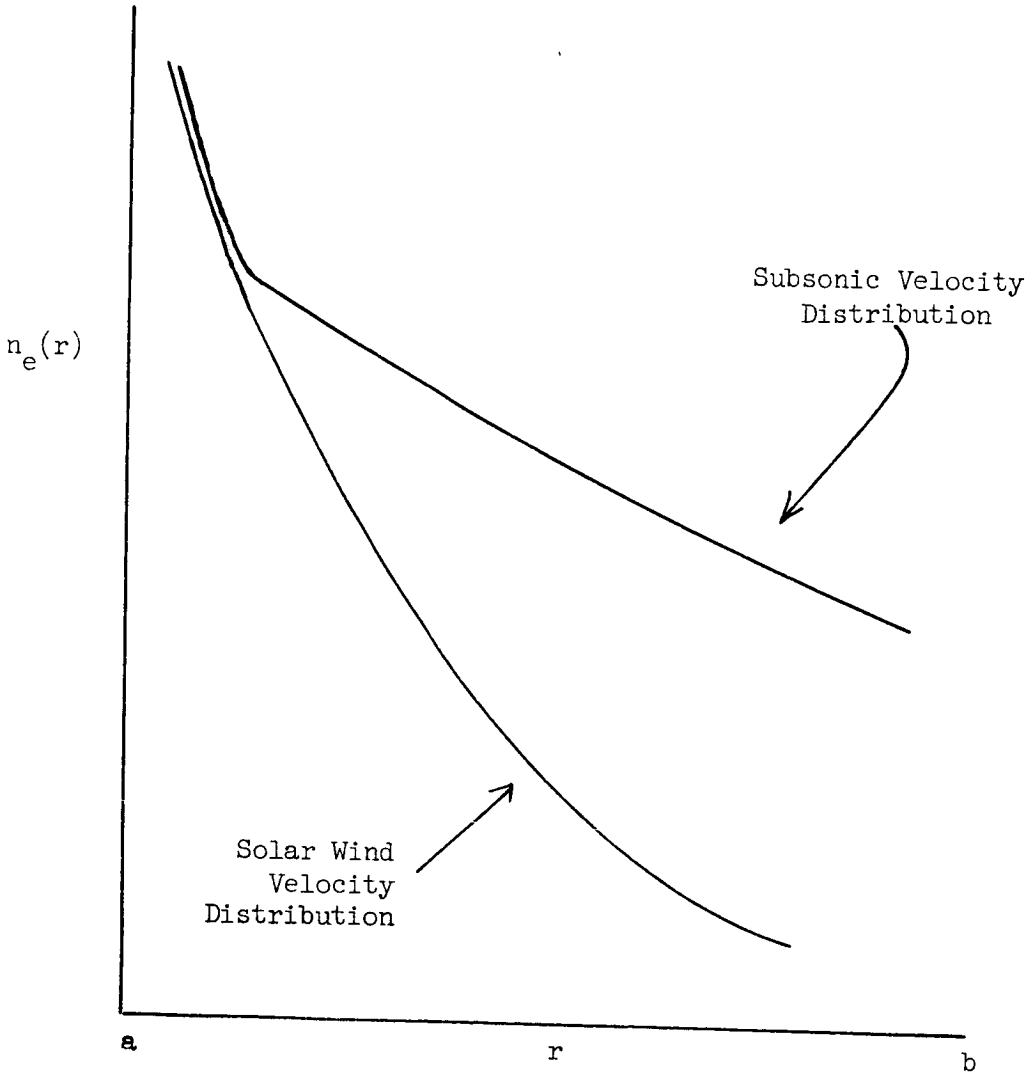
$n_e(r)$
Subsonic Velocity Distribution
Solar Wind Velocity Distribution
a
r
b

Figure 4

We now know that this conclusion is incorrect; nevertheless, a valuable new concept of the coronal energy balance evolved during this examination of a slowly streaming corona. Chamberlain (1961) assumed that the "external" heat source penetrates only into a thin shell near the coronal base; beyond this shell he reintroduced in the energy equation the thermal conduction term which Chapman had already shown to be important for a static corona. The equations to be solved are then those displayed in (III.1). The energy equation may be written as

$$\frac{5}{2}\vec{\nabla}\cdot(p\vec{u}) - (\vec{u}\cdot\vec{\nabla})p + \vec{\nabla}\cdot\vec{q} = 0 \qquad \text{(III.19)}$$

and this can be further simplified by evaluating $(\vec{u}\cdot\vec{\nabla})p$ using the momentum equation

$$-(\vec{u}\cdot\vec{\nabla})p \approx nmu^2\frac{du}{dr} - nu\frac{d}{dr}\left(\frac{GM_\odot m}{r}\right)$$

so that (III.19) becomes

$$\frac{5}{2}\frac{1}{r^2}\frac{d}{dr}(n\kappa T u r^2) + \frac{nmu}{2}\frac{du^2}{dr} - nu\frac{d}{dr}\left(\frac{GM_\odot m}{r}\right) - \frac{1}{r^2}\frac{d}{dr}\left(r^2 k\frac{dT}{dr}\right) = 0 \qquad \text{(III.20)}$$

The final simplification follows when (III.20) is multiplied by $(nu)^{-1} = r^2/(nur^2)$; since $nur^2 = c$ is constant, the differential equation can be integrated immediately, and we find

$$\frac{5}{2}\kappa T + \frac{mu^2}{2} - \frac{GM_\odot m}{r} - \frac{r^2 k(T)}{c}\frac{dT}{dr} = E \qquad \text{(III.21)}$$

where E is a new constant of motion. For variable temperature the momentum equation becomes

$$\frac{1}{2}\left(1 - \frac{\kappa T}{mu^2}\right)\frac{d(mu^2)}{dr} = -\frac{GM_\odot m}{r^2} + \frac{2\kappa T}{r} - \frac{d(\kappa T)}{dr} \qquad \text{(III.22)}$$

Chamberlain solved these two equations numerically for the solar breeze case with $E = 0$. Again he found $T \to r^{-1}$, $mu^2 \to r^{-1}$ as $r \to \infty$ and very moderate streaming speeds were predicted near the earth.

In the coronal base region $(1 < r/R_\odot \lesssim 20)$, "fair" agreement between the predicted and observed electron density distributions was found, but this came about only if $k(T)$, the thermal conduction coefficient for ionized hydrogen, was arbitrarily reduced by a factor of 8. (For $E = 0$ the hump in the $u(r)$ distribution is very gentle and no pronounced "knee" in the $n_e(r)$ curve results.) Although Chamberlain's slow solutions to these equations again resemble evaporation rather than the solar wind, it became clear that the correct thermal conduction term is of great importance, even in the presence of streaming. Parker (1962) speculated that thermal conduction alone could transfer heat over a sufficient distance to account for the presence of a nearly isothermal region in the case of fast expansion.

Various analytical treatments were carried out in order to assess the validity of this conjecture. De Jaeger (1962) inserted the Chapman $r^{-2/7}$ termperature distribution into the momentum equation and investigated the streaming. Parker (1963) showed that this procedure is correct only in the zero density limit, and he studied finite density corrections by analytical techniques. It should be clear, however, that the non-linear set of coupled equations for $u(r)$, $T(r)$ [Eqs. (III.21,22)] is sufficiently complex so that numerical techniques are needed. Before proceeding to a discussion of the numerical integration of (III.21), (III.22), it is useful, however, to discuss some general properties of the equations.

The momentum equation shows that the "sonic" transition (more precisely, the point $mu_c^2 = \kappa T_c$) occurs when

$$\left[\frac{d}{dr}(\kappa T)\right]_{r_c} = \frac{GM_\odot m}{r_c^2} - \frac{2\kappa T_c}{r_c} \qquad \text{(III.23)}$$

and thus the crossover radius and crossover temperature are related by

$$E = 3\kappa T_c - \frac{GM_\odot m}{r_c} + \frac{GM_\odot m k(T_c)}{c} - \frac{2\kappa T_c k(T_c) r_c}{c} \qquad \text{(III.24)}$$

This expression indicates that there are two types of solution. If r_c is sufficiently small, then a crossover near the sun occurs and

$$r_c \simeq \frac{GM_\odot mk(T_c)/c - E + 3\kappa T_c}{GM_\odot m} + \ldots \qquad \text{(III.25)}$$

This is the solar wind case with large streaming speeds near the earth. However, a transition at a very great distance from the sun is also possible. In this case

$$r_c \simeq \frac{GM_\odot mk(T_c)/c - E + 3\kappa T_c}{2\kappa T_c k(T_c)/c} + \ldots . \qquad \text{(III.26)}$$

The distant sonic transition occurs for the analog of the completely subsonic solutions discussed in the original Parker model. When thermal conduction is included, the gas continues to cool as it slowly coasts away from the sun. Ultimately, the thermal energy drops below the drift energy, and the flow becomes supersonic, no matter how slowly the gas is flowing. In fact, if we regard the solar breeze as a singular limit in which the sonic transition occurs at infinity, then it can be stated that supersonic flow and zero asymptotic pressure are indeed inevitable. Of course, this discussion is based on the incorrect idealization that the fluid equations are actually valid everywhere, but we insert this digression to indicate again that the role of a strict asymptotic pressure condition in determining the steady flow pattern is quite weak.

Study of the asymptotic behavior of Eqs. (III.21), (III.22) also shows that all physical solutions are supersonic at infinity, regardless of their behavior near the sun. If $T(r) \to 0$ as $r \to \infty$, then

$$\frac{mu^2}{2} - \frac{r^2 k(T)}{c}\frac{dT}{dr} \to E$$

and the general solution (Parker, 1964; Scarf and Noble, 1965) has

$$mu^2(r) \to 2(E - \kappa T_0 A\, \alpha^{7/2}/7) + \frac{2GM_\odot m}{r} - 16\kappa T(r) + \ldots$$

$$T(r) \to \alpha T_0 \left(\frac{GM_\odot m}{\kappa T_0 r}\right)^{2/7} + \frac{77}{9A\,\alpha^{3/2}} \left(\frac{GM_\odot m}{\kappa T_0 r}\right)^{4/7} \qquad \text{(III.27)}$$

with $A(T_0) = (2k(T_0)\, GM_\odot m/\kappa^2 T_0 c)$, where T_0 is an arbitrary reference temperature and α is an arbitrary dimensionless constant. In this case, the conductive term contributes everywhere and as $r \to \infty$, $T(r)$ tends to the Chapman distribution. Recently, Whang and Chang (1965) pointed out that another special asymptotic behavior is possible. If the fluid arrives at infinity with only kinetic energy, then

$$mu^2(r) \to 2E + \frac{2GM_\odot m}{r} - 12\kappa T(r) + \ldots$$

$$T(r) \to T_0 \left(\frac{35GM_\odot m}{2\kappa T_0 Ar}\right)^{2/5} + \ldots \qquad \text{(III.28)}$$

Both of these correspond to supersonic flow, and it is therefore of interest to inquire whether the equations with thermal conduction also allow subsonic solutions with $T \to T(\infty) > 0$, $u(r) \to 0$, $p \to p(\infty) > 0$ as in the adiabatic case. The answer is in the negative. Although it is possible to find a solution with $T(r) \to T(\infty) > 0$, the corresponding velocity distribution is not only unphysical, but supersonic, with $u^2(r)$ becoming infinite as $\ell g(GM_\odot m/\kappa T_0 r)$. (There is actually another formal but unphysical solution to Eqs. (III.21), (III.22). This has $T(r) \to 0$ at a finite radius.) Thus, when the thermal conduction is included, supersonic flow with $p(r) \to 0$, $r \to \infty$ arises for any finite value for E.

We are interested in the numerical solution of Eqs. (III.21), (III.22) which corresponds to the solar wind, with a sonic transition near the coronal base. In this case, it is preferable to integrate from the earth to the sun for an initial numerical search. This is so because the precise location of the crossover is not known until an integration is performed, and the outer boundary of the thin coronal "heating shell" has

not yet been determined. The first treatment of this problem was described by Noble and Scarf (1963). It was assumed that at the earth the solar wind streaming speed, temperature and total density are 352 km/sec , 2×10^5°K and $6.75/cm^{-3}$, respectively. A 90% hydrogen-10% helium admixture was also assumed, yielding $m = 0.62$ m (proton) . The equations were then integrated numerically on an IBM 7090 computer.

The only quantity not known or assumed initially was the value of (dT/dr) at the earth. Instead, a search procedure was performed by varying (dT/dr) to find the value at $r = 213R_\odot$ which would lead to $mu^2 \rightarrow \kappa T$ for some radius in the inner corona. Figure 5 shows the initial results of this series of integrations. Here $\psi = mu^2/\kappa T_0$, $\tau = T/T_0$, $\lambda = GM_\odot m/\kappa T_0 r$ and $\tau_1' = d\tau/d\lambda$ at $r = 213R_\odot$. (For $T_0 = 2 \times 10^6$°K , the earth is at $\lambda_1 = 0.027$, the coronal base is at $\lambda \sim 6$, and the dimensionless parameter $A = (2GM_\odot mk(T_0)/\kappa^2 T_0 c)$ is near 400 .) It can be seen that as we approach the sun (i.e., as λ increases), the temperature rises and the kinetic energy falls, so that $mu^2 \rightarrow \kappa T$ near $5.2R_\odot$ $(\lambda_c \simeq 1.36)$. However, all solutions shown in Fig. 5 are actually unphysical. The derivative $d(mu^2)/dr$ either vanishes or becomes infinite and the point $mu^2 = \kappa T$, $0 < d(mu^2)/dr < \infty$ is never reached.

This is a common difficulty with numerical integration across a singularity or saddle point such as the crossover at $mu^2 = \kappa T$; it is impossible to specify the initial conditions with sufficient numerical accuracy to avoid the unwanted solutions, but it is possible to use the results of Fig. 5 for interpolation and in the neighborhood of the singularity a power series expansion

$$\psi = \tau_c + a(\lambda - \lambda_c) + \ldots$$

$$\tau = \tau_c + \left(\frac{1 - 2\tau_c}{\lambda_c}\right)(\lambda - \lambda_c) + b(\lambda - \lambda_c)^2 + \ldots$$

can be used to integrate across the transition into the subsonic lower corona. The final result for this case is shown in Fig. 6. As $r \rightarrow R_\odot$,

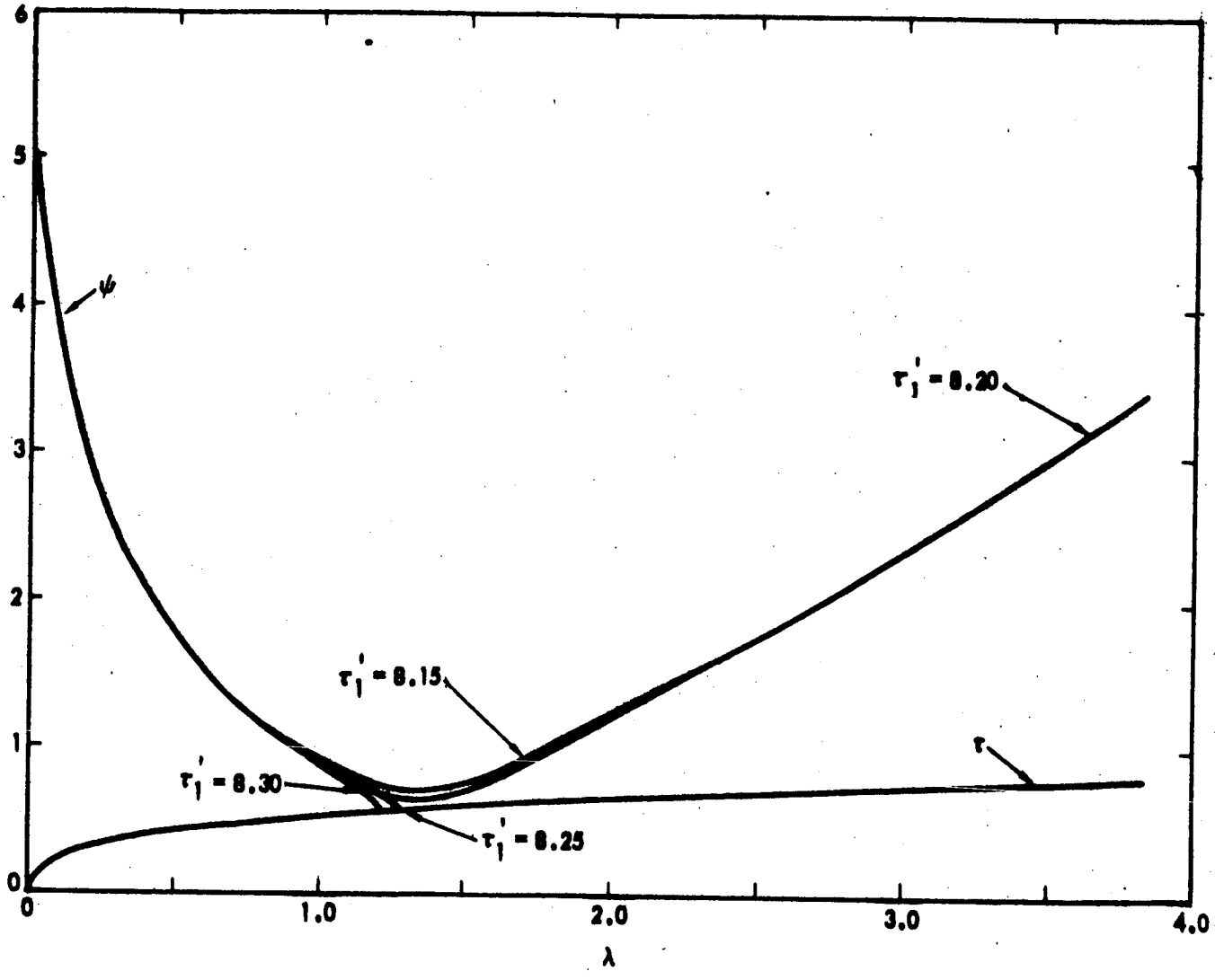

Figure 5. Some test solutions of Eqs. (III.21,22) obtained during a search procedure. The integration proceeds to the right from $\lambda_1 = 0.027$, and A, $\psi(\lambda_1)$, $\tau(\lambda_1)$ are fixed at 400, 4.8, 0.1, respectively. To the accuracy shown on this graph, all four $\tau(\lambda)$ curves are identical. [Note: $\tau'_1 = (d\tau/d\lambda)_{\lambda=\lambda_1}$, and the two lowest ψ curves have $d\psi/d\lambda \to \infty$ as $\psi \to \tau$.]

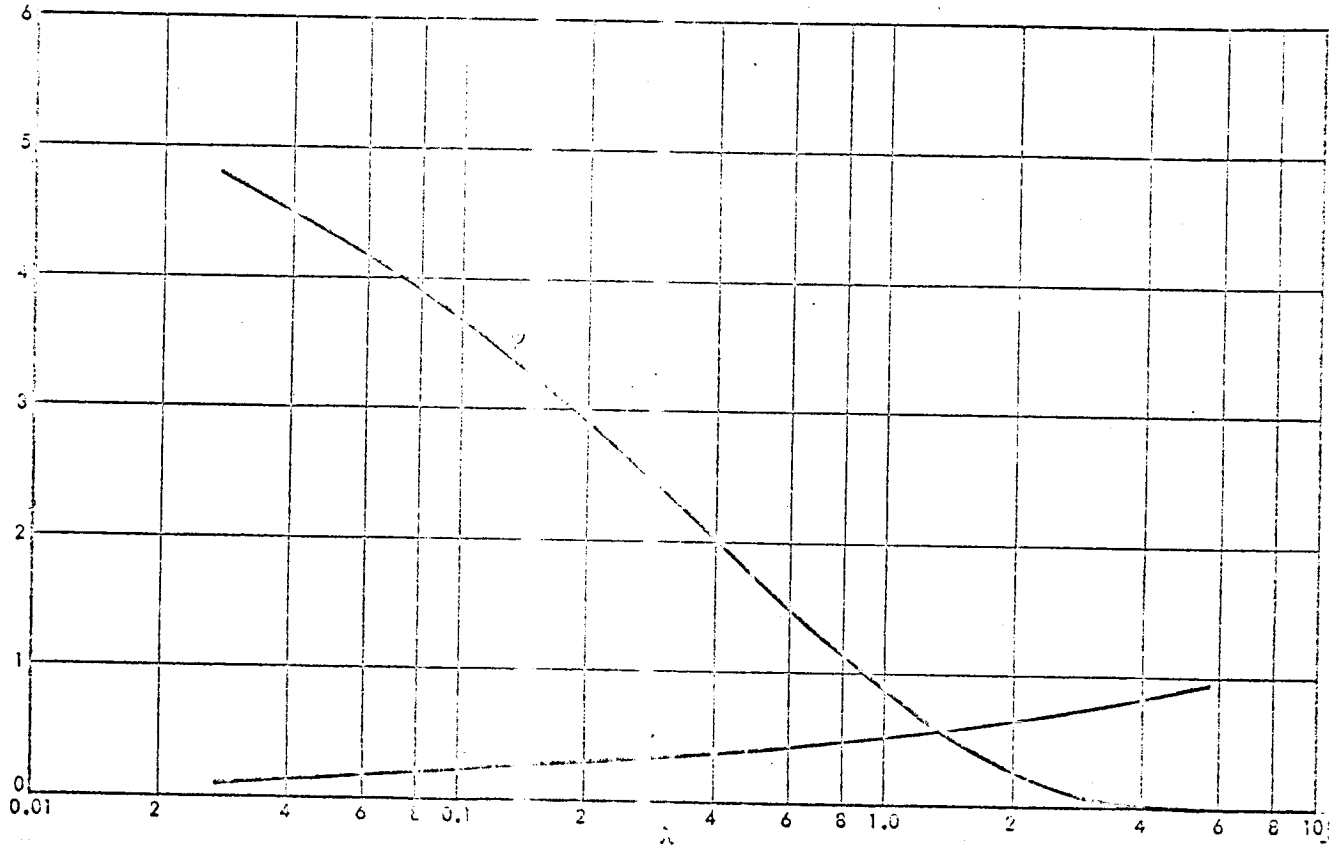

Figure 6. The critical solution which has $\lambda_1 = 0.027$, $\psi(\lambda_1) = 4.8$, $\tau(\lambda_1) = 0.1$ and $\tau'(\lambda_1) = 8.37$, for $A = 400$.

$\tau \to 1$ and hence $T \to T_0 = 2 \times 10^6$°K , while $mu^2(r)$ drops rapidly.

This first integration yields a very promising set of temperature and velocity profiles and in subsequent investigations an attempt was made to find the best fit to the observed coronal density profile. Some results reported by Scarf and Noble (1965) are shown in Fig. 7. The parameters T_0 and A were varied and $n_e(r)$ was computed for each case using $nur^2 = c$. The observed densities [references are given by Noble and Scarf (1963)] are not reliable in the outer corona (they are probably too high in the region $10R_\odot < r < 20R_\odot$). Thus, the striking agreement between theory ($A = 100$, $T_0 = 1.5 \times 10^6$°K) and observation in the inner corona, $2R_\odot < r < 10R_\odot$ is quite impressive. Some detailed properties of this best fit solution are listed in Table III.1; near the earth this corresponds to $n_e = n_i \simeq 5$ cm^{-3} , $u \simeq 300$ km/sec .

These numerical solutions do not answer all questions about coronal flow. Below $(2 - 2.5)R_\odot$ it appears impossible to reproduce the $n_e(r)$ observations, and it seems clear that the simple model based on spherical symmetry, no external heat source, negligible magnetic effects, etc., must become invalid. Nevertheless, these numerical investigations go a long way toward "explaining" the origin of the solar wind. If conditions in the coronal base are such that $T(2R_\odot)$ is maintained near 1.5×10^6°K , with $u(2R_\odot) \simeq 20$ km/sec , then thermal conduction naturally produces a very large region of high temperature so that the high pressure gradients can accelerate the fluid to yield the solar wind. Of course, these solutions only indicate the <u>possibility</u> of a solar wind. The conductive heating equations have other solutions that are subsonic everywhere near the sun. Figure 8 shows how an extremely small change in $\psi = mu^2/\kappa T_0$ near the base can convert the solar wind solution into a subsonic one. Thus, the numerical investigation of Eqs. (III.21), (III.22) explains how the corona can become a solar wind, but it cannot explain just why this occurs.

III.4. The Solar Magnetic Field

Solar magnetograms reveal a complex magnetic structure in the photosphere, and by examining the orientations of coronal streamers and

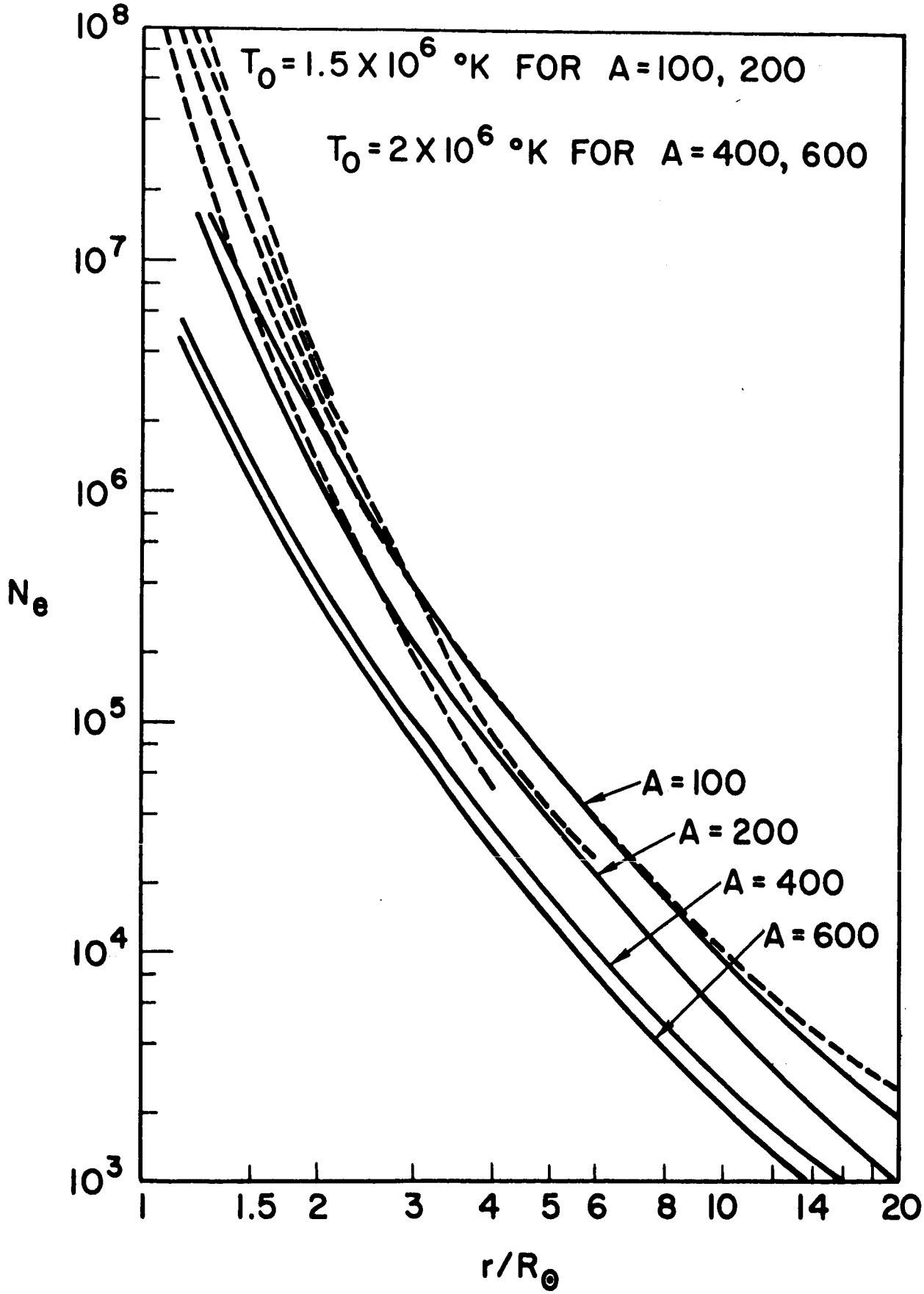
$T_0 = 1.5 \times 10^6$ °K FOR A = 100, 200
$T_0 = 2 \times 10^6$ °K FOR A = 400, 600
10^8
10^7
10^6
10^5
10^4
10^3
N_e
A = 100
A = 200
A = 400
A = 600
1
1.5
2
3
4
5
6
8
10
14
20
$r/R_\odot$

Figure 7

TABLE III.1

Solution of conductive heating equations for $A = 100$, $T_0 = 1.5 \times 10^6 °K$, $m = 0.62$ m (proton). The sonic crossover occurs at $r = 7.2 R_\odot$.

$r/R_\odot$	u(km/sec)	$n_e(cm^{-3})$	T(°K)
2	18.4	2.03×10^6	1.47×10^6
4.5	22.4	1.02×10^5	1.03×10^6
6.8	105	3.09×10^4	8.89×10^5
7.2	110	2.62×10^4	8.73×10^5
10	146	1.02×10^4	7.92×10^5

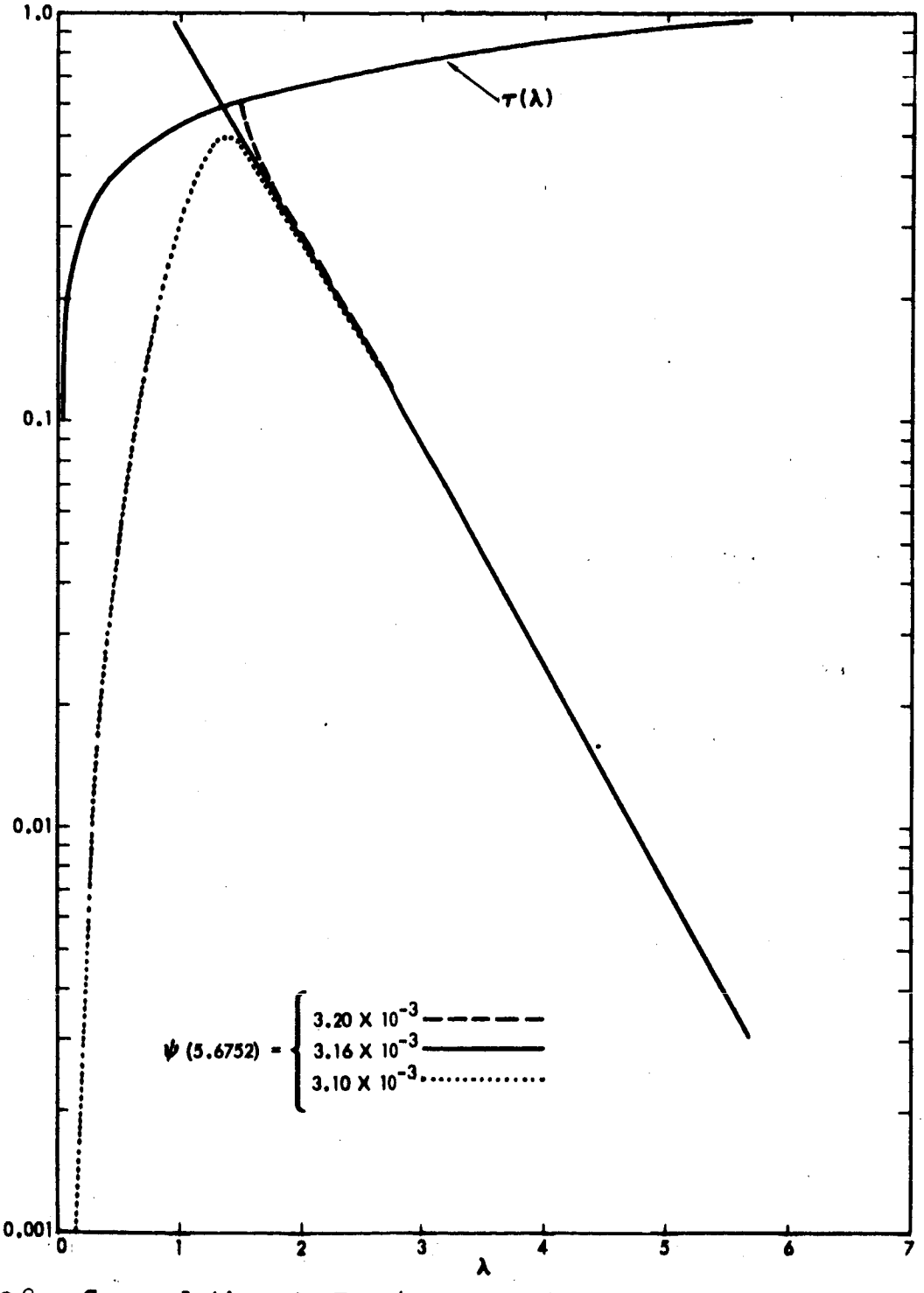

Figure 8. Some solutions to Eqs. (III.21, 22). The integration proceeds to the left and at $\lambda = 5.6752$, τ and τ' are fixed at 0.9564 and 0.621 respectively. These solutions illustrate the instability of the idealized model which has no viscous or magnetic corrections.

III.4. The Solar Magnetic Field

Solar magnetograms reveal a complex magnetic structure in the photosphere, and by examining the orientations of coronal streamers and density irregularities, it can be concluded that a similar configuration exists in the coronal base region. The most important aspect of this structure concerns the relatively weak but well-ordered general field which has a magnitude of about one gauss near the photosphere. This field is nearly radial at $r \simeq 1\ R_\odot$, and it appears to have opposite polarities in northern and southern latitudes.

If the solar atmosphere were not a streaming fully ionized gas, one might expect the general field to fall off as r^{-3}, representing a magnetic dipole. If this were so, the magnitude at 1 A.U. would be about 10^{-7} gauss $= 10^{-2}\gamma$. However, the streaming solar wind drastically modifies any such dipole-like behavior and the final configuration is completely determined by the hydrodynamic properties of the plasma.

As a first approximation, let us turn to the mhd conditions discussed in Chapter II. If $\vec{j}$ is bounded and η is small, then $(\vec{E} + \vec{u} \times \vec{B}/c)$ must vanish. However in a frame of reference in which the sun is at rest, there is no source of electric field, and hence $\vec{u} \times \vec{B}$ must be zero, so that $\vec{u}$ is parallel to $\vec{B}$. Suppose that we also consider a hypothetical sun which does not rotate. For this case, purely radial streaming is quite natural, and thus $\vec{B} = B_r \vec{i}_r$ will satisfy the mhd condition. However, $\vec{\nabla}\cdot\vec{B} = r^{-2} d(r^2 B_r)/dr$ must also vanish, so that $\vec{B} = B_0(\theta,\phi)(a^2/r^2)\vec{i}_r$ represents a possible solar magnetic field distribution. Near 1 A.U., this would give $B \simeq 2.5 \times 10^{-5}$ gauss $= 2.5\gamma$.

Thus far, the magnetic pressure gradient terms associated with $\vec{j} \times \vec{B}/c$ have been neglected in the momentum conservation equation, and now that a possible field configuration is at hand, it is necessary to examine the self-consistency of this approximation. To this end, we have tabulated in Table III.2 the thermal and kinetic energy densities [n, u, T taken from Table III.1], in order to compare

TABLE III.2 ENERGY DENSITIES (ergs/cm^3)

$r/R_\odot$	$n\kappa T$	nmu^2	$B^2/8\pi$
2	4.1×10^{-4}	7.1×10^{-6}	2.5×10^{-3}
4.5	1.45×10^{-5}	5.7×10^{-6}	9.5×10^{-5}
6.8	3.8×10^{-6}	3.58×10^{-6}	1.9×10^{-5}
7.2	3.14×10^{-6}	3.53×10^{-6}	1.48×10^{-5}

them with the magnetic energy density, $B^2/8\pi = B_0^2 a^4/8\pi r^4$. The table is constructed using $B_0 = 1$ gauss , $a = R_\odot$.

It can be seen that the magnetic energy density is considerably larger than the mechanical energy density throughout the inner corona. [The two become equal near $10\ R_\odot$; beyond this point $B^2 \sim r^{-4}$ and $nu^2 \sim u(r)r^{-2}$, so that $\beta = E_{mech}/E_{mag}$ rapidly becomes small.] Thus, the existence of the magnetic pressure gradient term

$$\vec{F}_B = -\frac{1}{8\pi}\vec{\nabla} B^2 + \frac{(\vec{B}\cdot\vec{\nabla})\vec{B}}{4\pi} \qquad \text{(III.29)}$$

cannot be ignored on numerical grounds for $r < 10\ R_\odot$. However, if $\vec{B} = B_0(\theta,\phi)\vec{i}_r(a^2/r^2)$ as assumed above, then it is easy to see that the magnetic force term has no radial component, so that the radial momentum equation needs no modification. On the other hand, Eq. (III.29) generally does yield finite forces in the θ and ϕ directions,

$$(\vec{F}_B)_\theta = -\frac{a^4}{8\pi r^5}\frac{\partial B_0^2}{\partial\theta} \quad ,$$

$$(\vec{F}_B)_\phi = -\frac{a^4}{8\pi r^5 \sin\theta}\frac{\partial B_0^2}{\partial\phi} \quad ,$$

since the anticipated variation in B_0 (to account for the north-south polarity reversal, for instance) implies $j_\theta, j_\phi \neq 0$. This means that our assumption of spherical symmetry cannot be strictly valid, and unless B_0 is constant, a three dimensional circulation must be considered. This type of complication has not yet been treated in any detail. It is generally anticipated that the space averaged values of j_θ, j_ϕ will vanish, so that the assumption of spherical symmetry remains valid for the mean flow pattern, but in view of the magnitudes shown in Table III.2, it is clear that major deviations from the simple model might be possible.

In fact, the expression $\vec{B} = B_r\vec{i}_r$ is seriously in error for another reason. The sun, which is the source of the solar field, is not at rest, but at the equator it undergoes one rotation every 24.7 days ($T = 27$ as seen by an observer on the moving earth. Furthermore, the

sun does not rotate as a rigid body. Its period is 24.7 days at the equator, and nearly 30 days at the poles). This rotation has several serious consequences. The plasma does not start from the sun with $\vec{u} = u_r \vec{i}_r$ but it is spun off with a finite angular momentum. Moreover, an inertial observer sees a rotating magnet and this means that in an inertial frame of reference a unipolar electric field must exist.

The correct treatment of these complications was indicated by Parker in his original solar wind paper. As $r \to \infty$, the mechanical flow velocity must become purely radial, in an appropriate non-rotating inertial frame. This means that if we were to transform to a rotating (primed) frame fixed to the sun, u'_ϕ would tend to $\Omega r \sin\theta$ as $r \to \infty$, where $\Omega = 2.94 \times 10^{-6}$ rad/sec. However, in this rotating frame u'_ϕ must vanish at the coronal base $(r = a)$ since the plasma is ejected radially. Thus, the flow pattern in the rotating frame may be of the form

$$\begin{aligned} u'_r &= u_r(r) \\ u'_\theta &= 0 \\ u'_\phi &= \Omega(r - F(r)) \sin\theta \end{aligned} \qquad \text{(III.30)}$$

with $F(a) = a$, $F(r) \ll r$, $r \to \infty$. It is convenient to start in the rotating frame for another reason. If the source of the magnetic field is fixed with respect to the observer, then there is again no source of electric field, and the mhd approximation again requires $\vec{u}' \times \vec{B} = 0$, or

$$u'_\phi B'_r = u'_r B'_\phi$$

For an axially symmetric field with $B'_\theta = 0$ this completely specifies $\vec{B}$ in terms of $u_r(r)$ and the function $F(r)$. Since $\vec{\nabla}\cdot\vec{B} = 0$, we find

$$\begin{aligned} B'_r(r,\theta) &= B_0(a,\theta)\left(\frac{a^2}{r^2}\right) \\ B'_\phi(r,\theta) &= \frac{\Omega[r-F(r)] \sin\theta \, B_0(a,\theta) a^2}{u_r(r) r^2} \end{aligned} \qquad \text{(III.31)}$$

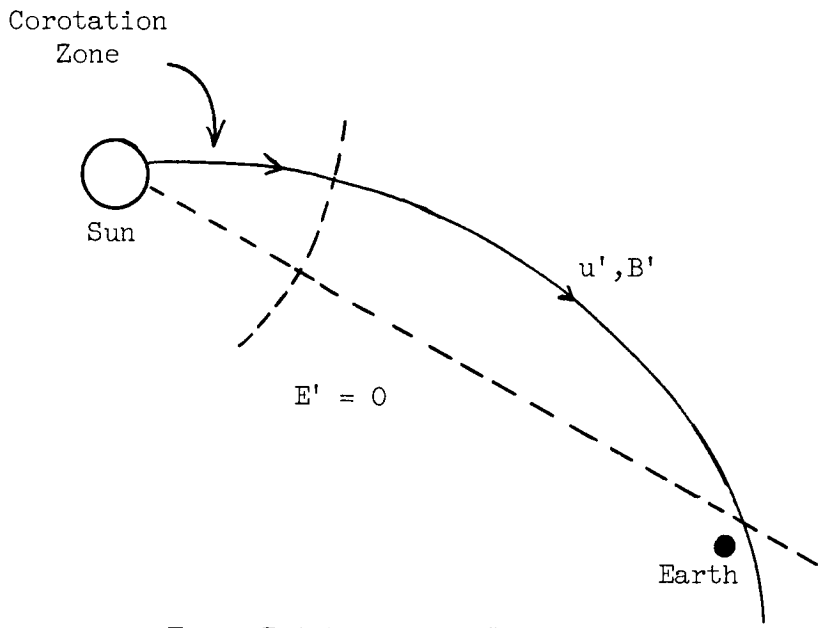

Frame Rotating with Sun

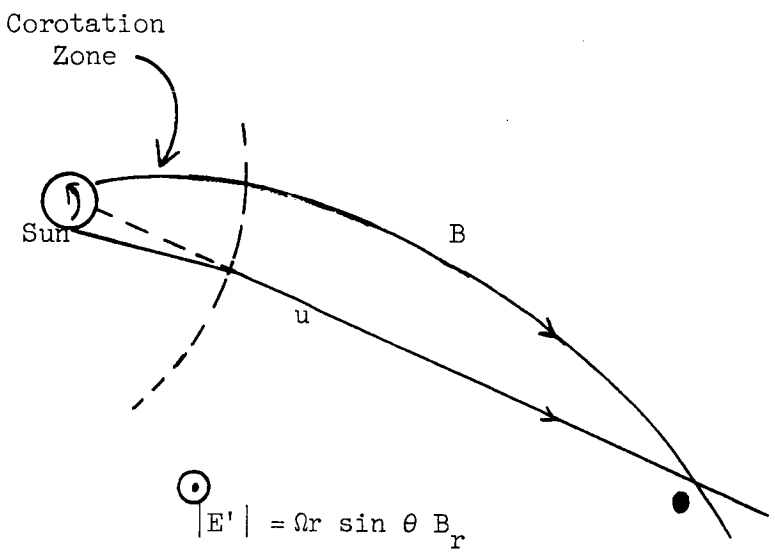

Figure 9. Inertial Frame

The field and flow configuration is shown in Fig. 9. If $B' = 1$ gauss at $r = a = 1.06\ R_\odot$ and $u(1\ \text{A.U.}) \simeq 400$ km/sec , then $B'_r \simeq 2.5 \times 10^{-5}$ gauss , $B'_\phi \simeq 2.7 \times 10^{-5}$ gauss at the earth (assuming $F(r) \ll r$ at $r = 1$ A.U.) .

It remains to transform Eqs. (III.30), (III.31) into an inertial system to facilitate comparison with observations. To order u'_ϕ/c we use

$$u_\phi = u'_\phi - \Omega r \sin\theta$$

$$B_\perp = B'_\perp \ , \qquad B_\parallel = B'_\parallel \tag{III.32}$$

$$E_\perp = E'_\perp - \frac{\Omega r \sin\theta}{c} B'_\perp$$

Note that non-relativistically $\vec{B}$ is an invariant, but since the source of B rotates with respect to an inertial observer, this observer sees the unipolar induction field $\vec{E} = -(\vec{u} \times \vec{B})/c$. The field arises to maintain the Galilean invariance of the Lorentz force $(\vec{E} + (\vec{u} \times \vec{B})/c)$, and it allows the stream to drift across the transverse component of the field B_ϕ with the appropriate local speed. The final equations in the inertial frame are

$$u_\phi(r) = -\Omega F(r) \sin\theta$$

$$B_r(r,\theta) = B_0(a,\theta)\left(\frac{a}{r}\right)^2$$

$$B_\phi(r,\theta) = \frac{\Omega[r-F(r)] \sin\theta\ B_0(a,\theta) a^2}{r^2 u_r(r)} \tag{III.32}$$

$$E_\theta(r) = -\Omega r \sin\theta\ B_0(a,\theta)\left(\frac{a}{r}\right)^2$$

and the new configuration is shown in the bottom section of Fig. 9.

The function $F(r)$ is inserted to account for the possibility that the large magnetic pressure gradients may force the corona to corotate with the sun in some complex fashion. If no corotation occurs, then

$F(r)$ is simply given by the form needed to conserve angular momentum, $F(r) = a^2/r$, and this obviously satisfies $F(a) = a$, $F(r) \ll r$, $r \gg a$. Other semi-empirical expressions have been considered. Parker (1958) discussed the case of strict corotation out to $r = b$ ($F(r) = r$, $a < r < b$; $F(r) = b^2/r$, $r > b$) with $b \simeq 20\ R_\odot$, and other authors have suggested that corotation might occur out to $(50 - 100)R_\odot$.

The magnetic pressure gradient terms are modified by the solar rotation since B_ϕ no longer vanishes. The expression for $(\vec{F}_B)r$ is

$$(\vec{F}_B)_r = - \frac{1}{8\pi} \frac{\partial}{\partial r} (B_\phi^2)$$

if azimuthal symmetry is assumed, and in the lower corona $(r < 10\ R_\odot)$ this is to be compared with $\partial(n\kappa T)/\partial r$. We have seen that $B_r^2/8\pi$ remains large to $n\kappa T$ in this region but this does not contribute to the radial momentum equation. However,

$$\frac{B_\phi^2}{8\pi} = \left[\frac{\Omega[r - F(r)]}{u_r(r)}\right]^2 \frac{B_r^2}{8\pi}$$

does appear in the radial equation and this could require considerable modification of the flow. To examine this, we note that

$$\frac{B_\phi^2}{8\pi} < \frac{\Omega^2}{r^2 u_r^2} B_0^2 a^4 \simeq \frac{n(r)}{u_r(r)}$$

For the solar wind, $u(r)$ increases smoothly and $n(r)$ falls rapidly so that even if corotation is ignored, $\partial(B_\phi^2/8\pi)/\partial r$ decreases rapidly in the inner region where $\beta < 1$. However, if we have "subsonic" flow, then $n(r)$ does not decrease so quickly beyond r_c, and $u_r(r)$ becomes very small just beyond r_c (see Figs. 4 and 8). In this case, the spiral field "wraps up" just beyond r_c, and $(\vec{F}_B)r$ is large, in a region where the magnetic energy density still dominates. Thus, for the slow solutions, the magnetic corrections must be extremely important. While it has not been demonstrated that no self-consistent

field-plasma configuration is possible, such a configuration would be very different from the predictions of Eqs. (III.21) and (III.22) unless the corona is in the solar wind state. The interaction of the rotating corona with the distorted solar field is generally believed to be the mechanism which insures that the streaming corona becomes a supersonic solar wind.

Chapter III. REFERENCES

S. Chapman, Smithsonian Contribution to Astrophysics, 2, 1, 1957.

E. N. Parker, Astrophys. J., 128, 664, 1958.

L. Spitzer, Jr., Astrophys. J., 116, 299, 1952.

H. Zirin, Smithsonian Contrib. to Astrophys., 2, 13, 1957.

J. Chamberlain, Astrophys. J., 131, 47, 1960.

J. Chamberlain, Astrophys. J., 133, 675, 1961.

L. Noble and F. Scarf, J. Geophys. Res., 67, 4572, 1962.

E. N. Parker, Planet. and Sp. Science, 9, 461, 1962.

C. de Jaeger, Space Research III, (North-Holland Pub. Co., Amsterdam), 1963.

E. N. Parker, Astrophys. J., 139, 72, 93, 1964.

L. Noble and F. Scarf, Astrophys. J., 138, 1169, 1964.

F. Scarf and L. Noble, Astrophys. J., 141, 1478, 1965.

Y. C. Whang and C. C. Chang, J. Geophys. Res. (in press), 1965.

General References

Parker, Inter. Dynam. Processes

LeGalley and Rosen, Space Physics

see previous lists

IV. INTERPLANETARY PLASMA AND FIELD MEASUREMENTS

In recent years it has become possible to make direct measurements of the interplanetary plasma and magnetic field by sending instruments aloft on probes or earth satellites with high apogee orbits. These experiments are difficult to carry out and many gaps in our knowledge remain. In this section the problems, the experimental techniques and the observations will be summarized briefly.

IV.1. General Problems of Interplanetary Plasma Measurements

Many diagnostic techniques are available for use with the laboratory plasma, but only a few of these have been applied in interplanetary space because of the special difficulties which are encountered there. Typical parameters anticipated for the solar wind at 1 A.U. are $u \simeq 400$ km/sec , $T_i \simeq T_e \simeq 2 \times 10^5 °K$, $n_e = n_i \simeq 5$ cm^{-3} , and we will use these numbers to discuss the magnitudes of the quantities to be measured.

Let us first consider the ratio of thermal or random velocities to the flow speed, u . If $\kappa T_e = (1/2) m_e a^2$, $\kappa T_i = (1/2) m_i A^2$, then we find $a = 2480$ km/sec , $A = 57$ km/sec , so that $A \ll u \ll a$. Thus, the ion stream is highly directed while the electrons are almost isotropic. This disparity is even more striking when energies are considered. The ion drift energy is 840 ev with $\kappa T_i \simeq 17$ ev . The electrons also have $\kappa T \simeq 17$ ev , but the drift or directed energy is less than 0.5 ev .

Because of these differences, the proton and electron currents to be measured are not the same. The proton current density in the wind is primarily convective with

$$j_p^{(0)} = \frac{neu_p}{c} = 3 \times 10^{-12} \frac{\text{esu}}{\text{cm}^2} = 3 \times 10^{-11} \frac{\text{amp}}{\text{cm}^2} \qquad \text{(IV.1)}$$

This is, of course, a very small directed current density and not easy to measure under any circumstances. On the other hand, the isotropic electrons in the solar wind can deliver a maximum current density on the order of (Jastrow and Pearse, 1957)

$$j_e^{(0)} = -\frac{ne}{c}\frac{\pi}{4}a$$

$$= 1.55 \times 10^{-10}\ \frac{\text{amp}}{\text{cm}^2} \qquad \text{(IV.2)}$$

(Note that the convective part of j_e is the same as (IV.1); Eq. (IV.2) represents the current delivered to a conducting surface.)

Actually, these numbers represent an impossible current distribution, since in the steady state the net current delivered to the spacecraft must vanish. If these currents were the only ones present, more electrons than protons would be acquired in any time period, and the spacecraft would develop a negative potential, $(-\phi)$. This would accelerate protons, reject the lower energy electrons, and balance the two currents at the spacecraft surface, with

$$u_p' = \sqrt{\frac{\pi\kappa T_e}{2m_e}} \int_{|e\phi|}^{\infty} \sqrt{\frac{E}{\kappa T_e}}\ \frac{dE}{\kappa T_e} \exp(-E/\kappa T_e)\ ,$$

$$\frac{m_p u_p^2}{2} + |e\phi| = \frac{m_p u_p'^2}{2} \qquad \text{(IV.3)}$$

Since the proton drift energy is large compared to κT_e, it is customarily assumed that the proton speed is almost unmodified by ϕ. In this case, $u_p' \simeq u_p$ and ϕ is determined by solving the integral equation

$$\int_{|e\phi|/\kappa T_e}^{\infty} dx\ x^{1/2} \exp(-x) = u_p \sqrt{\frac{2m_e}{\pi\kappa T_e}} \simeq \frac{1}{5.5}$$

This gives $|e\phi| \simeq (2 - 3)\kappa T_e$, showing that the high energy tail of

the electron distribution is sufficient to balance the ion current, so that only a fraction of the electrons arrive at the spacecraft, and these have speeds which are strongly modified by the electric field, $\vec{E} = - \vec{\nabla} \phi$.

The idealized potential distribution is given by Eq. (I.10), if the ion flux remains undistorted, and we then have a sheath region surrounding the spacecraft with $\phi \simeq - (2 - 3)\kappa T_e/e \simeq - (40 - 60)$ volts , and a radius on the order of $\ell_D = 6.9(T_e/n_e)^{1/2} \simeq 28$ meters . Thus, it would appear to be very difficult to measure solar wind electrons, although on the basis of the above discussion, no difficulties seem to be present for proton measurements, aside from the anticipated small currents.

Actually, several other complications are present. The one which is most well-understood is associated with the intense solar ultraviolet flux which is capable of ejecting photoelectrons from the spacecraft. Since the solar wind must be measured in sunlight, this effect is always present, and it has been estimated (Bonetti, et al., 1963) that the photoelectron current may be as large at 10^{-8} amp/cm^2 . (This depends to some extent on the nature of the spacecraft surface.) The photoelectrons flow outward over the sunlit part of the spacecraft, and the net inward positive current is then the sum of the proton current and the photoelectron current. This effect tends to make the spacecraft less negative and it may, in fact, acquire a net positive potential.

Other uncertainties arise because active sources of spacecraft potential bias may be present. Exposed wires in solar paddle circuits may collect excess numbers of electrons, and gas jets for attitude stabilization may produce varying charges by frictional electrification. Finally, it seems likely that plasma oscillations in the ambient medium can drastically perturb the sheath. The sheath size is a highly nonlinear function of the spacecraft-plasma potential difference, and therefore all of these effects can be quite significant.

The difficulties associated with measurement of the solar plasma can be summarized as follows:

(a) The anticipated proton current densities are extremely small, and since strong photoelectron currents occur when the probe looks at the sun (or solar wind), a serious source of contamination is present.

(b) The electron current is certainly seriously modified by sheath effects, which are influenced by photoelectrons and other sources of bias.

(c) Although the ion flux at the probe is not generally expected to be strongly modified by sheath effects, the non-linearity of the sheath and the possible existence of unknown sources of sheath scattering, focusing, etc., degrade the interpretation of these measurements.

Before turning to a discussion of the actual techniques and observations, it is worth noting that the same ambiguities and complications must be taken into account when one wishes to describe the interaction of the solar wind with any other boundary such as the lunar surface, the magnetosphere boundary, or even the chromosphere. In all of these cases, large deviations from quasi-neutrality must occur, and charge separation plays an important role in order to balance the currents. In fact, Parker (1963) has recently noted that, near the coronal base, separation of species with different values of q/m can produce a significant amount of coronal heating.

IV.2. Techniques and Observations

One of the simplest instruments used to measure solar plasma characteristics is a detector which might be called a retarding potential analyzer, a two-element ion trap, or a Faraday cup. This elementary configuration has a single retarding grid and a collector plate, as shown in Fig. 10a. Since the instrument is physically small compared to the Debye length, there is no difficulty in separating electrons and protons by biasing the grid with respect to the spacecraft (i.e., the bias field is shielded as $\exp(-k_D r)$, but this

produces a negligible correction). When a potential $V_G \lesssim -17$ volts is applied to the grid, all electrons are rejected and most ions enter (the grid transmission is not 100%) with negligible energy shifts. The collector is now biased positively with respect to the spacecraft, but if $V_c < (1/2)m_p u^2$, the protons still strike the plate. The retarding voltage V_c is then increased in some preassigned manner, and when V_c approaches $(1/2)m_p u^2$, the collector current begins to fall. As V_c is increased further, only the high energy tail of the Maxwell distribution contributes to the current, and the temperature may be extracted from the $j(V_c)$ curves, as shown in Fig. 10b.

The flux, $J = nu = I/eA$, where A is the effective collector area, is actually the total flux of all particles with $u_\perp > (2eV_c/m_p)^{1/2}$ where $u_\perp$ is the component of $\vec{u}$ perpendicular to the retarding plate. Thus, at any fixed V_c, this instrument yields an integral energy spectrum, and if the beam comes in off-axis, or is hot, geometric corrections are needed.

Actually, such a simple configuration would have essentially no chance of detecting the proton flux in the solar wind because of the large current of photoelectrons generated when the solar ultraviolet strikes the collector. To correct for this, a suppressor grid is generally inserted between the entrance grid and the collector. When this is biased at an appropriate negative voltage, most photoelectrons are returned to the collector, yielding a much smaller net photo current. However, in this three-element ion trap, solar radiation reflected from the collector can strike the suppressor, and liberate additional photoelectrons which then flow back to the collector. Three-element ion traps of this type are thus capable of measuring solar plasma, but they are relatively insensitive with J (threshold) $\simeq (1 - 2) \times 10^8$ protons/cm^2 sec. However the first interplanetary plasma measurements on Lunik I, Lunik II, Lunik III, and Venus I (see Table IV.1) were carried out with these instruments.

The Soviet observations are summarized by Bonetti, et al. (1963). On Lunik II, a flux of positive ions with $J \simeq 2 \times 10^8/\text{cm}^2$ sec, $E_p = (1/2)m_p u^2 > 15$ ev was found beyond $r = 39\ R_e$ (the probe was

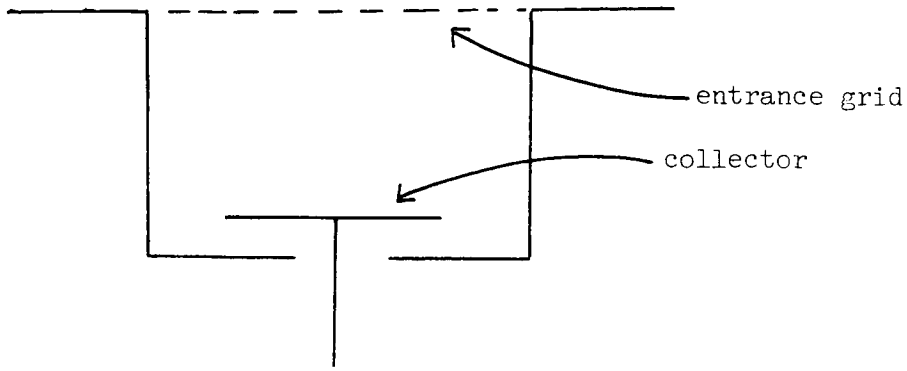

Figure 10a. Two-Element Ion Trap or Retarding Potential Analyzer

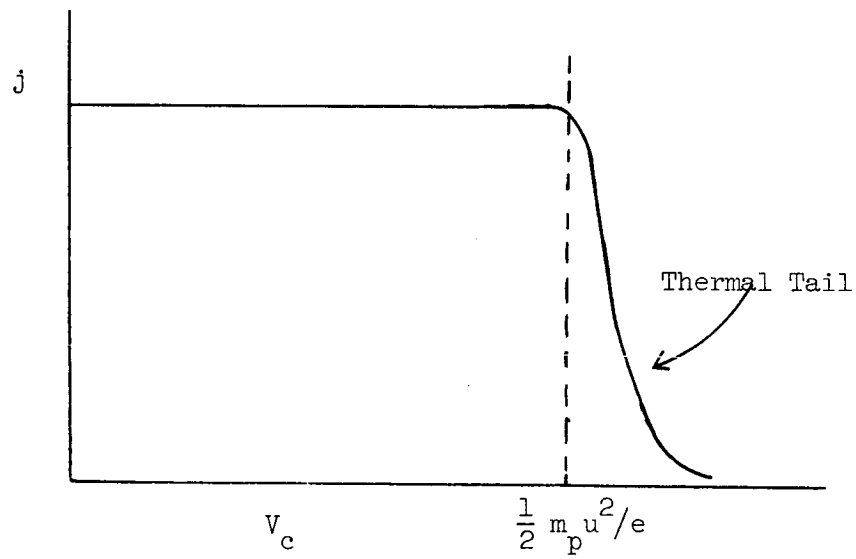

Figure 10b. Current-Voltage Characteristic

TABLE IV.1. INTERPLANETARY FIELD AND PLASMA EXPERIMENTS

Designation	LaunchDate	Orbit	Complement	Comments
Lunik I	1-2-59	heliocentric	3 element ion trap	Insensitive
Lunik II	9-12-59	moon impact	3 element ion trap	Insensitive, intermittent response
Lunik III	10-4-59	barycentric R = 291,000 miles	3 element ion trap	Insensitive, intermittent response
Pioneer 5	3-12-60	heliocentric	search coil magnetometer	$B_\perp$ only
Venus 1	2-12-61	heliocentric	3 element ion trap	Same as Lunik I, II
Explorer 10	3-25-61	geocentric R = 145,000 miles	AC Cup Rubidium vapor filled fluxgates	Not interplanetary, transition region protons detected
Explorer 12	8-15-62	geocentric R=48,000 miles	Analyzer CdS detector triaxial fluxgate	Not interplanetary, analyzer failed, transition region electrons detected
Mariner 2	8-26-62	heliocentric	Analyzer triaxial fluxgate	Attitude stabilized, $\simeq 100\ \gamma$ spacecraft field
Explorer 14	10-2-62	geocentric R=61,000 miles	Analyzer triaxial fluxgate	Generally not interplanetary or transition region
Explorer 18 (IMP-1)	11-26-63	geocentric R=122,000 miles	AC Cup Analyzer ion trap Rubidium vapor tilted fluxgates	Conflicting plasma results, magnetic bias small
Vela 3,4	7-17-64	geocentric R=69,000 miles	Analyzer search coil	Large magnetic spacecraft bias, $B_\perp$ only
OGO-1	9-4-64	geocentric R=93,000 miles	Analyzers AC Cup ion traps Rubidium vapor	Rubidium vapor failed to deploy, $B_\perp$ only, plasma results apparently conflicting
Explorer 21	10-3-64	geocentric R=59,000 miles	Same as IMP-1	Conflicting plasma results, magnetic bias small

fired away from the sun and presumably did not emerge into interplanetary space until r exceeded $30\ R_e$n) , and on Lunik III a single observation at $r = 20\ R_e$ (in the solar direction) revealed a flux of $4 \times 10^8/cm^2$ sec , $E_p > 20$ ev , but no flux above background was detected thereafter. The probe on Venus I was apparently even less sensitive (perhaps because this solar probe outgassed completely, while the Lunik may not have, so that higher photon fluxes were present) and the only plasma measurement reported was a burst of flux with $J \simeq 10^9/cm^2$ sec at $r = 297\ R_e$.

The M.I.T. plasma probe (Bonetti, et al., 1963) designed for the Explorer 10 flight is a device which resembles an ion trap, but several important modifications are incorporated to suppress the photocurrents and increase the sensitivity, with attainment of a minimum detectable flux on the order of $4 \times 10^6/cm^2$ sec . The instrument, usually called a Faraday cup, contains four grids and a collector. The entrance grid is maintained at the spacecraft potential and, as before, the final grid is maintained at a negative potential (-130 volts) to reflect collector photoelectrons. The second or modulator grid potential is varied by a square wave signal with a frequency of 1400 eps . Six different amplitudes were used for Explorer 10: 5 , 20 , 80 , 250 , 800 and 2300 volts.

The basic idea of the probe operation is that when the square wave varies between 0 and, say, 800 volts, the ion current hitting the collector varies between $J(E_\perp > 0)$ and $J(E_\perp > 800$ ev) (assuming singly ionized particles only). Thus, the output current is a constant $[J(E_\perp > 800$ ev)] plus a square wave modulated signal $[J(800$ ev $> E_\perp > 0)]$. By detecting and amplifying only the modulated part of the current (using a filter or synchronous detector), only the flux corresponding to the energy range 800 ev $> E_\perp > 0$ is recorded. At the same time, the photocurrents are suppressed. The currents generated in the collector-suppressor region are unmodulated and hence filtered out. (To ensure this lack of modulation, the third grounded grid is inserted between the modulator and suppressor; this reduces capacitative coupling.) Photoelectrons generated before the suppressor are rejected by the -130 volt bias.

Unfortunately, the orbit of Explorer 10 was such that it penetrated the transition region (see Fig. 2), but not interplanetary space; although apogee was near 43 R_e, the satellite went out along the evening magnetosphere boundary, and it had no solar paddles so that only one pass was possible. Nevertheless, Explorer 10 did detect plasma of solar origin, modified by the interaction with the distorted geomagnetic field. The observed flux varied between threshold, $4 \times 10^6/cm^2$ sec, and $3.5 \times 10^8/cm^2$ sec with a mean value near $1.5 \times 10^8/cm^2$ sec; the mean streaming energy seemed to be near 420 ev ($u \simeq 285$ km/sec) and the temperature ranged from 3×10^5°K to 8×10^5°K.

The next spacecraft to carry plasma detectors was Explorer 12. The payload included a cadmium sulfide (CdS) crystal energy flux detector sensitive to energy fluxes exceeding 1 erg/cm^2 sec ster (electrons with $E > 200$ ev, protons with $E > 1$ kev), and an electrostatic analyzer. The analyzer did not operate properly, and the spacecraft never penetrated past the transition region (see Table IV.1). However, in the transition region, the CdS detector found large fluxes of electrons ($J \simeq 10^{10}/cm^2$ sec, $E_e > 1$ kev) which presumably are produced by the interaction of the solar wind with the geomagnetic field (Freeman, 1964).

The Mariner 2 spacecraft, launched into solar orbit on August 26, 1962, had on board a JPL electrostatic proton analyzer, which gave the first strong and direct evidence for the existence of a continuous solar wind. This type of instrument differs considerably from the ion trap, and a typical configuration (for IMP-1) is shown in Fig. 11. The streaming plasma enters in the small slit ($A \simeq 0.5 - 1$ cm^2), and a voltage, V_a, is maintained across the analyzer plates. The quantity V_a is then varied in some predetermined manner, and the positive ion current to the collector is recorded as a function of V_a. Only a charged particle with $E = q V_a \pm (\Delta E/2)$ will follow the curved path between the analyzer plates, and thus the detector inherently gives a differential energy spectrum. Sensitivity to solar ultraviolet is eliminated by blackening the analyzer plates, and

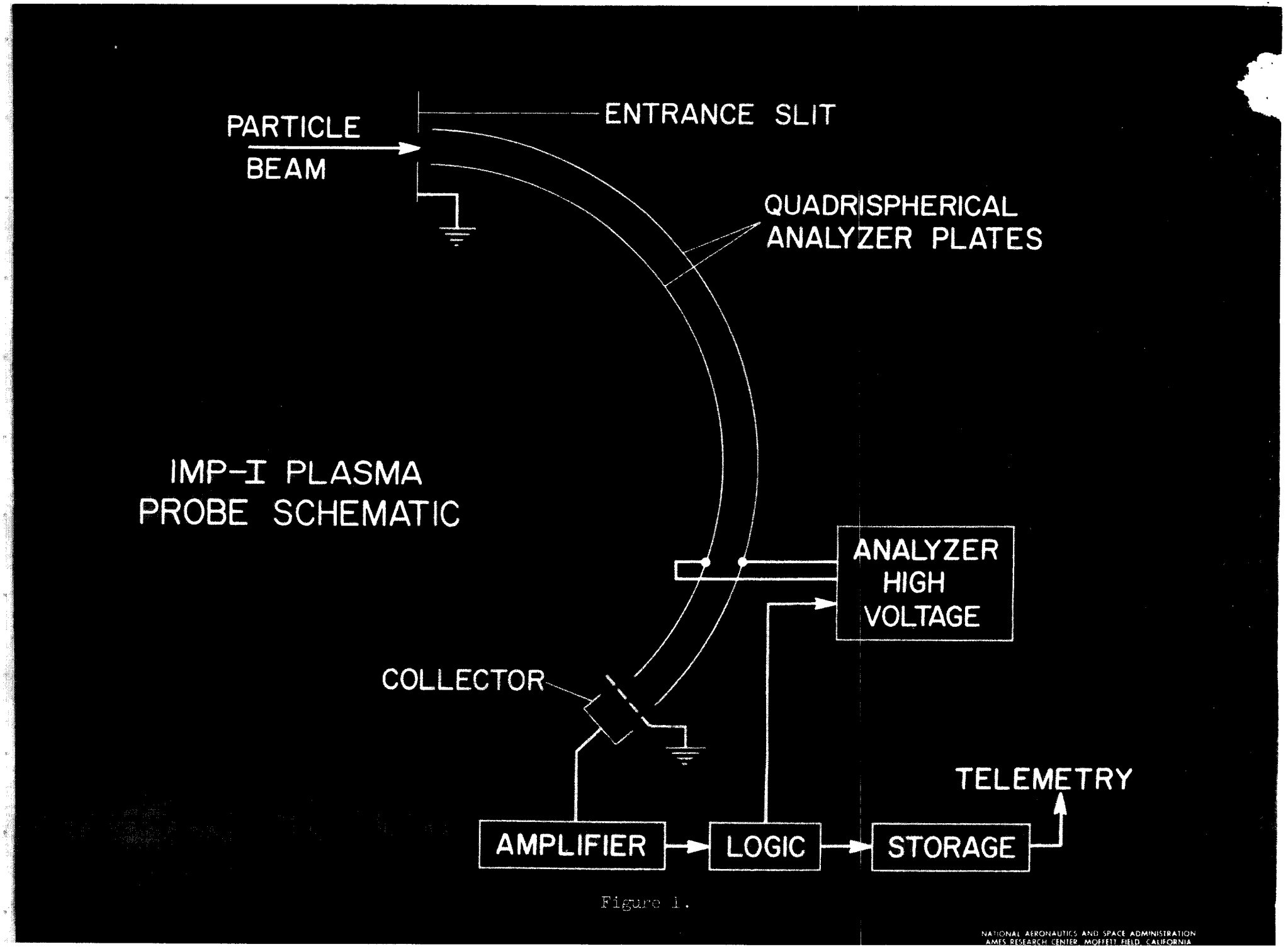
PARTICLE
BEAM
ENTRANCE SLIT
QUADRISPHERICAL
ANALYZER PLATES
IMP-I PLASMA
PROBE SCHEMATIC
ANALYZER
HIGH
VOLTAGE
COLLECTOR
TELEMETRY
AMPLIFIER
LOGIC
STORAGE
NATIONAL AERONAUTICS AND SPACE ADMINISTRATION
AMES RESEARCH CENTER, MOFFETT FIELD, CALIFORNIA

Figure 1.

sometimes a negative suppressor grid is inserted before the collector. These instruments typically have sensitivity ranges from 3×10^5 to $10^{10}/cm^2$ sec , over an energy range from 250 ev to about 20 kev . A disadvantage of a single channel analyzer is that when limited telemetry is available, it is impractical to have enough energy windows to cover completely the energy spectrum in a reasonable time. Since the window width, ΔE, is generally on the order of $6 - 10\%$ of E for fixed V_a , the measurements are therefore customarily performed with wide gaps between energy windows.

Thus, the Mariner 2 analyzer only measured positive ions with $E/q \simeq 231$, 346 , 516 , 751 , 1124 , 1664 , 2476 , 3688 , 5408 and 8224 electron volts. Furthermore, Mariner 2 was attitude stabilized and the 40,000 energy spectra obtained were all essentially one dimensional, with the probe pointing within 0.1^o of the sun. Aberration corrections have been applied and an attempt was made to sort out the doubly charged alpha particles $(E_\alpha = 2eV_a)$ from the high energy tail of the singly charged proton distribution. It was concluded (Snyder, Neugebauer and Rao, 1963) that the solar wind is always present with $300 \text{ km/sec} < u < 800 \text{ km/sec}$. The measured currents were generally consistent with densities ranging from 0.5 to $10/cm^3$, and the one dimensional temperature varied from $6 \times 10^4 °K$ to $5 \times 10^5 °K$ for 90% of the spectra. The Mariner 2 data also show that long-lived activity centers on the sun (M-regions) are associated with recurrent increases in streaming speed.

The Mariner plasma experiment was definitive in the sense that it confirmed the existence of a continuous solar wind, yet the measurements were really rather incomplete with respect to the energy spectrum, etc. When an analyzer with a narrow aperture and wide energy gaps is used to determine the characteristics of a cool streaming ion current, it may happen that the narrow peak will fall outside of any window, so that only currents near background $(I \simeq 10^{-13} - 10^{-14}$ amp or $J \simeq 10^5 - 10^6/cm^2$ sec) associated with the tail of the distribution, are detected. It is scarcely better if the narrow peak falls near a window, since any small fluctuation in $|\vec{u}|$ then causes the current to rise or fall exponentially; this is especially serious for an

attitude stabilized spacecraft because an angular fluctuation can also produce large current changes. Furthermore, it is necessary to assume a value of $\vec{u}$ in order to compute the aberration correction, which must then be related to the observed spectrum in a self-consistent manner. For the Mariner 2 experiment, this analysis was complicated by the choice of energy windows. That is, windows were not set at V_1, $2V_1$, V_2, $2V_2$, ..., and it was therefore difficult to detect protons with $V = E_p/e$ and alpha particles having the same speed, or $V' = E_\alpha/q_\alpha = 2E_p/e$.

For these reasons, the pioneering measurements on Mariner 2 were difficult to analyze, and many questions remained to be answered. It is therefore of considerable interest to examine data from subsequent experiments. The next spacecraft to be launched with a plasma probe was Explorer 14 (see Table IV.1). Although apogee was 16.5 R_e, the initial line of apsides made an angle of 72° with respect to the sun-earth line on the dawn side of the earth, and the apogee position steadily precessed around toward the geomagnetic tail. Thus, the spacecraft generally did not encounter solar, or even transition region, plasma.

However, on the fourth outbound orbit (October 7-8, 1962), the earth encountered a storm previously detected on Mariner 2, and for a period of 27 minutes, the NASA-Ames electrostatic analyzer (Wolfe and Silva, 1965) measured the characteristics of the interplanetary plasma. The data are particularly interesting for several reasons. First, Explorer 14 was spin stabilized and crude angular information was obtained. Second, a logarithmically decreasing voltage was applied across the analyzer plates so that the instrument continuously covered the energy range from 18,000 down to 200 ev/unit charge with a cycle time of about three minutes (energy resolution ~ 10%). Since the sweep period was not an exact integral multiple of the spin period, the streaming plasma was not observed at precisely the same window on successive sweeps, and this allowed the gaps between the windows to be filled in. Finally, this same storm was observed on Mariner 2 some 4 – 5 hours earlier, and it therefore was possible to have an independent check on Mariner data reduction techniques.

The Explorer 14 interplanetary spectrum for eight energy scans is shown in Fig. 12. The plasma came from the solar direction, and assuming that the primary peak at 1000 ev is due to protons alone, the resulting storm density is 94.1 protons/cm^3, with $u = 437$ km/sec. If the secondary peak at 2000 ev is primarily due to doubly charged helium with the same bulk velocity, then the resultant density is 8.7 alphas/cm^3, and the helium to hydrogen ratio is 0.092. The corresponding Mariner 2 spectrum is quite similar.

The next spacecraft which carried plasma probes into interplanetary space was unique in several respects. Explorer 18, or IMP-1, was launched in November, 1963, with a four-day orbit having initial apogee at 31.5 R_e near the subsolar point. Thus the spacecraft initially spent most of its time in interplanetary space, and there was at least some interplanetary penetration until pass 24, three months after launch. Moreover, the payload included both a NASA-Ames electrostatic analyzer with 14 energy windows (250 ev to 16 kev; $\Delta E/E \sim 6 - 9\%$; $J_{min} \simeq 3 \times 10^5/cm^2$ sec) and an M.I.T. Faraday cup with six windows (45 ev to 5.4 kev, for protons in five channels plus a 65 – 210 ev electron channel, $J_{min} = 6 \times 10^6/cm^2$ sec). Both probes were modified versions of the earlier Explorer detectors. Because of limited IMP telemetry, the analyzer angular scan was quantized into three roughly equal segments, with sector 2 centered on the solar direction and the boundary between sectors 1 and 3 in the antisolar direction. The cup modulation differed from the Explorer 10 format in that the square wave was varied from V_1 to V_2 (instead of 0 to V) in order to obtain $J(V_2 > eE > V_1)$. The positive ion channels were 45 – 105 ev, 95 – 235 ev, 220 – 640 ev, 560 – 2000 ev and 1700 – 5400 ev and the electrons and positive ions were collected on separate segments of a split plate. For the analyzer, the complete energy scan in a single angular sector took 36.5 seconds, but a complete energy and angular span cycle required five minutes and 28 seconds. However, for the cup an angular distribution in one energy channel required only about 3.5 sec, but the complete energy scan required 2.8 minutes (Wolfe, Silva and Meyers, 1965; Bridge, Egidi, Lazarus, Lyon and Jacobson, 1964).

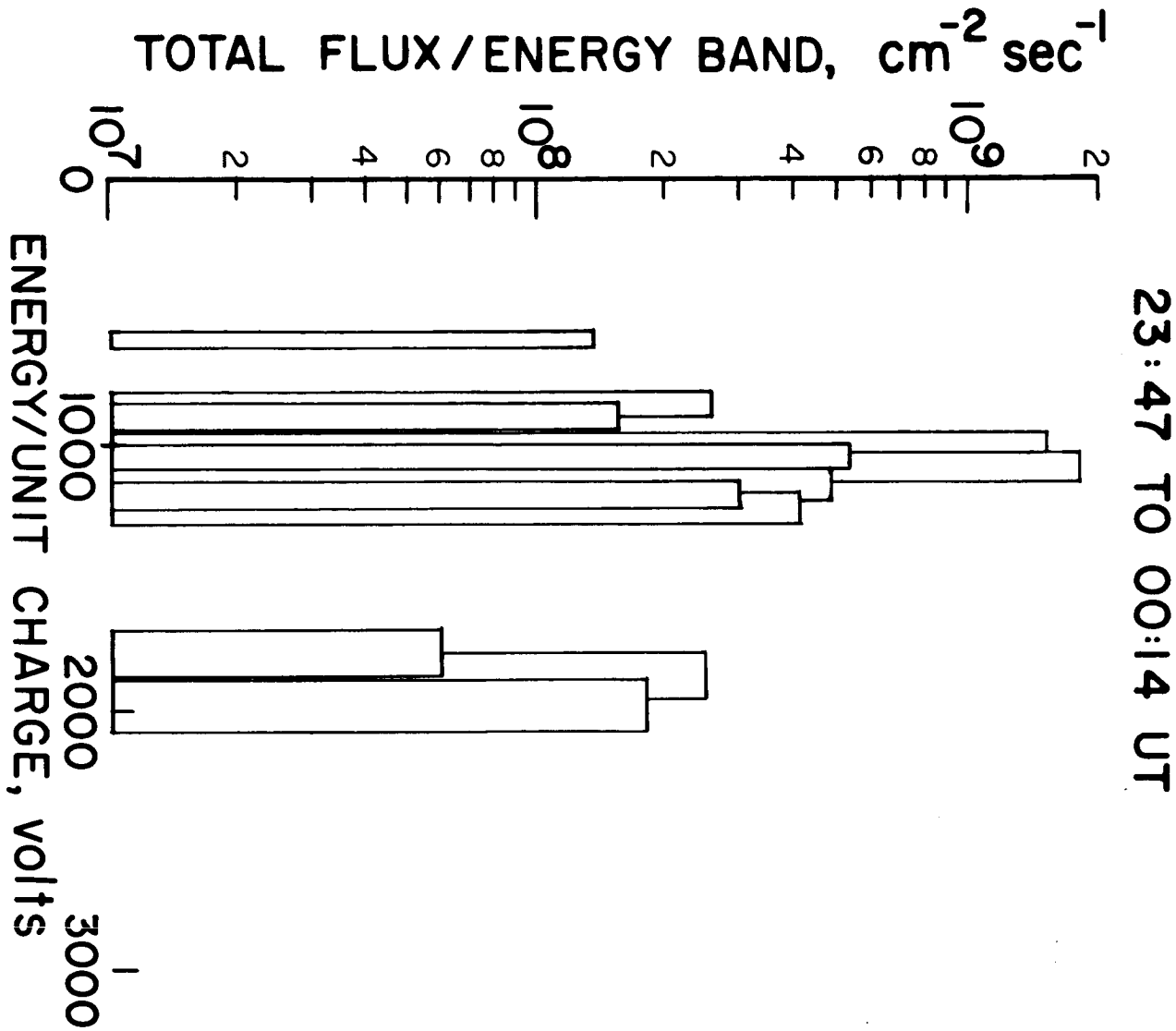

Figure 12 - page 77

The reason for going into this much detail about the instrumentation is quite simple; the data from the two plasma probes do not agree. Although the extent of the disagreement is quite moderate in interplanetary space (compared to the violent conflict in the transition region and magnetosphere, which will be discussed later), the differences are nevertheless striking and undoubtedly significant. The average solar wind velocity as determined by the IMP-1 analyzer was 378 km/sec , while the cup average was 319 km/sec . Moreover, the two groups report different ranges of variability. The M.I.T. probe indicated $250 \text{ km/sec} < u < 440 \text{ km/sec}$ as typical values, while the analyzer yields $250 \text{ km/sec} < u < 700 - 800 \text{ km/sec}$. Finally, the densities derived from the cup response are consistently higher than the indicated analyzer densities.

The origin of this discrepancy is not known at present. Since the probes agree when calibrated in the laboratory, it seems clear that some spacecraft sheath or external interference effect in interplanetary space causes a wide aperture AC probe and a narrow aperture DC probe to respond differently when exposed to the same plasma. It is not difficult to think of specific phenomena which could contaminate one probe or the other (e.g. a large amplitude density ripple associated with electrostatic plasma oscillations via Poisson's equation could broaden the effective cup window if the wave frequency were near 1.4 kc/s) but it is dangerous to speculate on the bias mechanism in the absence of any additional information. This discrepancy is presently a source of serious concern and various laboratory and spacecraft experiments are planned to analyze the difficulty.

The fact that the two kinds of probes disagree was confirmed upon launch of IMP-2 (Explorer 21). Although apogee was less than that of Explorer 14, the line of apsides was initially in the solar direction and the solar wind conditions apparently produced a smaller magnetosphere and transition region while IMP-2 was aloft. At any rate, during the first 25 passes, IMP-2 generally penetrated interplanetary space for part of the orbit. The payload contained somewhat modified versions of the IMP-1 probes, and again the cup and analyzer yielded different results.

During this time interval, the second launch Vela probes were also in orbit, and each of these carried a Los Alamos electrostatic analyzer. One of these usually operates in an electron mode while the other detects positive ions. No solar wind electrons have been detected to date, but this is not surprising in view of the sheath difficulties discussed earlier, and high energy windows. However, in the proton mode the Vela analyzer obtains both energy and angular distributions and these can be compared with the interplanetary observations on IMP-2. It is of considerable importance to make this comparison, since the Vela and IMP-2 experiments are carried out under quite different conditions. In particular, the spacecraft are not the same size and shape, and the surfaces are not of the same material. Thus, if sheath effects produce the discrepancies, then the Vela and IMP analyzers should perhaps require distinct corrections. Secondly, the spin axes of the two spacecraft are not the same so that any needed geometrical corrections should differ. Finally, the IMP and Vela analyzers have different time constants, different cycling periods, different energy windows and ranges, and even different detection techniques (current measurement for IMP versus particle counting for Vela). Thus, agreement between the Vela and IMP analyzer response would tend to indicate that none of these effects is related to contamination.

Figure 13 shows simultaneous Vela and IMP-2 interplanetary spectra, normalized in 5200 ev and 5500 ev channels, respectively (Wolfe, Silva and Meyers, 1965). It can be seen that the two curves agree extremely well, that the hydrogen and helium peaks are quite distinct, and that the curve deviates from a Maxwell-Boltzmann distribution only in the slight non-thermal tail which represents less than 1% of the total ion density. Furthermore, the Vela angular distribution is consistent with $T = 2 \times 10^5 °K$, the same value which can be used to fit the observed points (S. Bame and I. Strong, private communication).

The Vela plasma probes supply another point of interest. Although the results are quite preliminary, the data seem to be compatible with the deduction that the mean value of $\vec{u}/|\vec{u}|$ is not simply given by an aberration correction for radial flow; the deviation may be as much as two degrees (i.e., $u_\phi/u_r = -\tan 2° = -.0349$). For $\bar{u}_r \simeq 400$ km/sec ,

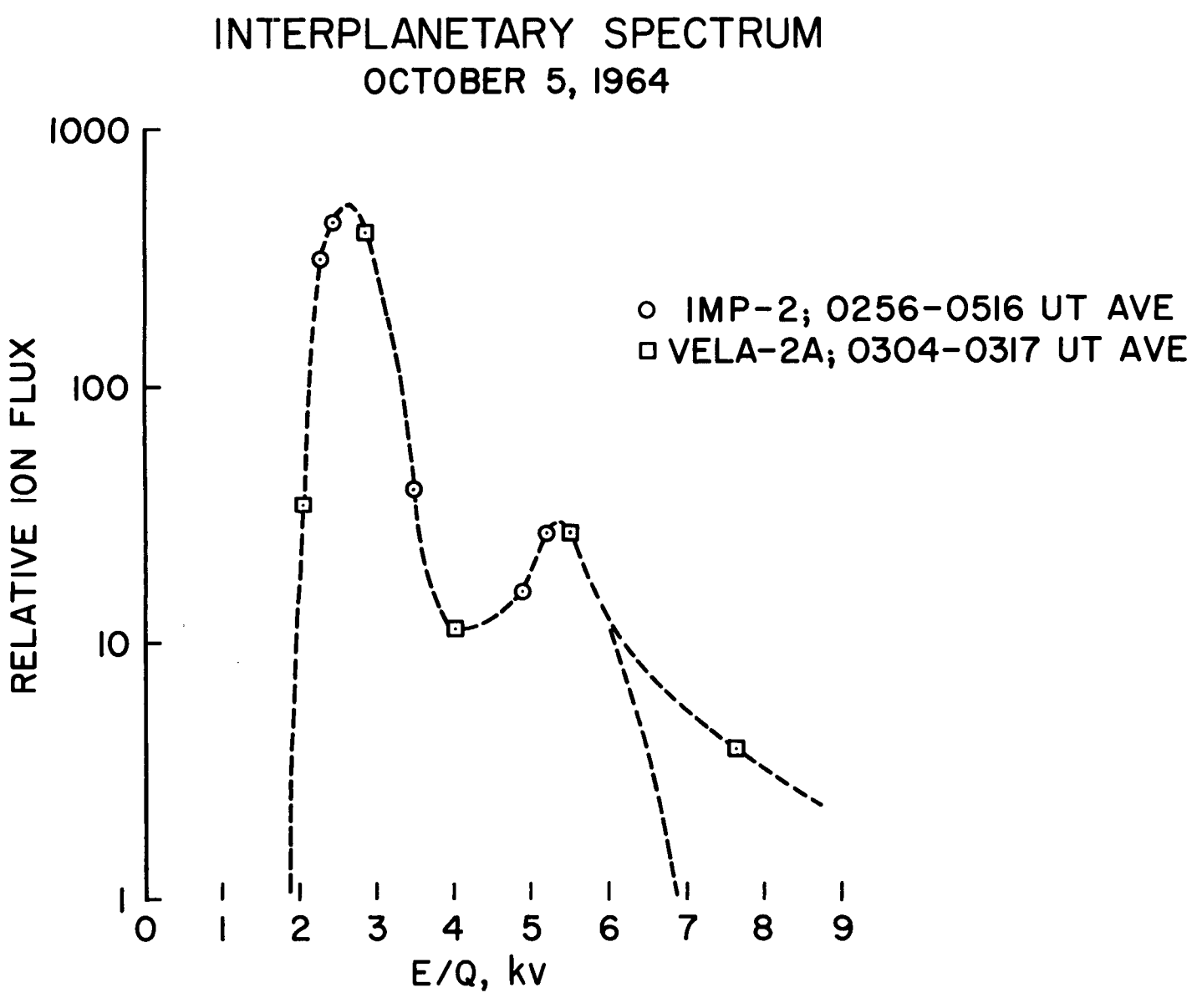

Fig. 13

A-34307-2

NATIONAL AERONAUTICS AND SPACE ADMINISTR
AMES RESEARCH CENTER MOFFETT FIELD CALIF

$|u_\phi|$ is then 14 km/sec . Assuming $F(r) = r$, $r < b$, $F(r) = b^2/r$, $r > b$, for $\theta = \pi/2$ we find

$$\frac{b^2}{r^2} = \frac{u_\phi}{\Omega r}$$

or $b \simeq 0.187$ A.U. $\simeq 40\ R_\odot$. While this number is not to be regarded as well founded, it is clear that any significant deviation from radial flow implies that coronal corotation is quite important.

We conclude that Parker's theory of the continuous solar wind is well verified by direct observation, but it is clear that further study of the actual distribution functions and their variation must await resolution of the experimental controversy.

IV.3. Interplanetary Field Measurements

It has been noted that, in a sense, a spacecraft in orbit in interplanetary space resembles a small boat proceeding in the ocean; only one point in space-time is sampled, and any attempt to chart the current, or magnetic field, is full of difficulty and ambiguity. Small fluctuations and irregularities mask the main circulation, and long range correlations are almost impossible. For these reasons, it seems likely that the most general confirmation of Parker's magnetic field model will not be derived from spacecraft measurements.

In fact McCracken's analysis (1962) of the arrival on the earth of energetic particles from solar flares, sunspot groups, etc., gives perhaps the best information on the interplanetary magnetic field. McCracken found that when an active sunspot group is on the far western portion of the solar disk, the magnetic lines of force connect it to the earth. The direction of earth impact was analyzed by examining the angular distributions and arrival times of groups of particles with various energies. Since $(\vec{E} + \vec{u}_{s.w.} \times \vec{B}/c) \simeq 0$, if the particles are superthermal $(|\vec{u}| \gg u_{s.w.})$ then $\vec{u} \times \vec{B} \simeq 0$, and the particles are guided along the interplanetary field, they can spiral around the field, as shown in Fig. 14. McCracken found an earth impact angle consistent with Parker's hose angle $(B_\phi/B_r = \tan \chi$, $\chi \simeq 45 - 50°)$, but the degree of isotropy for particles arriving at the earth was higher than anticipated for a regular spiral field. It was concluded that considerable disorder exists, and that the particles are scattered from small scale irregularities.

Actually, spacecraft measurements of the interplanetary $\vec{B}$ field were already available when McCracken's work was published, but the data analysis was still incomplete. Pioneer 5, launched toward Venus on March 12, 1960, had on board a search coil magnetometer. This type of sensor is an iron core coil rotating with the spacecraft and thus using the satellite's spinning motion to generate in the coil a sinusoidal EMF proportional to the component of ambient field along the coil axis. (This is usually designated as $B_\perp$ since it is perpendicular to the

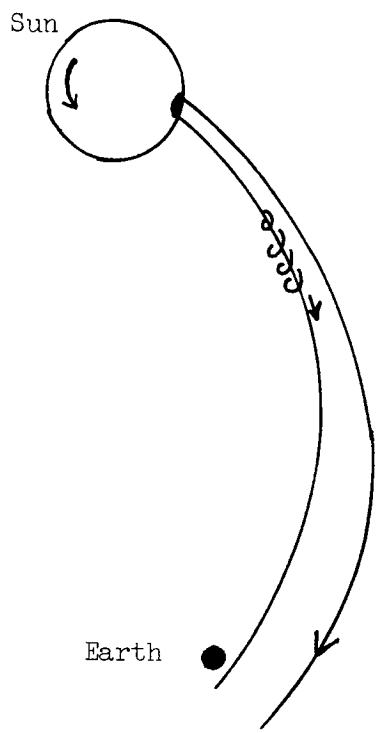

Figure 14

spin axis.) The phase $\phi = \tan^{-1}(B_x/B_y)$ of the field can also be determined by means of an aspect indicator (sun sensor plus timer), but this system which could have yielded the orientation of $\vec{B}_i$ with respect to the ecliptic did not operate on Pioneer 5.

The coil output was rectified, amplified according to a nonlinear response curve, digitized and telemetered to earth. Approximately 21,000 individual readings were taken during a 56-day period. The distribution of all points in interplanetary space is shown in Fig. 15. In order to interpret this, it is necessary to know the direction of the spin axis. For Pioneer 5, the spin vector was very nearly in the ecliptic plane and so oriented as to sweep from about 25 degrees east to 25 degrees west of the sun-satellite line during the data period. Since a large fraction of the individual transmissions showed the sharp peak near 2.7 γ indicated in Fig. 15, it was initially concluded (Coleman, et al., 1960) that the persistent return to around 2.7 γ implies that "1) the total ambient field vector must have remained nearly constant in magnitude and uniform in direction over the data period (in an inertial frame); 2) only field vectors of galactic origin or normal to the ecliptic would have been consistent with the measurements; and 3) total field magnitude must have been close to the measured figures."

This interpretation was made before the confirmation of the existence of the solar wind, and it seemed to rule out Parker's model, which required a spiral-like field in the ecliptic plane. In fact, this interpretation of the Pioneer 5 data was erroneous. Greenstadt (1965) spent several years analyzing the results and he fortunately chose to use the median, and other distribution percentiles, rather than the field reading with maximum density (the mode), for his statistical analysis. It was found that a temporal change in most percentiles occurred, and Greenstadt attributed this to the changing geometry of the spin axis, with respect to the probe-sun line. Using only subgroups of data associated with the same range of magnetic conditions on the earth (A_p or K_p) he tried to find the field configuration which would best fit the measured decline. The results

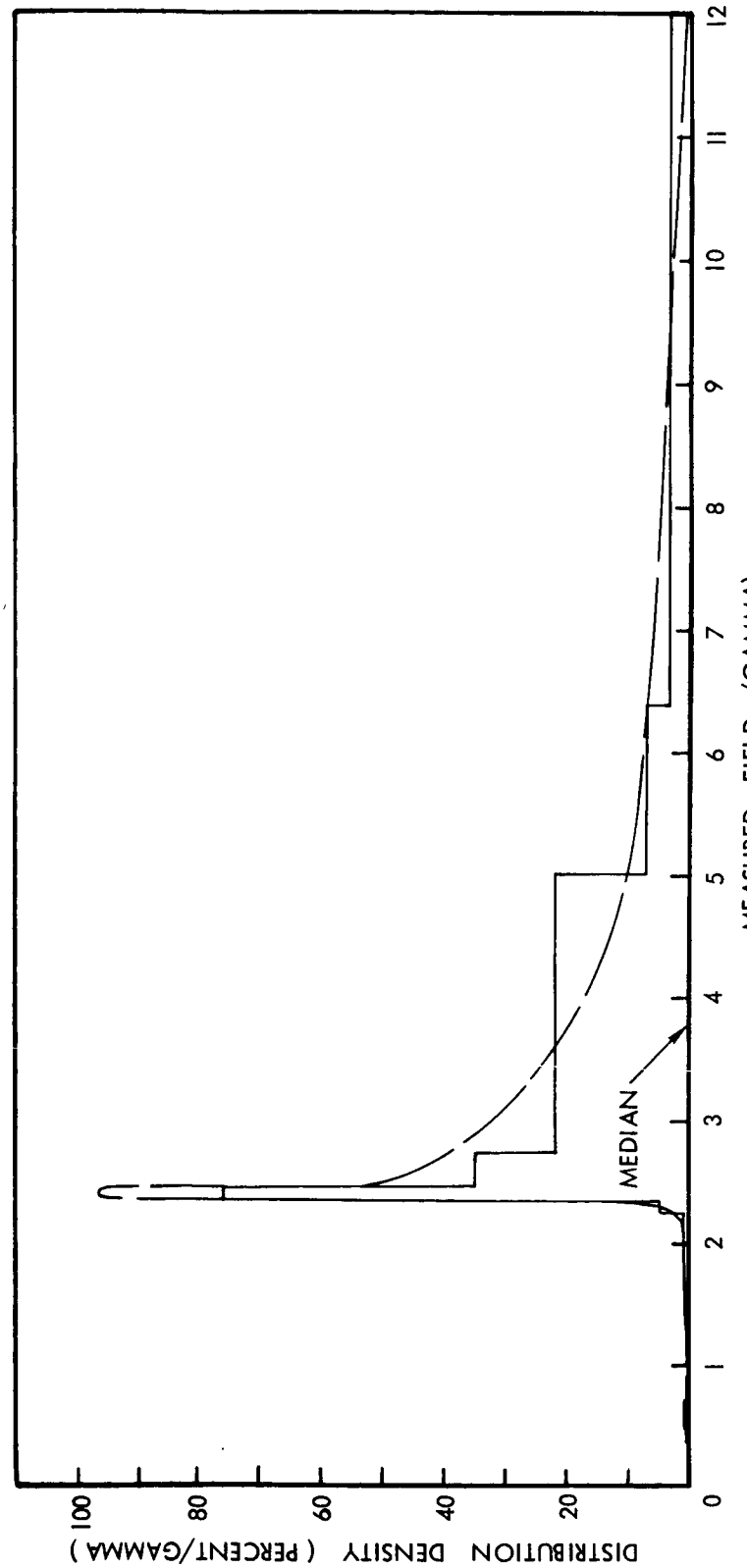

Figure 15. Pioneer V Magnetometer, Density Distribution of all Data in Interplanetary Region.

for median $|\vec{B}|$ are, in gamma:

	10 percentile	median	90 percentile
Calm	3.5	4.9	6.9
Disturbed	3.8	6.0	9.7

The mean hose or spiral angle was $45°$ and the mean vector was within $15°$ of lying in the ecliptic plane. The angular distribution of all best fit solutions is shown in Fig. 16, and it is clear that Parker's model is well verified.

Greenstadt's analysis avoided use of the peak near $2.7\ \gamma$, but some explanation for this was offered. Several sources of error were considered, and some were discarded (ambient field behavior, spacecraft contamination at ω_s, binary malfunction). The most likely source of this disparity is a calibration error which would attribute too narrow a window to each of the two windows near $2.7\ \gamma$, and hence too high a relative frequency. This can explain the observed distribution mode completely.

The next interplanetary probe to carry magnetometers was Mariner 2. The payload included triaxial fluxgate magnetometers which gave a complete vector field measurement each 37 seconds. This type of instrument is very different from a search coil, and the sensing element is usually a hollow cylinder of high permeability magnetic material surrounded by primary and secondary windings. The primary is driven (at say $5 - 10$ kc) so that the core saturates on each half cycle, but the point at which saturation occurs is shifted asymmetrically by any steady magnetic field component along the sensor axis. This produces in the secondary higher harmonics of the primary frequency and the amplitude of the second harmonic is approximately proportional to the field strength along the axis.

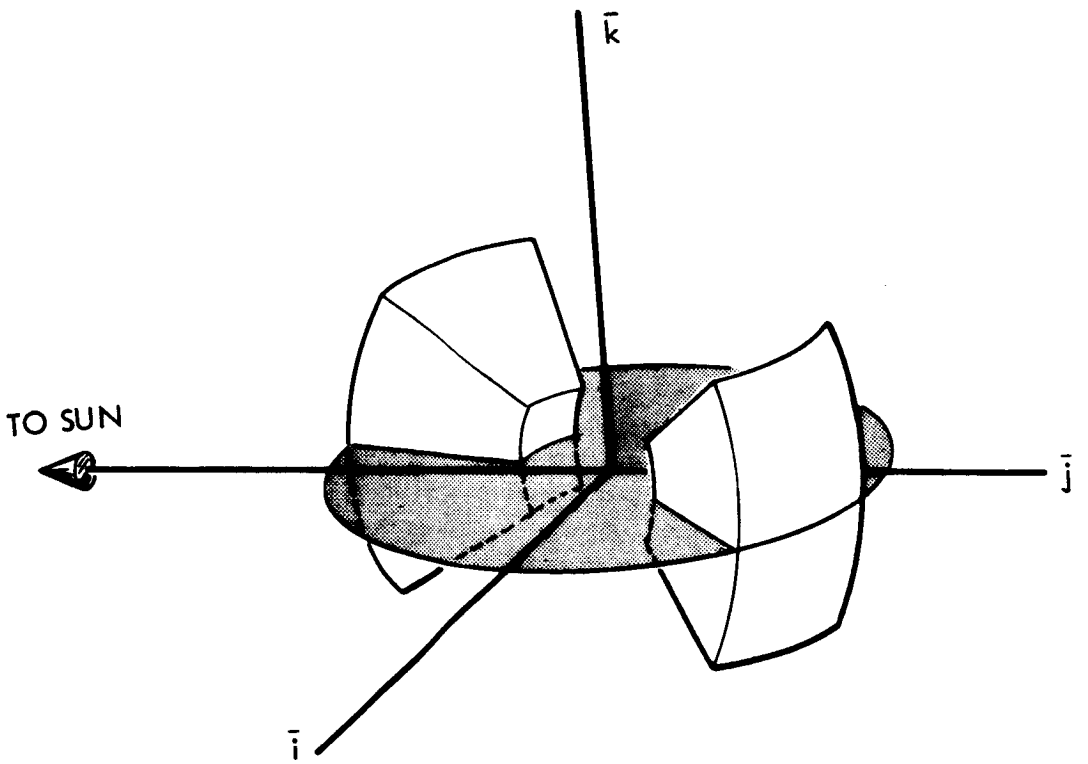

Figure 16. Pioneer V Magnetometer, Regions of Space Occupied by Best Fit Solution Vectors in i, j, k Frame of Figure IV-68.

The Mariner system had three fluxgates mounted at right angles, with one parallel to the attitude stabilized probe-sun line (the z-axis). Two dynamic ranges were possible ($0 - 64\ \gamma$ and $64 - 320\ \gamma$) ; however, this experiment was beset by difficulties associated with the spacecraft field. During the first $3 - 4$ days, Mariner was spin-stabilized about the z-axis, and the perpendicular ($B_x - B_y$) interplanetary field component was roll modulated while the spacecraft field was not. (The post-launch spacecraft field is generally not the same as the pre-launch value, which can be brought down to zero.) This enabled the experimenters to determine the $B_\perp$ contamination within $1\ \gamma$, but B_z (spacecraft) was never measured. Moreover, it is thought that $B_\perp$ (spacecraft) did not remain constant during the flight, and estimates of bias field as high as $100\ \gamma$ have been given (Smith, 1964).

Nevertheless, useful information was obtained. Smith has shown that $\Delta B_y / \Delta B_z \simeq 1$ which is consistent with an estimated average magnitude of $5\ \gamma$ at the Parker hose angle. The average value of ΔB_x (normal to the ecliptic) vanished, and large disorder in $\vec{B}$ was again found.

In many ways, the best interplanetary field experiment was carried out by Ness, et al. (1964) on IMP-1. Very stringent magnetic controls were imposed on the spacecraft and the experiments, and the three magnetometers were mounted on booms. In its worst ("permed") state, the bias field at the magnetometer was less than $12\ \gamma$, and IMP-1 was launched with minimum permanent or induced magnetic fields. The payload included a rubidium vapor magnetometer mounted on a boom along the spin axis and a pair of nonaxial fluxgates, mounted on opposite equatorial plane booms and tilted by $30°$ and $60°$, respectively, with respect to that plane.

The rubidium vapor magnetometer measures the absolute value of $\vec{B}$ by measuring the Zeeman splitting of the ground state of the atom. For the rubidium 87 isotope, the separation between adjacent levels is $6.996\ \text{cps}/\gamma$. One of the levels ($^2S_{1/2}$, $m = 2$) is selectively populated by optical pumping, and light is absorbed until this level is

filled. The gas cell then becomes transparent. However, if a weak magnetic AC field with $\omega = \omega_c = eB/mc$ is imposed, the population is redistributed to all levels, and the incident light is again absorbed. It is possible to couple the modulated light output to the coil producing the weak magnetic field in such a way that the system operates as an oscillator with $f = eB/2\pi mc$. In this feedback configuration the output frequency yields $|\vec{B}|$. By imposing additional known bias fields, it is also possible to obtain $\vec{B}$.

These magnetometers are not easy to operate on a satellite. The pumping lamp must be lighted (this doesn't always happen) and active thermal controls (i.e., heating coils) are required to stabilize the temperature.

The tilted IMP-1 fluxgates were used to supplement the rubidium vapor measurements. If we consider a fluxgate tilted at an angle α ($= 30°$ or $60°$) to the spin axis, in the presence of a field with fixed $B_\perp$, $B_\parallel$, then the instantaneous field along the sensor axis is

$$B_s = B_\parallel \cos\alpha + B_\perp \sin\alpha \cos\phi$$

where $\cos\phi$ gives the projection of $\vec{B}_\perp$ on the sensor axis-spin axis plane. If $B_\parallel$ and $\vec{B}_\perp$ remain fixed as the spacecraft rotates, then we have

$$B_s(t) = B_\parallel \cos\alpha + B_\perp \sin\alpha \cos(\omega_s t - \psi)$$

where ω_s is the spin frequency (22 – 24 rpm for IMP-1) and ψ is a phase angle with respect to some fixed direction (the probe-sun line on IMP-1, as indicated by an optical aspect sensor). Since α and ω_s are known, it is, in principle, possible to analyze $B_s(t)$ to obtain $B_\parallel$, $B_\perp$ and ψ, and hence to reconstruct $\vec{B}$. The analysis procedure of Ness, et al., was based on numerical treatment of the derivatives of the detector output current, assuming that the above relation is valid.

Of course, there are monumental loopholes in such a procedure, since it assumed that the output current only varies because the spacecraft spins. However, if $B_\perp = B_\perp(t)$, $B_\parallel = B_\parallel(t)$, $\psi = \psi(t)$, with frequency components near ω_s , this procedure fails completely. For instance, if $\vec{B}_\perp = 0$, $B_\parallel = B_1 + B_2 \cos \omega_s t$, this instrumentation falsely interprets the field at $\vec{B} = B_1 \vec{i}_\parallel + B_2 \vec{i}_\perp$. Thus, the tilted fluxgate arrangement yields a vector field only when the field is quiet or steady on a time scale, $2\pi/\omega_s$. Fortunately, this appears to be generally true in interplanetary space (with the exception of storm periods) but it seems that in the magnetosphere and transition region a tilted fluxgate arrangement cannot be used to obtain field vectors.

The spacecraft field after launch was examined by comparing the results of the three magnetometers. The fluxgate magnetometer zero levels were then to be calibrated on the basis of the absolute response of the rubidium magnetometer. It was found that fluxgate A data ($\alpha = 60°$) and the rubidium data agreed within $0.25\ \gamma$, while fluxgate B had a zero offset of $-2.1\ \gamma$. Ness, et al., assumed that the spacecraft field (which presumably is not the same at the equatorial plane and along the spin axis boom) was less than $0.25\ \gamma$, and fluxgate B was accordingly adjusted to agree with the others. However, Dessler has recently pointed out that certain features of the resulting data suggest that the spacecraft field may indeed have been $-2.1\ \gamma$ at fluxgate B, so that fluxgate A would then need to be offset. At any rate, there are at least two possible ways to reduce the data, and since the total field is generally less than $5\ \gamma$, the final results can be quite different.

A histogram of the IMP-1 field strength measurements is shown in Fig. 17. The median field of $4.95\ \gamma$ is very close to the Pioneer 5 "calm" value, which should be expected, since IMP-1 was in orbit during a very quiet period. The angular distributions are shown in Fig. 18. It can be seen that the ϕ distribution is quite broad, although it is clearly peaked near the Parker "hose" angles of $45°$, $225°$. However, the origin of Dessler's criticism can be seen

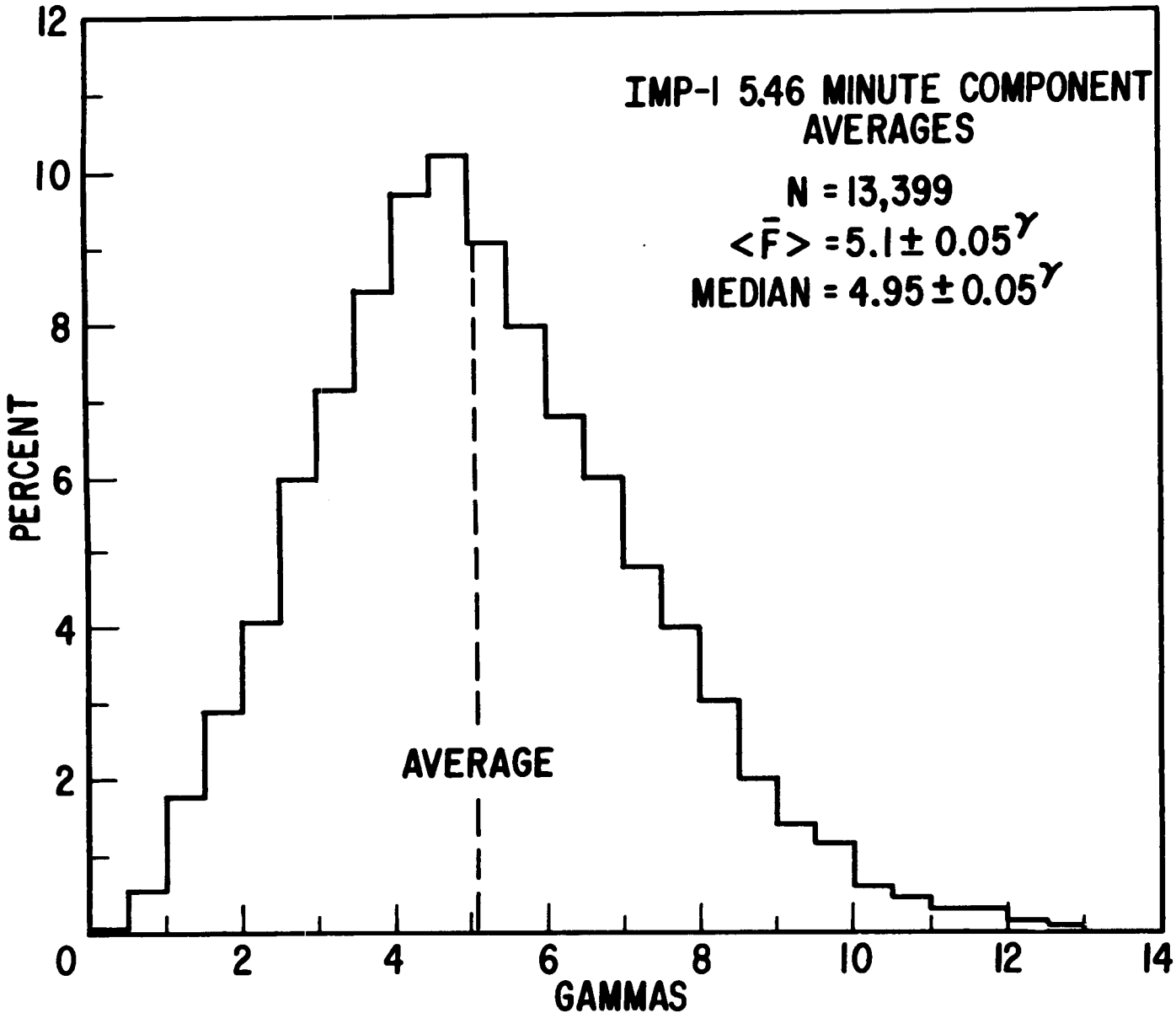

Figure 17. Statistical distribution of the interplanetary magnetic field magnitude for the same data corresponding to that shown in Figure 18. The uniformity of the distribution with an average value of 5.1 gammas is indicative of average photospheric fields of the Sun of a few gauss, according to Parker's model.

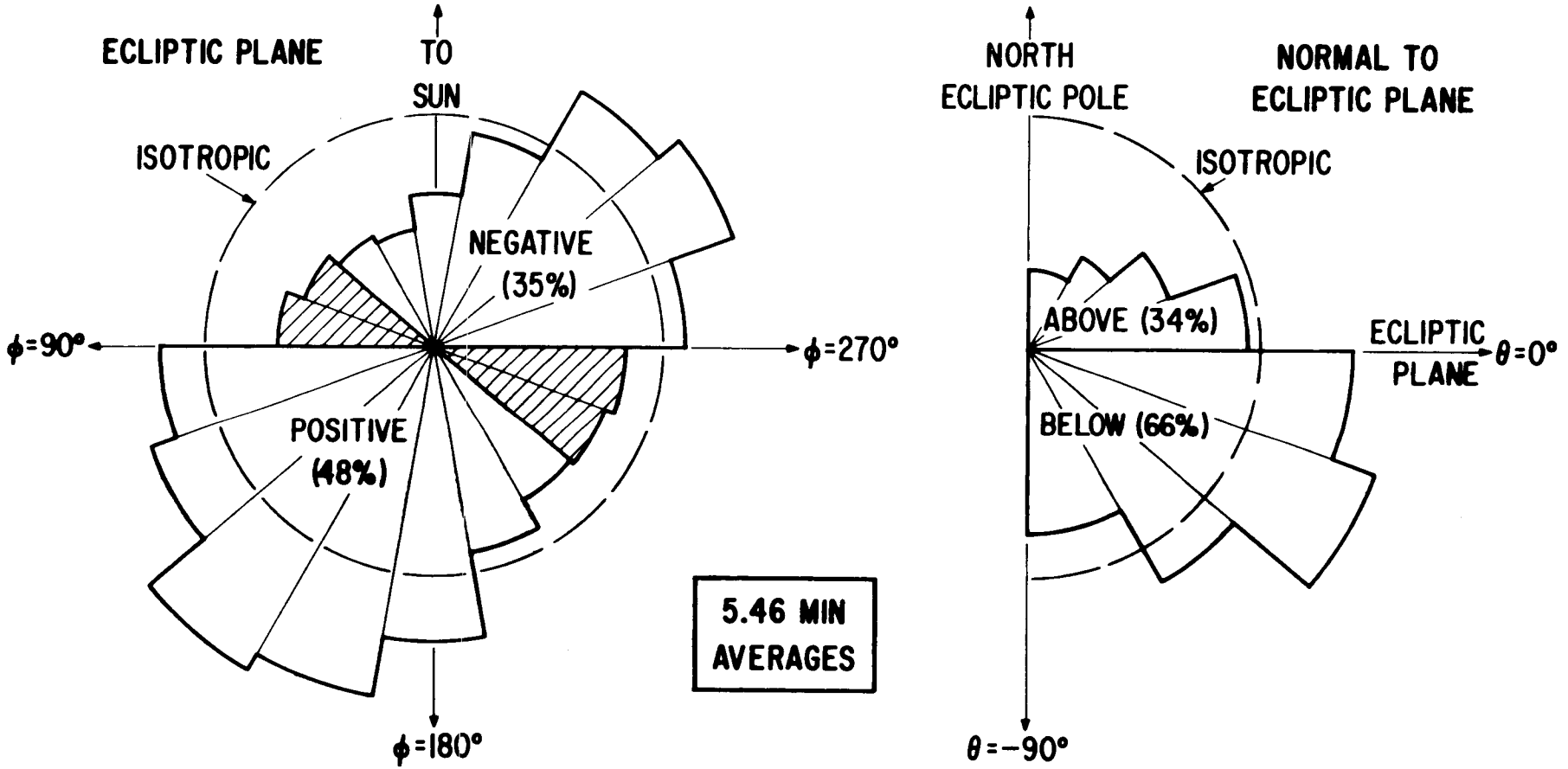

Figure 18. **Statistical distribution of the direction of the 5.46 minute component averaged interplanetary magnetic field as observed on IMP-I during solar rotations 1784-1786. The distribution in the plane of the ecliptic indicates a close correspondence with the theoretical model of a continual uniform solar coronal expansion developed by Parker. The field distribution normal to the plane of the ecliptic indicates a small but distinct southward directed component.**

from the θ -distribution also shown in Fig. 18. The unexpected large tilt below the ecliptic plane and the asymmetry about any given θ could possibly be associated with an incorrect choice for the spacecraft field, based on the fluxgate zero levels. It will be of interest to see how the distributions change if the data are analyzed using the other assumption. It should be noted that the plasma probes gave no indication that $\vec{u}$ (which should be parallel to $\vec{B}$) has an average southward component.

One very valuable result of the IMP-1 magnetometer experiment is independent of the question of spacecraft bias. Ness and Wilcox (1965) investigated the persistence of patterns or sectors in the interplanetary field and they related this to magnetic structure in the photosphere. The quantity which was studied is simply the direction of the field in a plus (outward from the sun) or minus (inward) sense. An autocorrelation of the 12-hour IMP (+) or (-) time series was constructed by combining four three-hour intervals and possible recurrence tendencies in the interplanetary field were investigated. It was observed that the data of the first eight days produced most of the exceptions to the recurrence tendency, but that the field seemed to have a more permanent configuration thereafter. The autocorrelation constructed with omission of data from the first eight days is shown in Fig. 192. It is clear that that directional pattern tends to recur with a 27-day period characteristic of the solar equatorial region. A cross-correlation was also performed between the IMP-1 twelve-hour series and a corresponding series representing the photospheric field, using observations made with the Mt. Wilson Observatory magnetograph. The cross-correlation depends significantly on the solar latitude under observation, and the highest correlation occurs when the interplanetary field is compared with the equatorial photospheric field (see Fig. 20).

It is also noteworthy that the field at the earth is best correlated with the photospheric field which passed the central meridian (i.e., the sun-earth line) 4 1/2 days earlier. This indicates that magnetic irregularities in the photosphere are transported to 1 A.U. with a mean speed of 385 kilometers/sec . This is in striking

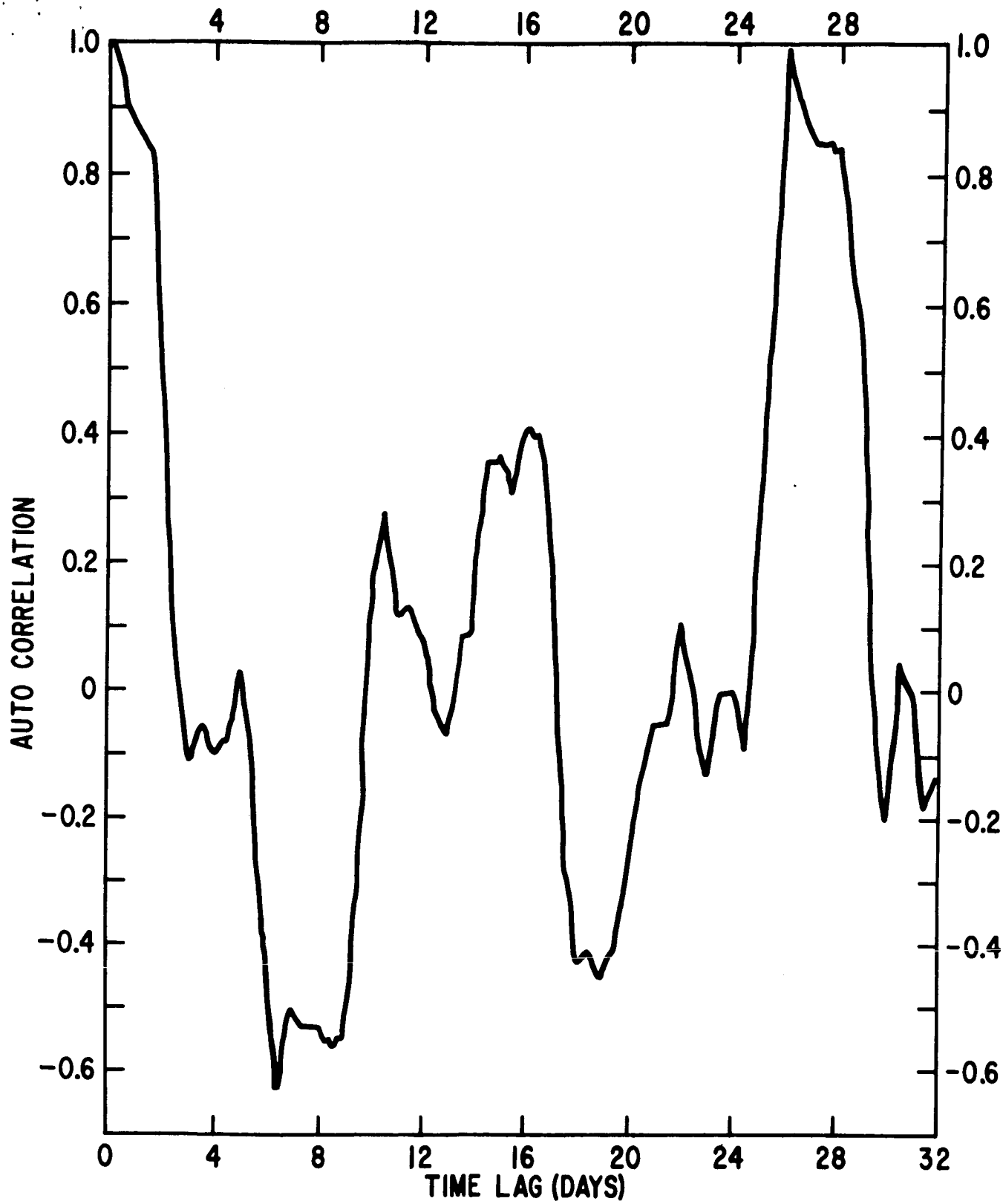

Figure 19. Auto correlation of the direction of the interplanetary magnetic field as observed by IMP-I. The direction of the field is defined to be either positive or negative according to Figure 18. The Auto correlation of this time series yields a significant peak at approximately 27 days.

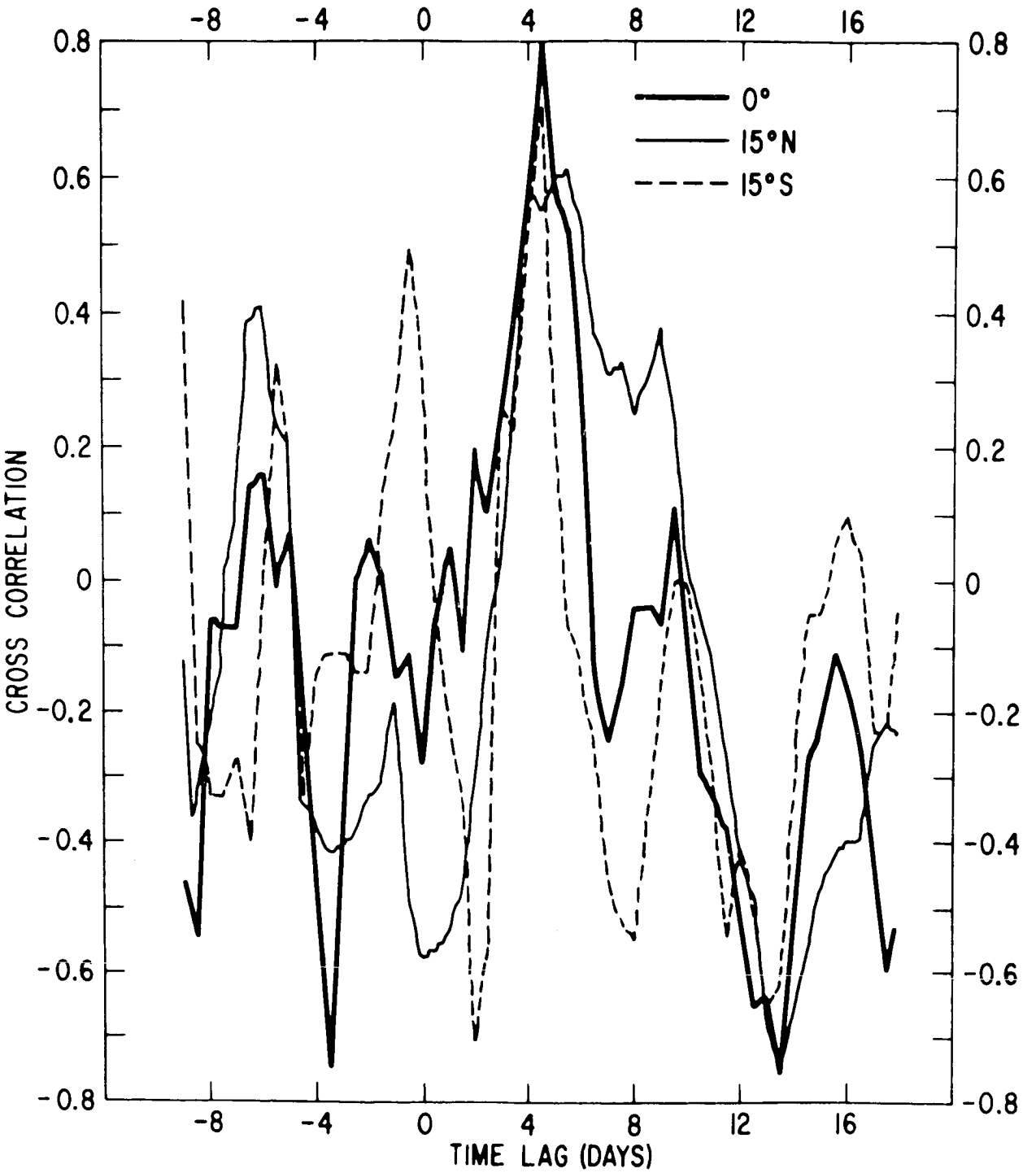

Figure 20. Cross correlation of the IMP-I interplanetary magnetic field data and the photospheric magnetic field for three latitudes illustrating the coherent and statistically significant peak at 4.5 days. This corresponds to a transport velocity of solar lines of flux to 1 AU of approximately 385 kilometers/sec.

agreement with the average value of 378 km/sec deduced on the basis of the IMP-1 analyzer results, but the correspondence with the IM-1 Faraday cup mean streaming speed (319 km/sec) is not so satisfactory.

IV.4. Comments

Great advances have been made in the measurement of interplanetary plasma and magnetic fields, and in a general sense all of the observations strongly support Parker's theory of a continuous solar wind, and an associated distorted spiral field. However, the measurements must be regarded as preliminary ones, at least until questions concerning the plasma probe discrepancies, the spacecraft sheath and the spacecraft magnetic bias are answered. A related problem has to do with the measurement of interplanetary electrons. IMP-1 also had on board a retarding potential analyzer (Serbu, 1964) which should have been capable of detecting isotropic electron fluxes in interplanetary space (energy range $0 - 100$ ev ; $J\ (\text{min}) < 10^7/\text{cm}^2$ sec , when not observing the sun). Although this probe did detect magnetospheric and transition region electrons on the first outbound pass, no interplanetary flux was measured. However, as noted above, if the spacecraft potential was zero or positive, the anticipated electron flux exceeds $3 \times 10^8/\text{cm}^2$ sec , for $T_e = T_i$. It is hoped that some of these questions will be answered by data from future experiments.

Chapter IV. REFERENCES

R. Jastrow and C. Pearse, J. Geophys. Res., 62, 413, 1957.

A. Bonetti, H. Bridge, A. Lazarus, B. Rossi, and F. Scherb, J. Geophys. Res., 68, 4017, 1963.

E. Parker, in The Solar Corona, ed. J. Evans, (Academic Press, New York), 1963.

J. Freeman, J. Geophys. Res., 69, 1691, 1964.

C. Snyder, M. Neugebauer and V. Rao, J. Geophys. Res., 68, 6361, 1963.

J. Wolfe and R. Silva, J. Geophys. Res., 70 (August 1, in press), 1965.

J. Wolfe, R. Silva, and M. Meyers, submitted to J. Geophys. Res., 1965.

H. Bridge, A. Egidi, A. Lazarus, E. Lyon and L. Jacobson, COSPAR, 1964.

J. Wolfe, R. Silva and M. Meyers, COSPAR, 1965.

K. McCracken, J. Geophys. Res., 67, 447, 1962.

P. Coleman Jr., L. Davis Jr., and C. P. Sonett, Phys. Rev. Lett., 5, 43, 1960.

E. Greenstadt, TRW Space Technology Labs. Report 9890-6001-RV000, 1965.

E. Smith, in Space Physics, 1964.

N. Ness, C. Scearce and J. Seek, J. Geophys. Res., 69, 3531, 1964.

N. Ness and J. Wilcox, Goddard Report X-612-65-79, 1965.

G. Serbu, Goddard Report, X-615-64-109, 1964.

V. PROBLEMS IN SOLAR WIND THEORY

The elementary theories of the solar wind (the isothermal-adiabatic model, the conductive heating model) appear to be capable of explaining the main features of the observed flow pattern and magnetic field configuration in the region $3R_0 < r < 215R_0$. In fact, when one takes a second look at the theory and at some of the observations, the basis for this gross agreement becomes less clear, and it is obvious that many problems remain to be solved before the coronal flow pattern is completely understood. In this chapter we wish to enumerate some of the problems and discuss some speculative attempts to solve them.

V.1. Deviations from Spherical Symmetry

It has already been noted that the magnetic pressure gradient terms generally preclude spherically symmetric flow. Other sources of anisotropy are present, and in certain regions of space, they are probably even more important than the above. Specifically, in the luminous region (say, $R_0 < r < 2R_0$), photographs show that rays, filaments, plumes, streamers, prominences, arches, etc., frequently extend up into the corona, and radio astronomy measurements confirm the presence of significant localized irregularities. Moreover, during solar minimum the gross density pattern is not even approximately spherically symmetric, and the equatorial coronal streamers are considerably larger and denser than the polar ones. In fact, it may be proper to describe the lower corona completely in terms of a filamentary model with gas being squeezed up through magnetic nozzles and to perhaps $(2 - 3)R_0$. It has been suggested (L. Davis, Jr., private communication) that such inhomogeneities could be the most important source of the discrepancy between predicted and observed density distributions in the coronal base; and since $B^2/8\pi > n(\kappa T + mu^2/2)$ here, magnetic filaments could very well produce the needed acceleration.

However, the strong magnetic field in the lower corona is a source of embarrassment for another reason altogether. It was noted in Chapter II that in the presence of a strong magnetic field the coefficient of thermal conductivity is modified with

$$k_{\parallel}(B,T) = k(T) \tag{V.1}$$

$$k_{\perp}(B,T) = \frac{k(T)}{1 + \omega_c^{e\,2}/\nu_e^2} \simeq \frac{\nu_e^2 k(T)}{\omega_c^{e\,2}}$$

where $\omega_c^e = eB/m_e c$ and $\nu_e \simeq 5\, n_e T^{-3/2} \ell n\, \Lambda$ (the electron collision frequency). For $B = 1$ gauss , $n_e = 10^8/cm^3$, $T = 1.5 \times 10^6 °K$, $\ell n\, \Lambda = 25$, it follows that $\omega_c^e \simeq 1.8 \times 10^7$ rad/sec , but ν_e is only about 7 collisions/sec . Thus, $k_{\perp}$ is completely quenched, and energy can be transferred by conduction only along the magnetic field. If $\vec{B}$ deviates from the radial direction (as it surely does) then $\vec{q}$ and $\vec{\nabla}T$ are related by a tensor conductivity coefficient, and drastic modifications of the conductive heating model are required.

The effect of possible corotation has also not been treated in an adequate fashion. If a region with complete corotation (i.e., $F(r) = r$, $r < b$) does exist, then it is useful to solve the flow equations in the rotating frame since for $r < b$, $u'_{\phi} = 0$, $\vec{B}$ can be radial, and no radial magnetic pressure gradient terms will then appear. However, in the rotating frame, the effective or apparent force is no longer simply given by the gravitational attraction of the sun. Instead we have

$$\vec{F}'_{eff} = -\frac{GM_{\odot} m \vec{r}}{r^3} + 2m(\vec{\Omega} \times \vec{u}'_r) - m\vec{\Omega} \times (\vec{\Omega} \times \vec{r}) \tag{V.2}$$

where the second term represents the Coriolus force and the third is the centrifugal acceleration term, $m\Omega^2 r \sin\theta$. In the solar equatorial plane, the radial component of $\vec{F}'_{eff}$ is

$$F'_r = -\frac{GM_{\odot} m}{r^2} + m\Omega^2 r \tag{V.3}$$

so that the solar gravity field is weakened by the rotation. For large b this effect could be quite significant. The net force vanishes for a particle rotating with the sun (i.e., in a synchronous orbit) at $r \simeq 37R_{\odot}$.

Finally, we must consider the fact that recurrent activity regions of various types are present on the sun. The Mariner 2, Explorer 14 storm of October 7-9, 1962, represents one kind of irregularity. It appears that the main feature of this event was a sudden increase (by at least an order of magnitude) in density, rather than velocity, and it is possible that an active filament near the base emitted many more particles than normal. If these were all emitted with negligible corotation, then the density irregularity would form a pattern in interplanetary space similar to the magnetic field spiral as shown in Fig. 21a. Although all velocities are radial, the source of the irregularity rotates with the sun and successive elements are emitted in different angular positions. [Actually, there is considerable doubt that the October 7 configuration resembled Fig. 21a. The time lapse between detection on Mariner 2 and Explorer 14 suggests an almost radial pattern near the earth (J. Wolfe, private communication), which could perhaps have resulted if the original direction of emission on the sun had been strongly tipped in the direction of corotation.]

More significant distortions must be associated with M-regions since these apparently produce enhancements in solar wind speed. The magnetic spiral angle, and the shape of the M-region boundary depend on $u_r(r)$ and a possible configuration is shown in Fig. 21b. It is clear that this kind of non-uniformity can produce serious perturbations. On the leading edge, we have an interaction region with fast plasma overtaking slower streams, and on the trailing edge a lowering of density occurs. We shall see below that very complex effects can occur when plasma streams collide, and in fact, these same phenomena must generally be induced by any temporal fluctuations in the plasma velocity.

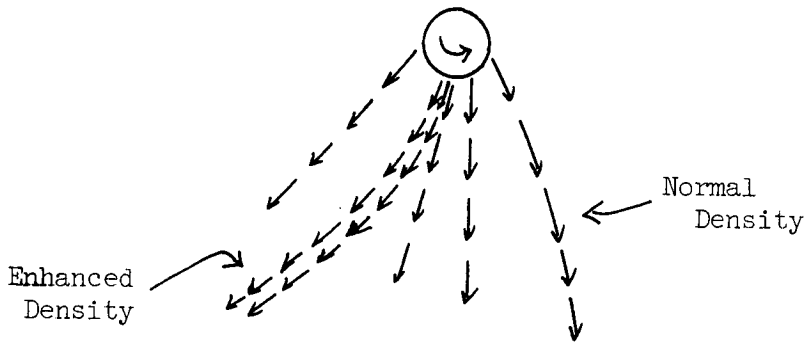

Figure 21a

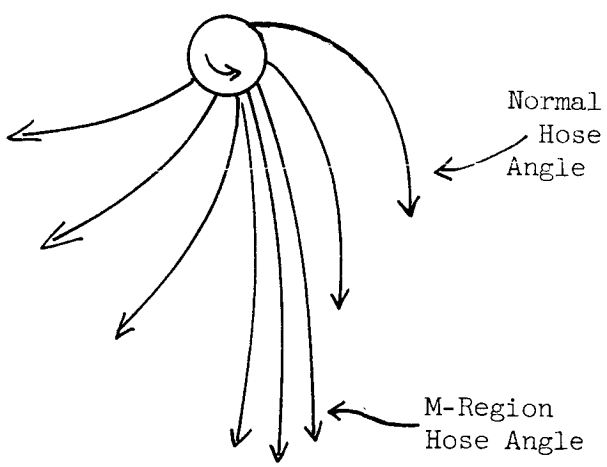

Figure 21b

The study of coronal and solar wind irregularities, circulation patterns, temporal variations and deviations from spherical symmetry has scarcely been started. At present, it can be stated that these phenomena may be extremely important but that complete observations will be difficult to perform, and the theory required will be extremely complex.

V.2. Viscous Effects

In the first discussion of solar wind theory, no detailed prediction of the flow pattern near the earth was given. For the best fit solution $nu \simeq 1.5 \times 10^{11}/cm^2$ sec at $r = 10R_\odot$ (Table 2) and the continuity relation, $nur^2 = c$, then yields an unambiguous flux value at the earth, $J_{av.} = 3.24 \times 10^8$ ions/cm^2 sec, but the proportions of n and u which make up this flux must be derived by solving the dynamical equations. Unfortunately, the validity of the Navier-Stokes equations becomes questionable long before the earth is reached.

The basic problem has to do with the assumption $\ell/L \ll 1$, used to derive the Navier-Stokes equation by the Chapman-Enskog technique and the correct L must first be identified. If L is simply defined by $L|dN/dr| \simeq N$, then the original solutions of the conductive heating equations indicate that $\ell \simeq L$ near $75 - 100 \cdot R_\odot$. However, the problem is not so easily solved, and the complications become important much closer to the sun. It has already been noted that these conductive heating equations possess unphysical solutions with $T(r) = 0$, $r < \infty$ and $T(r) \to T_\infty > 0$, $r \to \infty$; in each case $u \to \infty$ at the singularity. With the hope that these annoying solutions were only present because the viscous forces (which presumably inhibit large velocity gradients) had been artificially omitted, Scarf and Noble (1964, 1965) decided to introduce the appropriate viscous terms into the Navier-Stokes equations. The results of this investigation are rather surprising.

For spherically symmetric flow the complete Navier-Stokes equations have the form

$$nmu \frac{du}{dr} + \frac{d}{dr}(nkT) + \frac{nGM_\odot m}{r^2} = \frac{4}{3} r \frac{d\mu}{dr} \frac{d}{dr}\left(\frac{u}{r}\right) + \frac{4}{3} \mu \frac{d}{dr}\left[\frac{1}{r^2} \frac{d}{dr}(r^2 a)\right] \tag{V.4}$$

and

$$\frac{mu^2}{2} - \frac{GM_\odot m}{r^2} + \frac{5}{2}\kappa T - \frac{r^2 k(T)}{c}\frac{dT}{dr} - \frac{4}{3}\frac{\mu(T) r^2}{c}\left(u\frac{du}{dr} - \frac{u^2}{r}\right) = E \qquad (V.5)$$

where E and $c = nur^2$ are constants of motion. For fully ionized hydrogen, $\mu = \mu_0 (T/T_0)^{5/2}$, with $\mu(T_0)$ given in Eq. (II.33). However, unlike the conductive coefficient, $k(T)$, the viscous coefficient does change significantly as the gas composition is varied. The addition of 10% helium reduces μ to about 70% of its value for fully ionized hydrogen. Thus for the solar wind the Prandtl number, $\kappa\mu/mk$, is approximately equal to 0.013. This explains why viscous contributions had previously been neglected. When the thermal and kinetic energies and gradients are comparable, the viscous term in the energy equation is roughly (1 – 2)% of the conductive term and where $\kappa T > mu^2/2$, the ratio is even smaller.

This kind of argument is indeed appropriate when one discusses normal subsonic flow, but it should already be clear from Eq. (V.5) that a serious error is possible when the flow is supersonic. Even though $\mu(T)$ is numerically very small, if u is large and constant, the term $4\mu(T)u^2 r/3$ can play a very important role in the energy balance equation as r increases.

Numerical integration of Eqs. (V.4,5) confirms this expectation, but the way in which the viscous stresses modify the flow may, at first glance, appear to be unphysical. Figure 22 shows some typical results derived by integrating in both directions from the crossover. The parameter B is essentially the Prandtl number times $A = 2k(T_0)GM_\odot m/\kappa^2 T_0 c$ where T_0 is the temperature at the coronal base. For the case shown here, $A = 200$, $T_0 = 1.5 \times 10^6$°K, and the curve labeled $B \equiv 0$ is the one derived earlier, with no viscous terms at all. The velocity profile labeled $B = 2.46$ is the numerical solution of the Navier-Stokes equation with the appropriate coefficient of viscosity for the coronal gas, and to the accuracy shown in this figure, the temperature distribution is unchanged by the addition of viscosity.

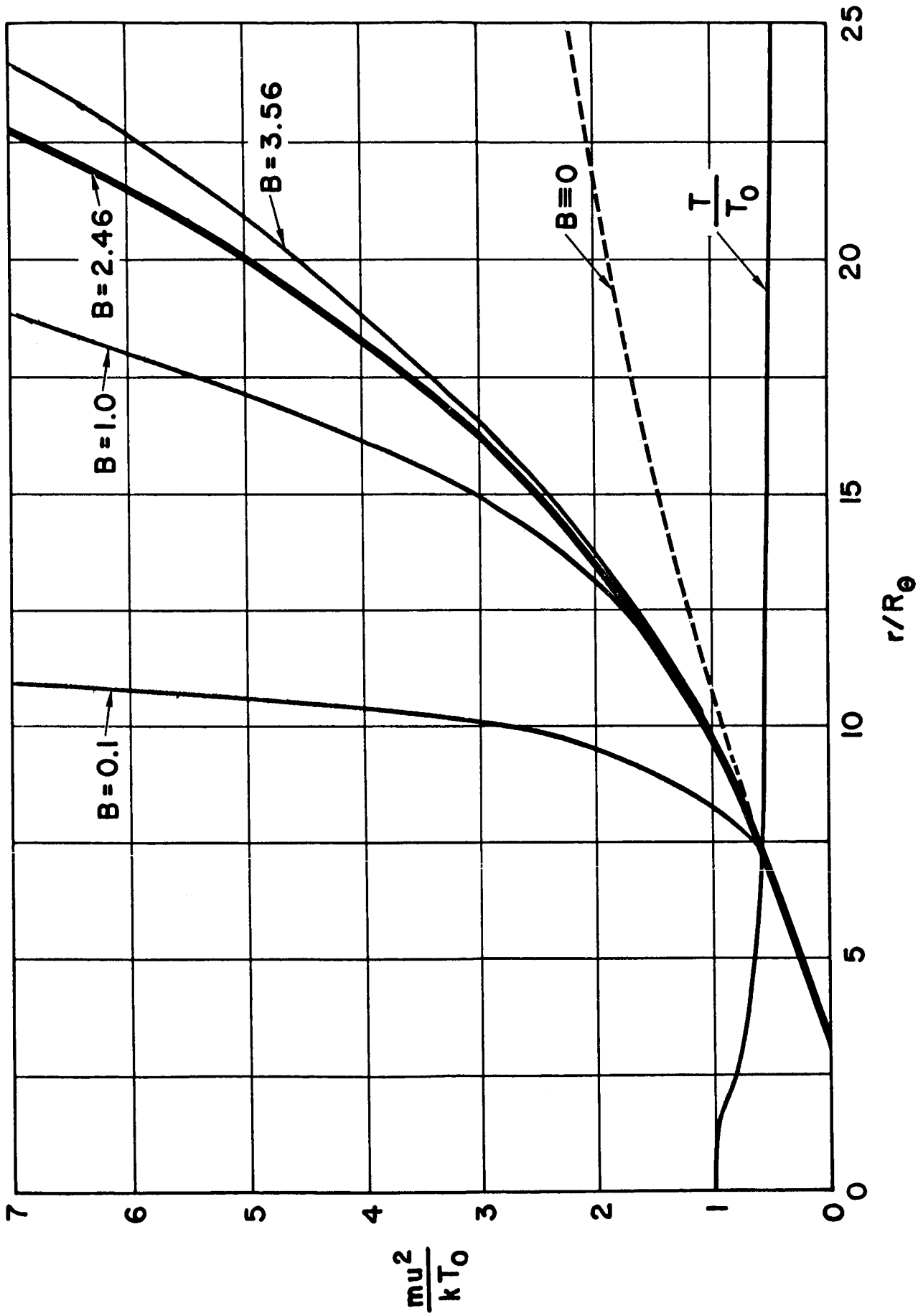

Figure 22

It can be seen that in the subsonic region the viscous terms produce a negligible change in $u(r)$. This is no surprise, because $\kappa\mu \ll mk$ and $(1/2)mu^2 \leq \kappa T$ here. It can also be seen that the viscous terms do induce a significant change in $u(r)$ in the supersonic region. Again, this is not unexpected; although $\kappa\mu/mk$ remains small, $(1/2)mu^2$ becomes large compared to κT , and the viscous contribution to the energy equation is comparable to the conductive term. What is most amazing about these curves is that $u(r,B)$ is greater than $u(r,B \equiv 0)$. Physically, one would expect viscous dissipation to yield a lower flow speed relative to the sun, and not a higher one.

The answer to this paradox was found by trying to vary the Prandtl number to approach $B = 0$. The curves shown for $B = 0.1$, 1.0 and 3.56 are calculated using artificial and unphysical values for $\mu(T_0)$, keeping $k(T_0)$ fixed. It can be seen that as $\mu(T_0)$ (or B) is increased, the flow speed at any given radius does indeed decrease in a physically sensible manner. However, as $B \to 0$, we do not approach the curve $B \equiv 0$ which is the solution of the non-viscous conductive heating equations.

In fact, the "paradox" has an exact analogy when thermal conduction alone is considered. If μ and k are both neglected, then the flow is adiabatic and $T(r) \to r^{-4/3}$. However, if only the viscous terms are omitted, then $T(r) \to (k(T_0)r)^{-2/5}$ or $(r^{-2/7} + Ck(T_0)^{-1}r^{-4/7} + \ldots)$. The solutions with finite thermal conductivity do not yield adiabatic flow in the limit $k(T_0) \to 0$, and similarly, the solutions with small but finite $\mu(T_0)$ do not go over to the $\mu(T_0) \equiv 0$ solutions as $\mu(T_0) \to 0$. From a mathematical point of view, this is also clear. The differential equations are of the form $dT/dr = G/k(T)$, $du/dr = F/\mu(T)$ and $k \equiv 0$, $\mu \equiv 0$ represent singularities. The result is well known to aerodynamicists. In "Flow of Rarefied Gases," Schaaf and Chambré (1961) remark on page 33, "Solutions are thus singular in the viscosity (or equivalently, the mean free path), and the boundary layer solution (for $\mu \to 0$) cannot be obtained by perturbation schemes starting with the inviscid solution."

If the $B = 2.46$ curve in Fig. 22 is regarded as the "correct" one, then this solution can be used to investigate the limits of the continuum or fluid models of the corona. The first question has to do with the precise meaning of the restriction $\ell/L \ll 1$. In particular, it must be ascertained which scale length is involved. This can be determined by examining the higher order terms in the Chapman-Enskog treatment. The successive approximations are

$$p_{ij}^{(0)} = 0 \quad ,$$

$$p_{ij}^{(1)} = \mu\tau_{ij} \quad , \tag{V.6}$$

$$p_{ij}^{(2)} = \mu\tau_{ij} + \frac{\mu^2}{n\kappa T}\,\tau_{ij}\vec{\nabla}\cdot\vec{u} + \ldots \quad ,$$

(Schaaf and Chambré, 1961, p. 30) and thus the Navier-Stokes equations should be valid if $\mu(du/dr)/n\kappa T \ll 1$. Since $\mu \approx nm^{1/2}(\kappa T)^{1/2}\ell$ [see Eqs. (I.13), (II.33)] this can be written as

$$\frac{\ell}{L}\left(\frac{mu^2}{\kappa T}\right)^{1/2} \ll 1 \quad , \qquad L\left|du/dr\right| \simeq u \tag{V.7}$$

and the appropriate scale length turns out to be the one associated with the streaming velocity. (This is not a statement of general validity. The complete expression for $p_{ij}^{(2)}$ contains temperature gradients as well. The Navier-Stokes equations become questionable whenever one of these terms is significantly large. In our case, the velocity gradients are steep beyond the crossover while the thermal gradients remain moderate.) By inspection of the numerical solution, Scarf and Noble (1964) have found that the above inequality is not satisfied beyond $r = 20\ R_\odot$.

In the language of aerodynamics, we pass from the continuum region to the "slip flow" region when the appropriate Knudsen number approaches unity. For a neutral gas, the slip flow regime is bounded by the region of continuum flow ($\ell \ll L$) and free molecular flow ($\ell \gg L$). Actually, because the solar wind is a magnetized plasma, there is no

region in which free flow occurs in the classical gasdynamics sense. Nevertheless, we can define three regions. For $(\mu\vec{\nabla}\cdot\vec{u}/nkT) \ll 1$, the full Navier-Stokes equations are valid. For $\mu(\vec{\nabla}\cdot\vec{u})/nkT \sim 1$, but $\ell\,|dT/dr| \ll 1$, the Navier-Stokes equations are not valid, but there are enough collisions to maintain a statistical distribution function with a well-defined temperature. For $\ell\,|dT/dr| \geq T$, ordinary two-body collisions are unimportant and the characteristics of the particle distribution functions are determined by other phenomena.

In ordinary gasdynamics no rigorous formulation of the equations of motion is available for slip flow. Various complex systems of equations (the Burnett equations, the Thirteen Moment equations) have been proposed to replace the Navier-Stokes equations for moderate Knudsen numbers, but these replacements introduce severe difficulties, and considerable doubt exists about their physical validity. (Schaaf and Chambré, 1961, pp. 31-34.) It seems likely that no moment equations will really be of use here, so that the flow patterns have to be obtained by solving the Boltzmann equation itself. However, it appears that the Navier-Stokes equations, with some modifications, provide a better description of the gas in the slip flow regime than the higher order systems.

This discussion indicates that at present no rigorous treatment of the solar wind flow is possible beyond $(15 - 20)R_\odot$. In order to obtain some bound to the range of flow patterns, Scarf and Noble (1964) arbitrarily assumed that the Navier-Stokes equations are strictly valid up to $17R_\odot$, with adiabatic continuum flow beyond $17R_\odot$. The results for a quiet solar wind are shown in Table V.1. Although these numbers obviously are subject to considerable revision as more realistic treatments of the region beyond $(15 - 20)R_\odot$ are considered, the entries can be used to evaluate roughly the range of importance of two-body collisions. We find $\ell(T,n)\,|dT/dr| \simeq T$ for $r \simeq 75\ R_\odot$, and two-body collisions cannot serve to maintain the Boltzmann distribution function beyond this radius. The radial flow itself tends to introduce a severe anisotropy in the absence of a randomizing mechanism (i.e., $T_\parallel$ is generally not equal to $T_\perp$ for collisionless spherical flow because the

TABLE V.1. MODEL QUIET SOLAR WIND

($A = 100$, $T_0 = 1.5 \times 10^6$°K , $m = 0.62\ m_{prot.}$)

$r/R_\odot$	u (km/sec)	N_e (cm^{-3})	T (°K)	Remarks
< 2	—	—	—	"heating region"
2	18.4	2.03×10^6	1.47×10^6	↑ Uninhibited conduction and viscosity
4.5	72.4	1.02×10^5	1.03×10^6	
6.8	105	3.09×10^4	8.89×10^5	
	(sonic transition near $r/R_\odot = 7$)			
7.2	110	2.62×10^4	8.73×10^5	
10	146	1.02×10^4	7.92×10^5	
12.6	190	4.95×10^3	7.55×10^5	
15	246	2.70×10^3	7.35×10^5	↓
20	267	1.40×10^3	4.8×10^5	Adiabatic continuum flow
40	286	3.27×10^2	1.8×10^5	
50	287	2.09×10^2	1.35×10^5	
80	290	81.5		Collisionless flow dominated by scattering from magnetic and electric fluctuations
120	290	35.8		
200	290	12.9		
215	290	11.2		

particles with $\vec{v}$ parallel to the mean flow direction tend to migrate farther than those with finite $v_\perp$; in the presence of a central force field this anisotropy is even more marked, because the particles travel on ballistic orbits). Thus, the close agreement between the distribution observed at the earth (see Chapter IV) and a Boltzmann distribution indicates that some mechanism other than two-particle scattering binds the solar wind into a fluid and maintains the statistical spectrum beyond $(70 - 100)R_\odot$.

V.3. Hydromagnetic Instabilities

Parker (1957, 1958) first proposed that in the solar wind plasma particle scattering from waves could replace particle-particle scattering and maintain the fluid-like behavior in the collisionless region. In particular, Parker showed that an anisotropic plasma is unstable with respect to production of hydromagnetic waves of the Alfvén variety. Thus, these waves must grow in amplitude (in modern terminology of plasma physics, the system is "overstable" when the waves grow) until many particles are scattered, resulting in a distribution which is sufficiently isotropic to quench the instability.

The formalism is based on a modified version of the mhd equations suitable for a collisionless magnetized plasma. The change involves the expression $P_{ij} = n\kappa T\, \delta_{ij}$, $(\mu \equiv 0)$. If there are no collisions, then there is no reason to expect that $T_\parallel$ (i.e., parallel to $\vec{B}$) is equal to $T_\perp$. In fact, any charged particle will simply spiral forward around the field line, and it is reasonable to assume $T_\perp \neq T_\parallel$, in general. A plausible field oriented tensor expression for P_{ij} which reduces to the correct form as $\vec{B} \to 0$ or $T_\perp \to T_\parallel$ is then

$$P_{ij} = n\kappa T_\parallel \left(\frac{B_i B_j}{B^2}\right) + n\kappa T_\perp \left(\delta_{ij} - \frac{B_i B_j}{B^2}\right) \tag{V.8}$$

When this is inserted in Eq. (II.28), Parker's modified hydromagnetic equation is obtained. For $\vec{\nabla}\phi \simeq 0$, it follows that

$$nm \frac{\partial \vec{u}}{\partial t} + nm(\vec{u}\cdot\vec{\nabla})\vec{u} = -\vec{\nabla}\left(n\kappa T_\perp + \frac{B^2}{8\pi}\right) + \frac{(\vec{B}\cdot\vec{\nabla})\vec{B}}{4\pi}\left(1 - \frac{4\pi\, n\kappa(T_\parallel - T_\perp)}{B^2}\right) \tag{V.9}$$

and $\vec{u}$ and $\vec{B}$ are also related by

$$\frac{\partial \vec{B}}{\partial t} = \vec{\nabla} \times (\vec{u} \times \vec{B}) \tag{V.10}$$

In order to examine the effect of the anisotropy, let us consider a transverse perturbation $\vec{b} = b(z,t)\vec{i}_y$ on a static uniform field $\vec{B} = B\vec{i}_z$. If n, $T_{\|}$ and $T_{\perp}$ are constant, and $\vec{u} = u(z,t)\vec{i}_y$, then Eq. (V.9) yields

$$nm \frac{\partial u_y}{\partial t} \simeq \frac{B}{4\pi}\left[1 - \frac{4\pi\, nk(T_{\|} - T_{\perp})}{B^2}\right]\frac{\partial b}{\partial z} \tag{V.11}$$

with neglect of the quadratic terms. Equation (V.10) gives

$$\frac{\partial b}{\partial t} = B \frac{\partial u_y}{\partial z} \tag{V.12}$$

and the wave equation for b is

$$\frac{\partial^2 b}{\partial t^2} = \frac{B^2}{4\pi nm}\left[1 - \frac{4\pi\, nk(T_{\|} - T_{\perp})}{B^2}\right]\frac{\partial^2 b}{\partial z^2} \tag{V.13}$$

If $T_{\|}$ were equal to $T_{\perp}$, Eq. (V.13) would simply describe an Alfvén wave, or transverse disturbance propagating along the magnetic field with speed $B/(4\pi nm)^{1/2}$. The speed is reduced for $T_{\|} \gtrsim T_{\perp}$; however, if

$$nkT_{\|} - nkT_{\perp} > \frac{B^2}{4\pi} \tag{V.14}$$

overstability results. The perturbation is then of the form

$$b \simeq b_0 \cos kz \exp(t/\tau) \tag{V.15}$$

and the field irregularities grow exponentially in time. The time constant is

$$\tau = (4\pi nm)^{1/2}/Bk \left| \frac{4\pi\, nk(T_{\|} - T_{\perp})}{B^2} - 1 \right|^{1/2} \tag{V.16}$$

and if B is weak (as it is in interplanetary space)

$$\tau \rightarrow [(4\pi)^{1/2}/k][m/(\kappa T_{\parallel} - \kappa T_{\perp})]^{1/2} \qquad (V.17)$$

which is independent of the gas density and magnetic field.

Instability of a somewhat different nature also occurs when $T_{\perp}$ exceeds $T_{\parallel}$. In this case the analog of Eq. (V.14) is

$$\frac{(n\kappa T_{\perp})^2}{n\kappa T_{\parallel}} > \frac{B^2}{8\pi} \qquad (V.18)$$

(Thompson, 1962), and it can be seen that large deviations from thermal isotropy are forbidden by these hydromagnetic instabilities, although quite different physical processes produce wave growth in the two cases. Equation (V.14) describes a "firehose" instability where the centrifugal acceleration around the curving (i.e., perturbed) magnetic field gives rise to a current which enhances the irregularity. Equation (V.18) describes the onset of a "mirror" instability. The plasma flows into those parts of the wave where the field is weak, increasing $p_{\perp}$, and forcing the field lines farther apart, thus further weakening the field.

In Parker's original discussion of Eq. (V.14) (1958), a fairly dense solar wind ($n_i \simeq 10^3/cm^3$) was assumed. For this case $\ell\,|dT/dr| \simeq T$ near the earth, with $T \simeq 4 \times 10^5 °K$. Thus, Parker anticipated that magnetic disordering would commence near the earth, and it was conjectured that a highly disordered magnetic shell might surround the inner solar system at, say, $r \simeq 2$ A.U. Such a configuration had been hypothesized earlier to account for the slow decay of solar cosmic rays produced in connection with solar flares (Meyer, Parker and Simpson, 1956). The cosmic ray flux at the earth tapers off very gradually, and after the highest energy particles arrive first along field aligned paths, the other particles arrive from all directions, suggesting that they are scattered from a distant heliocentric shell.

The density used by Parker is possibly appropriate for a great storm or blast wave, and in this case the flare effect decay may be represented by the disordered shell picture. However, another possible explanation for the isotropy and long life of the bulk of the storm particles will be presented in the next section, and this question is still unresolved. At any rate, in the quiet solar wind the densities are considerably lower and the instability must become significant near $(50 - 80)R_\odot$, if it is important at all.

At $50\ R_\odot$, $B_r \simeq 45\ \gamma$ and $B_\phi \ll B_r$. If $n_i \simeq 200/cm^3$, $T \simeq 1.5 \times 10^5 °K$ (see Table V.1) then $B^2/4\pi \simeq 1.6 \times 10^{-8} ergs/cm^3$ and $n_i \kappa T \simeq 4.1 \times 10^{-8}$ ergs/cm^3, so that it appears possible to generate the firehose instability with a thermal anisotropy of $(10 - 20)\%$. (The electron contribution to $n\kappa T$ is expected to be isotropic.) If this occurs, one would expect the thermal and magnetic energy densities to remain comparable, since the magnetic scattering presumably produces the nearly statistical distribution. However, when the field begins to spiral, $B^2/4\pi$ decreases relatively slowly with $B_\phi \sim r^{-1}$ and $n(r) \sim r^{-2}$. Thus, this kind of randomization would yield a negligible change in temperature from $r \simeq 50\ R_\odot$ to $r \simeq 1$ A.U.

V.4. Plasma Oscillations

In recent years, more and more attention has been given to the role of plasma oscillations in space physics. These waves are not described by the mhd equations, but some properties of the plasma oscillation spectrum can be determined approximately by examination of the individual moment equations for the electrons and the ions. If $\vec{B} = 0$, $\vec{\nabla}\phi = 0$ and there are no collisions, Eqs. (II.24) and (II.26) yield

$$\frac{\partial n_e}{\partial t} + \nabla\cdot(n_e u_e) = 0$$

$$n_e m_e \frac{\partial u_e}{\partial t} + n_e m_e (\vec{u}_e\cdot\vec{\nabla})\vec{u}_e + \vec{\nabla} p_e = - e\vec{E} \qquad (V.19)$$

with a corresponding set for the ions. Poisson's equation requires

$$\vec{\nabla}\cdot\vec{E} = 4\pi e(n_i - n_e) \qquad (V.20)$$

In order to determine the characteristics of small amplitude density perturbations, we set $n_e = N + n'$, $n_i = N + n''$, and again neglect the quadratic terms in the momentum equations. Then

$$\frac{\partial^2 n'}{\partial t^2} = - \frac{\partial}{\partial t} (\vec{\nabla}\cdot(\vec{n}_e \vec{u}_e))$$

$$\simeq - N \vec{\nabla}\cdot\frac{\partial \vec{u}_e}{\partial t} \qquad (V.21)$$

$$\simeq \frac{\nabla^2 p_e}{m_e} + \frac{Ne}{m_e} \vec{\nabla}\cdot\vec{E} \quad .$$

If $p_e \sim n_e^{\gamma}$ and $n' \sim n'_0 \exp(i\omega t - \vec{k}\cdot\vec{r})$, it follows that

$$- \omega^2 n' \simeq - \frac{\gamma k^2 p_e n'}{N m_e} + \frac{Ne}{m_e} \vec{\nabla}\cdot\vec{E} \qquad (V.22)$$

or

$$n' \simeq - \frac{Ne}{m_e} \frac{1}{(\omega^2 - k^2 a^2)} \vec{\nabla}\cdot\vec{E} \qquad (V.23)$$

with $\gamma p/Nm_e = \gamma \kappa T_e/m_e = a^2$. A similar expression is easily derived for n'' ; here $e \rightarrow -e$, $m_e \rightarrow m_i$, $a \rightarrow A$.

When these relations for the density perturbations are inserted into Poisson's equation an expression of the form $D(\omega,k)\vec{\nabla}\cdot\vec{E} = 0$ is obtained. Since finite $\vec{\nabla}\cdot\vec{E}$ is desired, the allowed modes of the field must obey the dispersion relation $D(\omega,k) = 0$, or

$$1 = \frac{\omega_p^2}{\omega^2 - k^2 a^2} + \frac{\Omega_p^2}{\omega^2 - k^2 A^2} \qquad (V.24)$$

This equation generally has two real roots. If $\omega^2 \simeq k^2 a^2$, the fact that $\Omega_p^2 = (m_e/m_i)\omega_p^2$ is small compared to ω_p^2 can be used, and the second term can be treated as a perturbation. Then Eq. (V.24) yields

$$\omega^2 = \omega_p^2 \left[1 + \frac{m_e}{m_i} \left(1 + \frac{\gamma_e k^2}{K_D^2} \right) \right] + \frac{\gamma_e \kappa T_e}{m_e} k^2 + \ldots \qquad (V.25)$$

where K_D is the electron Debye wave number, $(4\pi N e^2/\kappa T_e)^{1/2}$. As $T_e \to 0$, this solution tends to $\omega_p(1 + m_e/m_i)^{1/2}$, and we recognize these high frequency electrostatic oscillations as the electron plasma oscillations discussed in Chapters I and II. (There it was assumed that $m_e/m_i = 0$.) If the plasma is cold, this is the only solution to the dispersion relation, but if T_e is finite, another mode is possible. To find this low frequency mode, assume $\gamma_e = \gamma_i$ and let

$$\omega^2 = C\, k^2 a^2 \frac{m_e}{m_i} \qquad (V.26)$$

where C is to be determined by solving the dispersion relation. For $\omega^2 \ll k^2 a^2$, we have

$$1 = -\frac{\omega_p^2}{k^2 a^2} + \frac{m_e}{m_i} \frac{\omega_p^2}{\left(C k^2 a^2 \frac{m_e}{m_i} - k^2 a^2 \frac{T_i}{T_e} \frac{m_e}{m_i} \right)} \qquad (V.27)$$

and this yields

$$C \simeq \left[\frac{T_i}{T_e} + \frac{1}{(1 + \gamma_e k^2/k_D^2)} \right] \qquad (V.28)$$

These ion plasma oscillations are extremely significant for several reasons. First, they travel very slowly, since the phase velocity is on the order of $(\kappa T_e/m_i)^{1/2} \simeq 40$ km/sec for $T_e = 2 \times 10^5$°K. This means that it is very easy to Doppler shift the frequency by means of a small velocity increment with respect to the plasma frame of reference. Second, any particle traveling with $u > (\omega/k)_{\text{ion wave}}$ should be able to radiate ion waves by a Cerenkov process, and one would therefore expect these waves to be associated with a strong drift or two stream instability. Third, unlike the electron plasma oscillation spectrum which is sharply peaked near ω_p, the ion spectrum is very broad. For plasma oscillation wave numbers between zero and K_D, ion waves with

$0 < \omega \lesssim \Omega_p$ are allowed. In the solar wind frame of reference, this implies $0 < f < 470$ cps for $n_i \simeq 5/cm^3$, and in a spacecraft frame of reference, f_{max} can be Doppler shifted up to kilocycles. Finally, since this wave represents an oscillating electric field with a frequency near the interplanetary electron gyrofrequency ($f_c = eB/2\pi m_e c \simeq 140$ cps for $B = 5\gamma$), it can be anticipated that electron cyclotron heating will occur if the properties of the dispersion relation are not drastically changed in the presence of a magnetic field.

Further analysis of these possibilities requires a more sophisticated approach, because it is not true that all electrons, for instance, contribute equally to the dispersion relation. More explicitly, it is necessary to start with the Boltzmann equation for the velocity distribution function in order to obtain the correct dispersion relation. The subsequent analysis follows closely the development outlined in the beginning of this section. The Vlasov equation (Boltzmann equation with no collision) term for the electrons is

$$\frac{\partial f_e}{\partial t} + \vec{v}\cdot\vec{\nabla} f_e - \frac{e}{m}\vec{E}\cdot\vec{\nabla}_v f_e = 0 \qquad (V.29)$$

and a similar relation describes the ion distribution function, f_i. Poisson's equation becomes

$$\vec{\nabla}\cdot\vec{E} = 4\pi e \int d^3v (f_i - f_e) \qquad (V.30)$$

and the perturbation approximations are of the form $f_e = f_0 + f'$, $f_i = F_0 + f'$. If f', f'' and E vary as $\exp(i\omega t - \vec{k}\cdot\vec{r})$, the resulting dispersion relation is

$$1 = \frac{\omega_p^2}{k^2}\int d^3v \frac{[\vec{k}\cdot\vec{\nabla}_v f_0 + (m_e/m_i)\vec{k}\cdot\vec{\nabla}_v F_0]}{[\vec{k}\cdot\vec{v} - \omega]} \qquad (V.31)$$

The integration over the singularity is specified by choosing a contour which passes below the point $v = \omega/k$, in the imaginary v plane. This specification, which is required to obtain a causal response, introduces the main modification. Landau damping (Landau, 1946) of the

wave now occurs, and ω is generally a complex function of k. Physically, Landau's damping represents a nonlinear interaction between particles traveling with speed v, and the wave with phase velocity ω/k. If $v < \omega/k$, the particle gains energy from the wave, and if $v > \omega/k$, the wave gains energy from the particle. Since f_0', F_0' generally decrease with increasing v, this interaction generally leads to a net damping of the wave.

Fried and Gould (1961) have examined the consequences of (V.31) in some detail. For $f_0 = (a/\pi)(a^2 + v^2)^{-1}$, $F_0 = (A/\pi)(A^2 + v^2)^{-1}$, the dispersion relation is

$$\frac{k^2}{\omega_p^2} = \frac{1}{(\omega/k + ia)^2} + \frac{m_e}{m_i}\frac{1}{(\omega/k + iA)^2} \tag{V.32}$$

and the two branches are

$$\omega \simeq \omega_p\left[1 + \frac{m_e}{2m_i}\left(1 - \frac{ika}{\omega_p}\right)^{-2}\right] - ika$$

$$\omega \simeq ka(m_e/m_i)^{1/2}(1 + k^2a^2/\omega_p^2)^{-1/2} - ikA \tag{V.33}$$

The solution for the electron plasma oscillation branch resembles Eq. (V.25) for $k \ll K_D^e$. However, if $k \gg K_D^e$, $|\mathrm{Im}\,\omega| > \mathrm{Re}\,\omega$, and the Landau damping is so strong that no true oscillations are possible.

This change is even more important for the ion wave branch, if $T_e = T_i$. In this case, $a(m_e/m_i)^{1/2} = A$, and Eq. (V.34) predicts extremely large damping for any k, in contrast to the undamped solution derived from the moment equations. Thus, it would seem from (V.34) that ion waves would never have to be considered.

In fact, this conclusion, while correct under the circumstances described above, is generally not valid. Consider a plasma with $T_e \gg T_i$. Then $A \ll \omega/k \sim \sqrt{\kappa T_e/m_i}$, and the Landau damping is negligible. We can also modify the damping drastically by introducing

an electron-ion current or drift (i.e., $F_0 \rightarrow A/\pi(A^2 + (v - u)^2)^{-1}$) . In essence, the damping is proportional to the fraction of ions having the speed ω/k . If $u = 0$, $T_e = T_i$, then ω/k is near the mean thermal ion speed and the damping is enormous. However, if the ions are cool, their distribution is very narrow. When we modify the wave speed (by heating the electrons, or letting the electrons drift with respect to the ions) so that $F_0(v = \omega/k)$ becomes small, the damping rapidly goes down. In fact, if the drift is sufficiently large $(u > \omega/k)$, the system is unstable and growing ion waves appear. For Maxwellian distributions, Fried and Gould have shown that the critical drift speed varies from $0.925(1 + (m_e/m_i)^{1/2})a$ for $T_e = T_i$ to about $4A$ for $T_e/T_i \gtrsim 12$.

This nonlinear behavior appears to be extremely significant in interplanetary space. The interplanetary electric field, $\vec{E}_I = - \vec{u} \times \vec{B}/c$, is very large and its fluctuations could produce currents big enough to trigger ion wave instabilities. For $u \simeq 400$ km/sec , $B = 5$ gauss , $E_I \simeq 2 \times 10^{-5}$ volts/cm . The criterion of large size involves comparison with the runaway field

$$E_R \simeq \kappa T_e/e\ell \qquad (V.35)$$

$$\simeq 2 \times 10^{-8}\ n/T_e \text{ volts/cm}$$

(see Chapter II). For $n = 10/\text{cm}^3$, $T_e = 2 \times 10^5 {}^\circ\text{K}$, $E_R \sim 10^{-12}$ volts/cm , and $E_I \sim 2 \times 10^7\ E_R$. Now actually this result must be interpreted with care. The quiet interplanetary field is normal to $\vec{B}$, and runaway can only occur if a large electric field is imposed parallel to $\vec{B}$. However, it is clear that normal fluctuations in $\vec{B}$, $\vec{u}$ and the angles can easily allow $(\vec{E}_I)_{\parallel}$ to exceed E_R . If this does occur, a very complex sequence of changes takes place.

First, the electron current increases as eEt/m_e . This continues until the electron drift speed exceeds the ion wave speed, and the current instability then sets in (Field and Fried, 1965). The waves grow and scatter electrons, reducing the drift speed as shown in Fig. 23. The

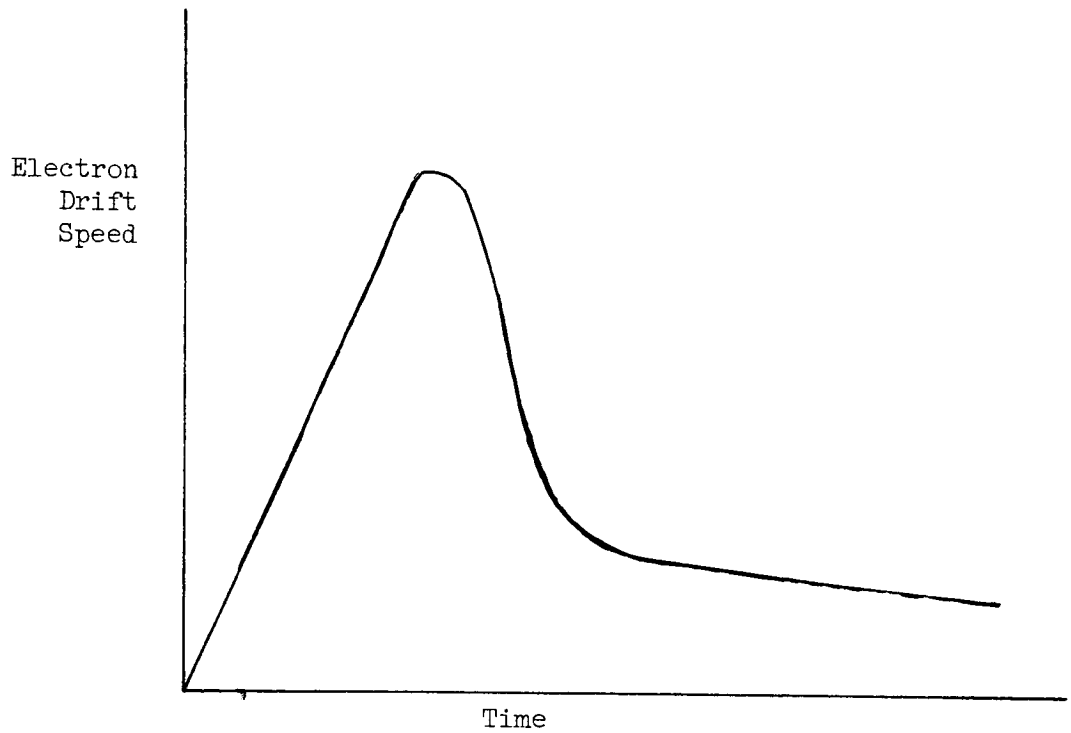

Figure 23

electrons are heated somewhat by the scattering and it is not known at present just what the form of the final state is. It may happen that the drift speed falls sufficiently so that the instability momentarily quenches itself, in which case we might expect a repetition of the process.

At any rate this picture of a collisionless plasma differs considerably from the hydromagnetic one. It is anticipated that fluctuations in $\vec{u}$, $\vec{B}$ or θ trigger ion wave instabilities throughout the collisionless region. These waves could undoubtedly heat some electrons by a subsequent gyroresonance with

$$\ddot{\vec{r}} - \dot{\vec{r}} \times \vec{\omega}_c = - \frac{e}{m_e} \vec{E}$$

$$\vec{E} = - \vec{\nabla}\phi \quad , \qquad \phi = \phi_0 \cos (\vec{k} \cdot \vec{r} - \omega t) \tag{V.36}$$

The ultimate acceleration limit for a given ϕ_0 is not known at present, but calculations by Fredricks, et al. (1965) show that energy multiplication by factors of at least 25 occur in times on the order of milliseconds. If this process is repeated in some stochastic manner one might then expect to find superthermal electron generation throughout interplanetary space, especially during disturbed periods. Parker (1965) has recently speculated that some such generation mechanism may provide an alternate explanation for the slow decrease of isotropic flux following a great storm.

Chapter V. REFERENCES

F. Scarf and L. Noble, AIAA Journal, 2, 1158, 1964.

F. Scarf and L. Noble, Astrophysical Journal, 141, May 15, 1965.

S. Schaaf and P. Chambré, Flow of Rarefied Gases, Princeton University Press, 1961.

E. N. Parker, Phys. Rev., 107, 923, 1957.

E. N. Parker, Phys. Rev., 109, 1874, 1958.

W. Thompson, An Introduction to Plasma Physics, Addison-Wesley, 1962.

P. Meyer, E. Parker and J. Simpson, Phys. Rev., 104, 768, 1956.

B. Fried and R. Gould, Phys. Fluids, 4, 139, 1961.

E. Field and B. Fried, Phys. Fluids, 7, 1937, 1964.

R. Fredricks, F. Scarf and W. Bernstein, J. Geophys. Res., 70, 21, 1965.

E. Parker, Phys. Rev. Lett., 14, 55, 1965.